EXPLORING THE ROLE OF PANNEXIN1A IN AN ACUTE EXPERIMENTAL MODEL OF PARKINSON'S DISEASE

Georg Stefan Otto Zoidl

A THESIS SUBMITTED TO THE FACULTY OF GRADUATE STUDIES IN PARTIAL FULFILLMENT OF THE REQUIREMENTS FOR THE DEGREE OF MASTER OF SCIENCE

GRADUATE PROGRAM IN BIOLOGY

YORK UNIVERSITY

TORONTO, ONTARIO

July 2022

Abstract

In the nervous system Pannexin1 channels are major ATP and glutamate release sites. The channels are implicated in neurodegenerative disorders including Parkinson's disease, but the underlying mechanisms remain unclear. Here, an interdisciplinary approach tested roles of the mammalian Pannexin1 ortholog Pannexin1a in a zebrafish model of MPTP-induced early stages of Parkinson's disease at molecular, systems, and behavioral levels. The short-term treatment of wild-type TL and gene-edited Panx1a-KO larvae caused metabolic stress, regulated inflammatory pathways, and reduced ATP production. Local field potentials recorded from three regions of the ascending visual pathway showed complex changes in the beta- and gamma-band power and in the coherence between these regions. MPTP treatment produced significantly impaired movements which were partially rescued by targeting the NLRP3 inflammasome. The main findings of this research provide evidence that Panx1a serves a neuroprotective role in an acute MPTP model of Parkinson's disease.

Acknowledgments

Many incredible people have helped guide, grow and shape me on my way to complete my Master's degree. Here, I would like to express my gratitude to them.

I would like to express my appreciation for my supervisor Dr. Connor and my advisor Dr. Donaldson for guiding and advancing my research over these past two years.

Furthermore, I am grateful for all the great people in the lab past and present who helped me on my way to become a better scientist; Amanda, Anna, Cherie, Daria, Don, Fatema, Ksenia, Nickie, Paige, Parisa, Ryan, Sarah and Simin. Thank you for passing on your knowledge to me and all the great memories and good times we had in the lab or on conference trips.

I am also very grateful to Janet and Veronica in the vivarium for their help and knowledge when it comes to zebrafish husbandry. Their incredible work has helped me several times throughout this thesis.

A big thank you to everyone on the York Lions Tennis team and my coaches. You've helped me grow as a student-athlete and gave me a break from the hectic lab life.

Last, but not least I'm grateful to my parents and family as they guided and supported me throughout these past two years.

Table of Contents

List of Abbreviations

µM	Micromolar
ºC	Degrees Celsius
6-OHDA	6-hydroxydopamine
95%CI	95% Confidence Interval
ANOVA	Analysis of variance
ATP	Adenosine 5'-triphosphate
BCC	Bicuculline
BLAST	Basic Local Alignment Search Tool
bp	Base pair
CaMKII	Calcium-calmodulin kinase
CD	Endonuclease
cDNA	Complementary deoxyribonucleic acid
Cryo-EM	Cryo-Electron Microscopy
C-terminus	carboxyl-terminus
CY-09	4-[[4-Oxo-2-thioxo-3-[[3-(trifluoromethyl)phenyl]methyl]-5-thiazolidinylidene]methyl]benzoic acid
DESeq2	Differential expression analysis
Dexamethasone	(11β,16α)-9-Fluoro-11,17,21-trihydroxy-16-methyl-pregna-1,4-diene-3,20-dione
DL	Hippocampus
DM	Amygdala
DNA	Deoxyribonucleic acid
dpf	Days Post Fertilization
EtBr	Ethidium bromide
ETC	Electron transport chain
FC	Functional connectivity
FDR	False discovery rate
FPKM	Fragments per kilobase of transcript per million mapped reads
$GABA_A$	γ-aminobutyric acid type A receptor
GSDME	Gasdermin E
GO	Gene ontology
GPI	glycosyl-phosphatidylinositol
Hz	Hertz
IL-18	Interleukin 18
IL-1β	Interleukin 1 beta
INF39	Ethyl 2-(2-chlorobenzyl)acrylate
KEGG	Kyoto encyclopedia of genes and genomes
KO	Knockout
LFP	Local Field Potential
logFC	Log fold change
MAPK	Mitogen-activated protein kinase
MCC950	N-[[(1,2,3,5,6,7-Hexahydro-s-indacen-4-yl)amino]carbonyl]-4-(1-hydroxy-1-methylethyl)-2-furansulfonamide sodium salt

Metformin	N,N-Dimethylimidodicarbonimidic diamide hydrochloride
min	Minutes
MK-801	(5S,10R)-(+)-5-Methyl-10,11-dihydro-5H-dibenzo[a,d]cyclohepten-5,10-imine maleate
mL	Milliliter
mm	Millimeter
MPP+	1-methyl-4-phenylpyridinium
MPTP	1-methyl-4-phenyl-1,2,3,6-tetrahydropyridine
mV	Millivolt
MΩ	Megaohm
N, N′-dimethyl-4,4′-bipyridinium dichloride	Paraquat
NaCl	Sodium chloride
NADPH	Nicotinamide adenine dinucleotide phosphate
NF-κB	Nuclear factor kappa B
NLRP3	NOD-, LRR- and pyrin domain-containing protein 3
NMDAR	N-Methyl-D-aspartate Receptor
OT	Optic tectum
P	Phosphorylation
padjust	Adjusted P-value
Panc	Pancuronium bromide
Panx1	Pannexin1
PCR	Polymerase Chain Reaction
PD	Parkinson's disease
PROB	Probenecid
proIL-1β	IL-1β precursor
pS	Pico Sievert
REST	Relative expression software tool
RNA	Ribonucleic acid
RNA-seq	RNA sequencing
ROS	Reactive oxygen species
RT-qPCR	Reverse Transcription - quantitative PCR
sec	Seconds
SEM	Standard error of the mean
SFK	Src-family kinase
TALEN	Transcription activator-like effector nucleases
TCAG	SickKids Centre for Applied Genomics
TL	Tupfel long fin
ZFIN	Zebrafish international network

List of Tables

List of Figures

1. Introduction

1.1 Pannexin1: Discovery, structure, and localization

Pannexin 1 (Panx1) is an integral membrane protein that is part of the vertebrate pannexin glycoprotein family (Jin et al., 2021), which includes three members (Panx1, 2, and 3). Panx1 was first identified by Panchin et al. (2000) in the early 2000s via a BLAST search of the GenBank. The discovery was more of an accident as they initially tried to compare innexin homology between mollusks and flatworms. Innexins are gap junction proteins found exclusively in invertebrates. The gap junction forming proteins of vertebrates are called connexins. Panchin et al. (2000) named the new family of proteins pannexins, for 'pan,' which is Latin for ‘all, and nexus’ in analogy to them forming gap junction connections between cells.

Following the initial discovery of pannexins, several groups conducted further research on their structure and localization. Researchers demonstrated that pannexins were present in mammalian genomes, including humans (Baranova et al., 2004). The human Panx1 gene, which contains five exons and four introns, was found on chromosome 11q14.3 (Baranova et al., 2004). Panx1 genes have been identified in all vertebrates, from fish to humans (Wang et al., 2009).

Like innexins and connexins, pannexins contain four transmembrane regions, two extracellular loops, one intracellular loop, and intracellular N and C termini **(Figure 1)**. Different from innexins and connexins, all pannexin proteins are glycosylated (Penuela et al., 2009). The formation of large glycosylated structures prevents docking of pannexin channels and gap junction formation (Whyte-Fagundes & Zoidl, 2018). Today, the pannexins primarily act as

channel proteins and not gap junction proteins, although a few exceptions are known (Bruzzone et al., 2003; Dahl & Locovei, 2006; Lai et al., 2007; Sahu et al., 2014).

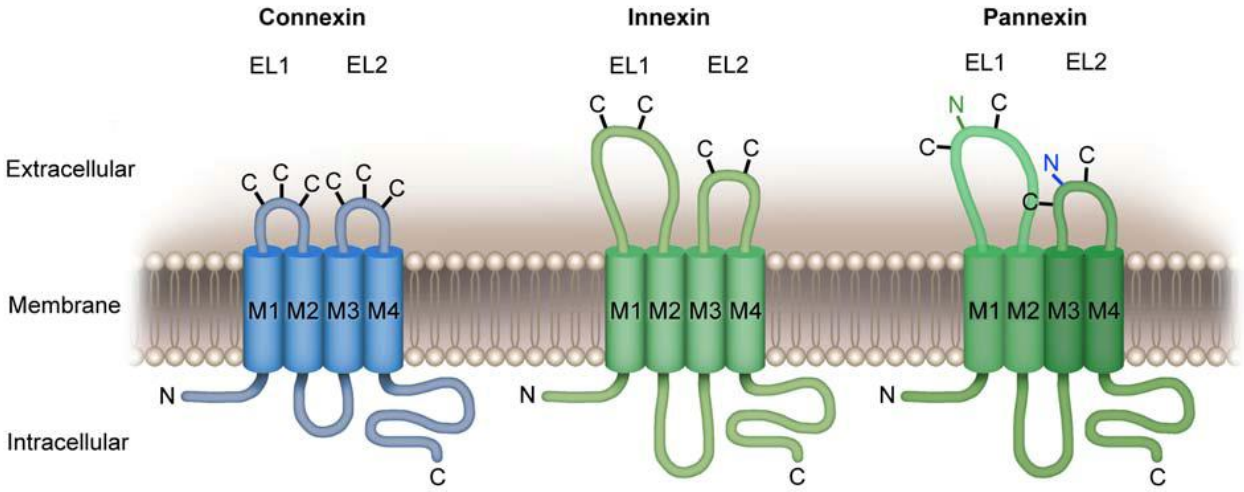

Figure 1. Structure of connexins, innexins, and pannexins. The three gene families share tetra-span transmembrane domains (M1-M4). Amino-terminal (N) and carboxy-terminal (C) ends are located in the cytoplasm. Innexins and pannexins lack the third conserved cysteine motifs (C) required for docking of connexins when forming gap junctions. Pannexins differ from connexins and innexins by N-glycosylation motifs (Figure created by Photoshop).

Initially, Panx1 was predicted to form a hexameric channel based on single-channel recordings, size exclusion tomography, and negative stain electron microscopy (Boassa et al., 2007; Chiu et al., 2017; Wang et al., 2014). More recently, the cryo-EM structure of human and frog Panx1 revealed a heptameric structure about 105Å long and 100Å wide (Jin et al., 2020; Michalski et al., 2020; Mou et al., 2020). Both hexameric and heptameric forms may exist since Panx1 channels can form two types of channels; highly selective chloride channels (<100pS) and large pore ATP-release channels (300-500pS) (Mim et al., 2021).

In rodents Panx1 is ubiquitously expressed in many different systems and cell types. Panx1 is expressed in the central nervous system, skeletal muscle, heart, cochlea, skin, cartilage,

spleen, kidney, reproductive systems, prostate, and small intestine (Baranova et al., 2004; Bruzzone et al., 2003; Penuela et al., 2007, 2008; Ray et al., 2005, 2006; Wang et al., 2009). Panx1 expression has also been localized to neuronal cells, astrocytes, and microglia (Mousseau et al., 2018; Ray et al., 2005; Suadicani et al., 2012). In the nervous system, Panx1 is localized at the postsynaptic density in proximity to N-methyl-D-aspartate (NMDA) receptors (Zoidl et al., 2007). While ubiquitously expressed throughout the central nervous system some regions express Panx1 strongly. In adult mice expression was especially high in the motoneurons of the hindbrain, the hippocampus, the amygdala, and the deep cerebellar nuclei (Ray et al., 2005).

1.2 Panx1 function *in vivo*

Panx1 channels are activated by several stimuli, including voltage, mechanical stimuli, and small molecules such as potassium and calcium (Michalski et al., 2018; Whyte-Fagundes & Zoidl, 2018). Panx1 can also be activated by interaction with ionotropic purinergic receptors such as P2X7 or G-protein coupled receptors of the P2Y family (Locovei et al., 2006; Pelegrin et al., 2008). Other channels in the postsynaptic density, such as NMDA receptors, open Panx1 channels through Src family kinases (S. Li et al., 2018). Panx1 has been associated with critical neurodevelopmental and plasticity functions such as neuronal network development, dendritic spine formation, and synaptic plasticity (Ardiles et al., 2014; Horton et al., 2017; Prochnow et al., 2012; Sanchez-Arias et al., 2019). Loss of function in Panx1 knockout mice caused learning and memory deficiencies and altered hippocampal plasticity (Flores-Muñoz et al., 2020; Gajardo et al., 2018; Prochnow et al., 2012).

An essential function of the Panx1 channels is the release of ATP (Dahl, 2015). In neurons, ATP release through Panx1 channels has both excitatory and inhibitory effects through signaling with purinergic receptors, voltage-gated calcium channels, or NMDA receptors (Boyce & Swayne, 2017; Shuo et al., 2018) (**Figure 2**). In the pannexin field, it is generally agreed that the excess release of ATP through Panx1 channels into the postsynaptic cleft can mediate enhanced NMDA receptor activation and the overstimulation of purinergic signaling, leading to augmented aberrant bursting activity, neuroinflammation, and cell death (Lim et al., 2021; Makarenkova et al., 2018). Cell death can be mediated by the release and accumulation of ATP in the synaptic cleft, acting as a "find-me" signal which recruits phagocytes to apoptotic cells (Chekeni et al., 2010; Medina et al., 2020). Another way Panx1 can mediate cell death is through the cleavage of the C-terminus by caspases leading to an irreversible commitment to cell death when the channel is permanently opened. Due to Panx1's diverse functions, this channel has been implicated in neurodegenerative disorders such as Parkinson's disease (PD), Alzheimer's disease, Huntington's disease, schizophrenia, and epilepsy (Frederiksen et al., 2019). However, there is consensus that present knowledge in the field only has scratched the surface of the diverse roles this channel has in both health and disease.

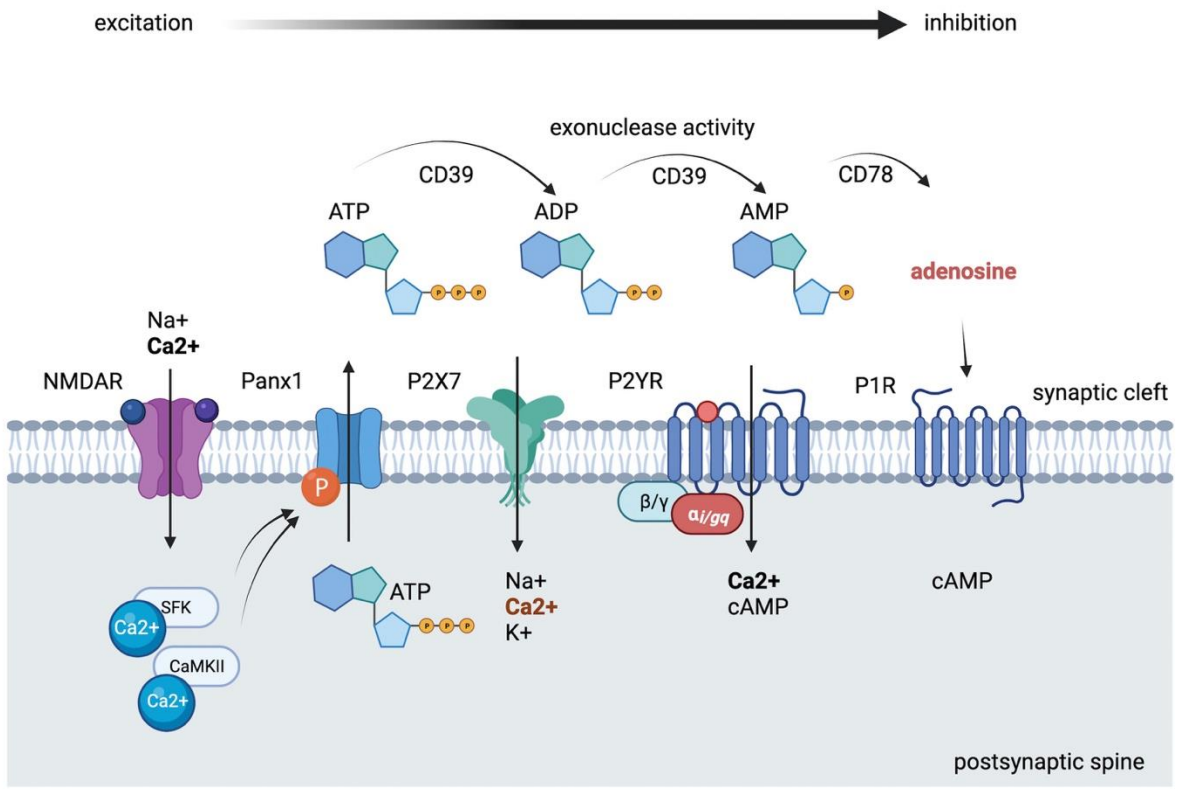

Figure 2. Model of the role of Panx1 in the postsynaptic membrane. Panx1 is a large pore channel in the postsynaptic membrane. It allows for the passage of molecules such as potassium and ATP. When NMDA receptors in excitatory neurons open, the influx of calcium can activate Src-family kinases (SFKs) and calcium-calmodulin kinases (CaMKII) which open Panx1 channels by phosphorylation (P). The released ATP from Panx1 channels plays essential roles in purinergic signaling as a P2X, P2Y, and P1 receptors ligand. In this process, ATP is metabolized by endonucleases (CDs) localized in the synaptic cleft. Once ATP is broken down to adenosine, it can trigger P1 receptors, which typically dampens the activity of excitatory neurons. It is worth noting that P1 receptors are also known to be pro-inflammatory, as once activated, they can promote the release of pro-inflammatory cytokines. (Image generated with BioRender.com).

1.3 Introduction to Parkinson's disease

Parkinson's disease is the second most prevalent neurodegenerative disorder after Alzheimer's disease (Fleming et al., 2022). The progression of PD is marked by the loss of dopaminergic neurons over time, especially in regions such as the substantia nigra pars compacta

and the striatum (Poewe & Mahlknecht, 2009). The most common hallmarks of PD are motor-based, such as tremors and bradykinesia, but there are also many non-motor symptoms such as hyposmia, sleep disturbances, and cognitive deficits (Antony et al., 2013). The progression of these symptoms has been linked to the loss of dopaminergic neurons in the brain.

The two dominant theories of how PD develops are brain-first and gut-first hypotheses. The brain-first hypothesis is built on evidence that the α-synuclein pathology arises in the brain, with secondary spreading to the peripheral nervous system (Horsager et al., 2020). A more recent hypothesis, named the dual-hit hypothesis, suggests that PD may originate from the gut (Breen et al., 2019; Houser & Tansey, 2017; Klann et al., 2022) **(Figure 3)**. The authors proposed that inflammation in the gut causes a breakdown of the intestinal lining. This breakdown allows molecules such as α-synuclein to escape the gut and travel up the vagus nerve to the brain. Once in the brain, α-synuclein accumulates and misfolds, forming Lewy bodies over time (Grazia et al., 1998). Lewy bodies can cause inflammation and eventually lead to the common dopaminergic neuron loss associated with PD (Beach et al., 2008, 2009; Gelb et al., 1999). Therefore, evidence is building that the initial events leading to PD may start long before any clinical symptoms are observed. The rethinking of the origin of PD puts a spotlight on understanding alterations of the inflammatory response as a critical target to tackle this neurodegenerative disease.

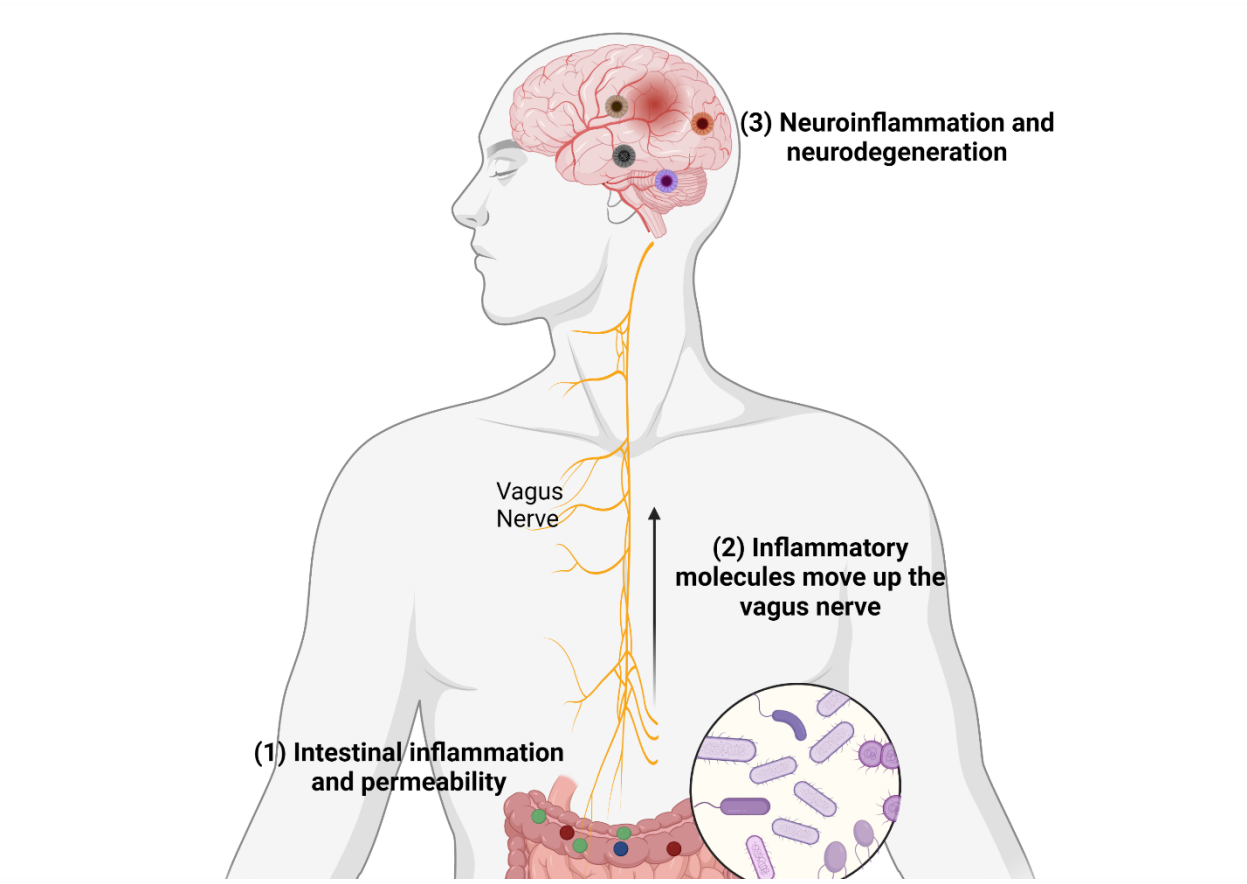

Figure 3. A current hypothesis of how Parkinson's disease originates. (**1**) Excessive inflammation in the gut caused by gut microbiota leads to the breakdown of the intestinal wall. The increased intestine permeability allows molecules to leave, such as α-synuclein. (**2**) α-synuclein travels up the vagus nerve to the brain. (**3**) The α-synuclein protein accumulates and misfolds in the brain. Accumulation of misfolded α-synuclein causes the formation of highly inflammatory complexes called Lewy bodies. The accumulation occurs over time in areas, with the first areas affected being the substantia nigra pars compacta and the striatum. The inflammation leads to the loss of neurons, especially dopaminergic neurons. (Image generated with BioRender.com).

1.3.1 Panx1 involvement in inflammation and Parkinson's disease

Panx1 has been implicated with inflammation and Parkinson's disease in several studies as a potential risk factor and drug target (Ahmadian et al., 2019; Frederiksen et al., 2019; Ling et al., 2021). Silverman et al. were the first to provide compelling evidence that Panx1 proteins

activate the inflammasome in neurons and astrocytes (Silverman et al., 2009, 2008b). The same authors demonstrated that Panx1 proteins interact with proteins of the inflammasome complex, causing activation of caspase-1. Caspase-1 plays an essential role in for maturation of pro-inflammatory cytokines (proIL-1β and IL-18) into IL-1β and IL-18.

In neurons, Panx1 activity has also been shown to increase when oxidative stress increases, suggesting a close relationship between the two in PD (Ahmadian et al., 2019). The activation of Panx1 leads to the release of ATP into the synaptic cleft. Excess ATP in the synaptic cleft triggers the P2X7 receptor leading to efflux of potassium from the cell and NADPH oxidase activation, which generates more reactive oxygen species (Wilkaniec et al., 2017). The ROS build-up along with low potassium levels can trigger NLRP3 inflammasome assembly and eventual cell death. Furthermore, Panx1 facilitates cell death through apoptosis, pyroptosis, and autophagy (Crespo et al., 2017). Apoptosis generally does not cause inflammation since dying cells advertise their presence. The release of ATP acts as a "find-me" signal that attracts immune response cells such as microglia, macrophages, and monocytes to the area to facilitate removal (Chekeni et al., 2010; Ravichandran, 2010). Pyroptosis causes cell lysis resembling a form of necrosis, which generates inflammation. Furthermore, autophagy and apoptosis constitute functionally distinct mechanisms for the turnover or destruction of cytoplasmic structures within cells and of cells within organisms, respectively.

Panx1 is considered a pro-cell death channel that helps in the propagation and clearance of inflammation, but the literature is not without conflicts. Some reports argued that Panx1's ability to form large pore channels which mediate ATP release and its interaction with purinergic receptors is a driver of inflammation (Crespo, Yanguas et al., 2017; Koval et al., 2021; Yang et al., 2020). However, there have been contradictions with other reports finding that the presence

of Panx1 was beneficial, ameliorating induced neuroinflammation (Ling et al., 2021). In this research, Panx1 was crucial in controlling reactive astrocytes to intervene in the inflammatory response and protect neurons. Finally, some groups suggested that Panx1 does not play a role in inflammasome activation, providing evidence that Panx1 is dispersible for canonical and non-canonical inflammasome activation (Chen et al., 2020; Qu et al., 2011). Taken together, it seems likely that Panx1 channels can take on diverse roles depending on the molecular, cellular, and physiological context.

1.4 Pannexin genes in the zebrafish

Pannexin genes in the *Danio rerio* (zebrafish) differ from other vertebrates. A phylogenetic tree analysis showed that the evolutionary relationship between Panx1 and Panx3 is closer than that of Panx2 (Kurtenbach et al., 2013). Previous studies have shown that pannexins had two rounds of duplication in the evolution of vertebrates about 400–600 million years ago. The first was the appearance of Panx2, and then the emergence of Panx1 and Panx3, which originated from a common ancestor (Bond et al., 2012; Kurtenbach et al., 2013). They are part of two rounds of genome duplication that occurred at the early stage of vertebrate divergence (Vandepoele et al., 2004). Panx1a and Panx1b genes most likely originated from the third major whole genome duplication event in teleost fish, which occurred about 320–350 million years ago (Bond et al., 2012; Prochnow et al., 2009).

In addition, the tissue expression of the two Panx1 genes in zebrafish showed significant differences. The expression pattern of zebrafish Panx1a was ubiquitous, while Panx1b was abundant in the brain and eyes (Bond et al., 2012; Kurtenbach et al., 2013). The biophysical

properties of Panx1a and Panx1b revealed shared and unique gating properties, with both channels forming large pores. Like mammalian Panx1 channels, Panx1a channels release ATP and can be blocked with the Panx1 inhibitor probenecid (PROB) (Silverman et al., 2008b). The recently reported phenotypes of global knockout of both Panx1 genes using engineered transcription activator-like effector nucleases (TALEN) demonstrated distinct changes to the visual system. Results indicated that loss of Panx1a channels specifically affected the expression of gene classes representing the visual system's development and visual processing. Abnormal swimming behavior in the dark and the expression regulation of pre-and postsynaptic biomarkers suggested changes in dopaminergic signaling (Safarian et al., 2020). The loss of Panx1b channels compromised the final output of luminance, motion detection, and the circadian clock system (Safarian et al., 2021).

1.5 *Danio rerio* as a Parkinson's disease model

Zebrafish are a high-throughput animal model extensively used to study vertebrate development. Today, zebrafish are also used to model human disease or for drug discovery (McGrath & Li, 2008; Roberts et al., 2013; Rubinstein, 2003; Veldman & Lin, 2008). Zebrafish are suitable for large *in-vivo* assays due to their small size, fast reproductive cycle, transparency at the larval stage, as well as rapid physical and cognitive development (Vaz et al., 2018). The first study of a zebrafish model for PD established clear neurochemical and behavioral changes (Anichtchik et al., 2004). This initial research was followed up by several other studies laying the foundation for Parkinson's studies today (Bretaud et al., 2004; Razali et al., 2021; Rink & Guo, 2004). These studies took advantage of zebrafish's non-invasive uptake of water-soluble drugs, which simply required adding compounds to the tank water.

Today, Parkinson's disease models in *Danio rerio* include chemically induced and genetic models. Chemically induced models include treatment with 1-methyl-4-phenyl-1,2,3,6-tetrahydropyridine (MPTP) (Bashirzade, Cheresiz, Belova, Drobkov, Korotaeva, Azizi-arani, et al., 2022; Lam et al., 2005; McKinley et al., 2005), 6-hydroxydopamine (6-OHDA) (Feng et al., 2014; Vijayanathan et al., 2017), rotenone (Ünal et al., 2019; Wang et al., 2017), and N, N′-dimethyl-4,4′-bipyridinium dichloride (paraquat) (Nellore & Nandita, 2015; Wang et al., 2018). Genetic models include modulation of early and late-onset Parkinson's disease genes such as Parkin, Pink1, and Lrrk2 (Brown et al., 2021; Fett et al., 2010; Sheng et al., 2010).

In this study, MPTP was used to induce Parkinson-like symptoms. MPTP was first synthesized as a potential opioid analgesic in 1947 by Lee and Ziering (Lee & Ziering, 1947). Later on it was discovered by Langston et al. (1984) that single injections of MPTP into squirrel monkeys resulted in Parkinsonism. Nowadays MPTP is used to simulate the disease to study the physiology and possible treatment options for Parkinson's disease.

MPTP is a Complex I inhibitor of the electron transport chain (ETC) of the mitochondria, which has been extensively studied in relation to Parkinson's disease across different animal models (Abolaji et al., 2018; Meredith & Rademacher, 2011; Ofori & Schorderet, 1987). MPTP is converted to its toxic form MPP+ by monoamine oxidase B, following its selective up take in dopaminergic neurons through the dopamine transporter (Przedborski et al., 2000). The inhibition of ATP production causes metabolic cell stress, which promotes cell death of dopamine-producing neurons. In this study, we used MPTP to chemically induce Parkinson-like symptoms in zebrafish larvae because of the non-invasive uptake through water and the well-characterized mechanism of action.

1.6 What are Local Field Potentials, and why do they matter?

This research tried to address the question of how to assess brain activity at the earliest stages of Parkinson's disease when neurodegeneration is not yet detectable. There are different ways to analyze and quantify brain activity. For example, light-sheet fluorescence microscopy allows for the volumetric 3D scanning of the whole zebrafish brain when larvae express genetically encoded calcium indicators or voltage indicators (Ahrens et al., 2013; Keller et al., 2015; Nakai et al., 2001; Royer et al., 2016; Siegel & Isacoff, 1997). Since instrumentation for recording whole brain activity by light-sheet microscopy was unavailable, an electrophysiological method to record local field potentials (LFPs) was implemented based on published expertise in the group (Safarian et al., 2019). LFPs represent composite signals deriving from the postsynaptic activity of neuronal sources located in the vicinity of an electrode (Herreras, 2016) (**Figure 4a**). When the local activity is composed of correlated events, the analysis of this averaged activity can give insight into the network. Together with data from single-unit spike recordings (**Figure 4b**), a combined Spike-LFP analysis can provide deep insight into the activities of neuronal networks in health and disease (Weinberger et al., 2006). In contrast to spiking activity, which originates from a single neuron close to the electrode tip, LFPs represent a summation signal of excitatory and inhibitory dendritic potentials from a population of neurons in the neighborhood of the recording site (Herreras, 2016; Teleńczuk et al., 2017). The raw LFP signal can be decomposed into five frequencies in the range of 0-300 Hertz (Hz) (**Figure 4c**). The frequency bands are delta (1-3), theta (3-7Hz), alpha (7-13Hz), beta (13-30Hz), and gamma (>30Hz) (Abhang et al., 2016). As shown in **Figure 4**, each frequency range represents a different state of brain activity in humans. The beta and gamma bands are associated with an awake state, critical

thinking, and cognitive processing. Activity changes to beta- and gamma-bands have been demonstrated in PD (Feldmann et al., 2022; Guerra et al., 2022; Swann et al., 2016).

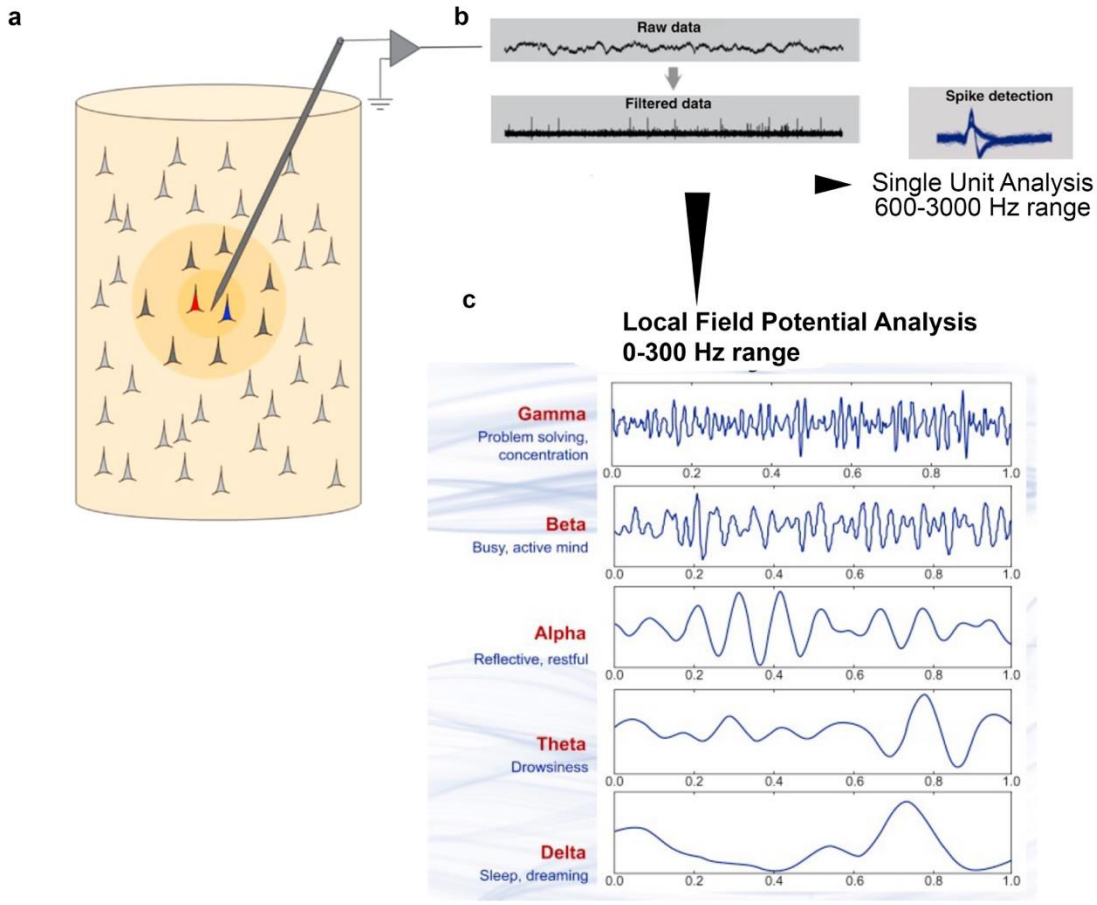

Figure 4. The recording of local field potentials. **a**) An electrode records the activity of neurons in the vicinity. **b**) The raw data output from LFP recordings. This data must be further filtered to be analyzed. LFP recordings can either be used for spike analysis or for analyzing brain waves. **c**) The local field potential analysis of the different frequency bands. The five different frequency bands are contained inside the raw signal and can be extracted with the help of various tests such as the power spectral density analysis. (Image generated with BioRender.com).

1.7 Behavioral analysis of zebrafish larvae

A benefit of working with zebrafish larvae is the robust behavioral phenotypes that become increasingly more complex from larval to adult stages (Roberts et al., 2013). A robust way to evaluate the behavioral phenotype of zebrafish larvae is to quantify the locomotion response when larvae are exposed to different light conditions (MacPhail et al., 2009). Larvae show distinct swimming patterns in response to light and dark conditions as soon as four days post fertilization (dpf) after developing a swim bladder (Basnet et al., 2019).

Here, a light-ramp stimulus was used to evaluate the larvae's movements in response to light**.** This test is a variation of the visuomotor response test, which was developed to quantitate the swimming of larval zebrafish in response to light increments and decrements (Emran et al., 2008). In this test, Emran et al. (2008) recorded responses of larvae to Light-ON/OFF conditions focusing on a brief spike of motor activity upon lights ON, known as the startle response, followed by a return to lower-than baseline activity, called a freeze. Larvae sharply increased their locomotor activity immediately following lights OFF and only gradually returned to baseline locomotor activity when the retina was intact. The light ramp assay suppresses the spike and freeze response and reports general locomotion activity when the light intensity is gradually ramped up, reaching a plateau of swimming activity at around 30% (1200 lux) light intensity as shown previously (Safarian et al., 2021).

2. Objectives and research design

This thesis aimed at addressing knowledge gaps related to the roles of Panx1 in the early stages of Parkinson's disease. **The hypothesis was that the genetic and pharmacological targeting of Panx1a alleviates the severity of an MPTP-induced PD-like phenotype.**

This goal was pursued by inducing acute inflammation with MPTP. As summarized in Section 1.4, the effects of chronic treatment with MPTP are well documented and have been used efficiently in animal models such as primates and rodents, as well as in the zebrafish model (Christensen et al., 2020; Mustapha & Mat Taib, 2021; Porras et al., 2012). Here, the first goal was to establish an acute MPTP model, which has not been done before in zebrafish larvae to the best of our knowledge. We speculated that by investigating a four-hour treatment with MPTP, we might be able to separate the initial events of inflammation from the endpoints reached by chronic treatment, thus gaining insight into the earliest stages of PD. Gene-edited Panx1a-KO larvae were chosen since our group previously reported that a global loss of Panx1a function regulates dopaminergic signaling in 6dpf larvae (Safarian et al., 2020). The pharmacological inhibition of Panx1a and Panx1b with the Panx1 inhibitor PROB was used to contrast the long-term effects of genetic loss of Panx1a from the acute effects caused by blocking both Panx1a and Panx1b channels.

The experimental strategy was designed to investigate MPTP-induced phenotypes in zebrafish larvae at three levels, from molecular, to systems, to behavior. The aims were:

- Investigating the molecular effects of MPTP by analyzing RNA-seq data and performing RT-qPCR and ATP assays. The goal was to elucidate the effects of acute MPTP treatment on gene regulation, pathway regulation, and metabolic effects.

- Investigating the brain activities of awake *in-vivo* larvae treated with MPTP using electrophysiological recording to evaluate changes to local field potentials. The strategy aimed at recording from three regions of the zebrafish brain, which are part of the ascending visual pathway. The rational was that in PD patients the visual system is affected for example with alterations of visual acuity and contrast sensitivity (Armstrong, 2011; Weil et al., 2016). The goal was to determine whether loss of Panx1a affected the visual-sensory responses to simple Light-ON/Light-OFF stimuli before or after treatment with MPTP. This goal required the development of a two-electrode local field potential recording and analysis protocol to determine local changes in the three brain regions or whether two regions became more coherent.
- The last goal was to use robust behavioral phenotyping of locomotion behavior before and after MPTP treatment to investigate changes in the visual-motor system. A sub-aim was to rescue the MPTP-induced phenotype by pharmacologically inhibiting the inflammasome.

3. Methods

3.1 Animal Handling

3.1.1 Adult zebrafish husbandry

Animal work was conducted at York University's zebrafish vivarium following the regulations set by the Canadian Council for Animal Care and after the approval of the protocol by the Animal Care Committee (GZ: 2020-7-R3). The wild-type strain was Tüpfel long fin (TL) bred in-house. The Panx1a knockout (Panx1a-KO) line was generated in-house (Safarian et al., 2020). The Zebrafish International Network (ZFIN) assigned the name panx1a$^{yku1/yku1}$. Adult

zebrafish were maintained in the vivarium's recirculation system (Aquaneering Inc., San Diego, CA) and kept at 28ºC on a 14-hour light and 10-hour dark cycle. Zebrafish were separated by sex a week before breeding and placed in the same tank separated by a transparent divider a day before breeding. Adults were bred in the morning, and eggs were washed and submerged in an E3 medium.

3.1.2 Maintenance of zebrafish larvae

Larvae were kept in the E3 medium from 0dpf to 7dpf. The use of larvae was kept to a minimum. Larvae were sacrificed at 7dpf according to the Animal Care Protocol guidelines. Behavioral, electrophysiological, and molecular assays were conducted on 6dpf larvae.

3.2 Quantitation of extracellular ATP

Larvae (~50 pooled larvae per sample) were incubated with (or without) 10µM MPTP for 4 hours at 28ºC (**Figure 5**). Next, larvae were collected and weighed before flash freezing and storage at -80ºC. Pooled samples were homogenized for 1min at 30Hz using the TissuelyserLT (Qiagen) set to 4ºC in phosphate-buffered saline (PBS) containing 100µM ARL-67156 (Sigma-Aldrich) and Halt Protease inhibitor (Thermo-Scientific) (1:100), to prevent excessive proteolytic and ATP degradation. Homogenates were transferred to cold Eppendorf tubes (-20ºC) and centrifuged at 12,000 rpm for 2min. Supernatants were collected and immediately used to measure extracellular ATP performed in 96-well format (Greiner Bio-One) using the Molecular Probes® ATP determination Kit as described by the manufacturer (Life Technologies). Samples were measured in replicates of 6 using the Synergy H4 Hybrid Multi-well Plate Reader (Biotek) as reported previously (Whyte-Fagundes et al., 2018). ATP concentrations in experimental

samples were determined from ATP standard curves (concentrations range: 0-1µM) included with each assay. The Gen5 Data Analysis Software (Biotek) controlled the luminescent assay parameters; internal temperature set to 28ºC, low intensity shakes of the plate for 3sec prior to reading, a 5sec integration time per well, and gain setting at 150.

Data were exported and analyzed in Excel. GraphPad's Welch's t-test was used to test for the statistical significance of differences between groups. ATP was presented as a normalized concentration per mg of protein to account for biological variance in larval size. It was previously reported that a linear relationship exists between pooled larvae's weight and the homogenate protein content (Whyte-Fagundes et al., 2018).

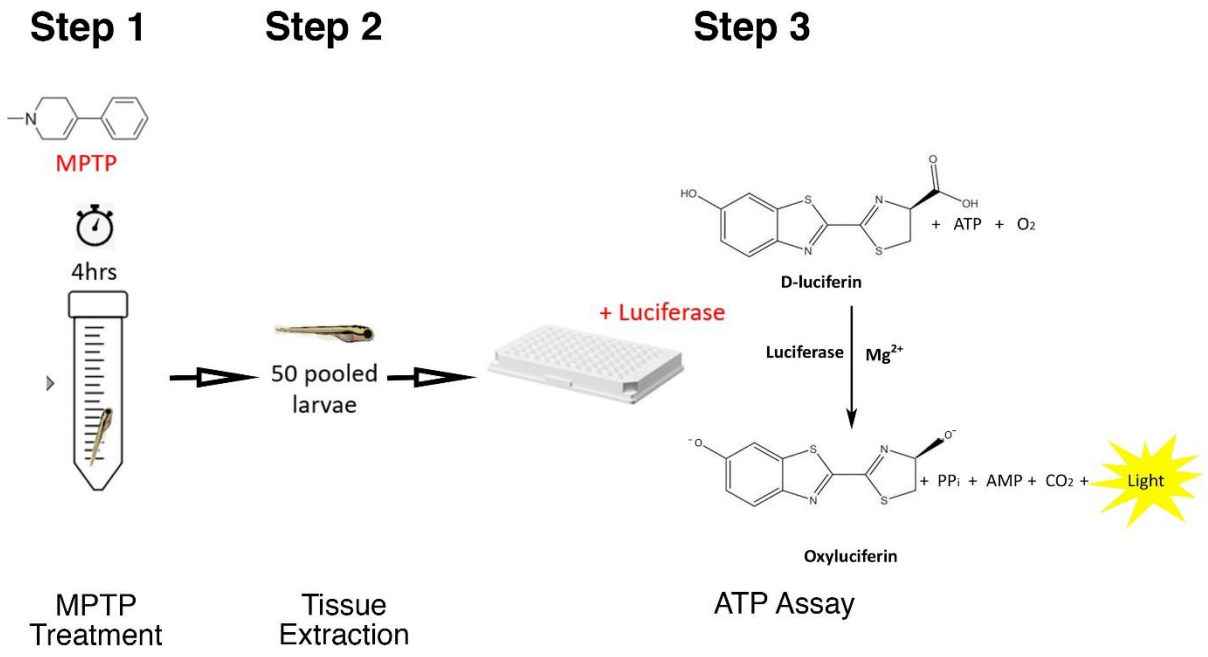

Figure 5. Workflow for determining extracellular ATP concentrations via a Luciferase assay in zebrafish larvae. Six-day post fertilization, *Danio rerio* larvae were incubated with MPTP for four hours in a 15mL Falcon tube (Step 1). Following the treatment, 50 larvae were taken and pooled in an Eppendorf tube. Excess water was removed, and the larvae were homogenized (Step 2). In Step 3, the Synergy H4 Plate Reader quantified light output generated by the firefly luciferase enzyme assay. Light was emitted from the reaction of D-luciferin to oxyluciferin. (Image generated with BioRender.com).

3.3 RNA-seq Analysis

The transcriptomes of TL and Panx1a zebrafish lines were analyzed by RNA-seq (NGS-Facility, The Center for Applied Genomics, SickKids, Toronto, ON). Larvae were either untreated or incubated with MPTP (50μM) before RNA-seq analysis. The Bioinformatics Group at Sickkids provided a Differential Transcript Expression Analysis (RSEM and DESeq2). In brief, a transcript abundance estimation used RSEM version 1.3.3 (http://deweylab.github.io/RSEM/) and bowtie2 version bowtie/2.3.4.2 (http://bowtie-bio.sourceforge.net/index.shtml) to estimate the expression level of each sample. For each sample, RSEM reports read counts, estimated lengths, and FPKM for each transcript and gene. In the second step, a differential expression analysis was performed using the estimated read counts for each transcript from the RSEM output. This transcript expression matrix was supplied to DESeq2 (https://bioconductor.org/packages/release/bioc/html/DESeq2.html) v.1.22.2 to detect differentially expressed transcripts. Filtering the low expressed transcripts to increase power was automatically applied via independent filtering on the mean of normalized counts within the DESeq2 results() function. Adjusted P-values (padj) were derived from Benjamini-Hochberg multiple testing. Here, a cutoff of 0.01 was used to select differentially expressed genes for further analysis.

Gene ontology (GO) enrichment of biological processes from the FishEnrichR database was used to identify regulated biological processes (Mi et al., 2019). After applying a cut-off of padj (<0.01), genes were sorted as up-or down-regulated using the log2FC values. GO biological processes analysis performed a Fisher's exact test and a false discovery rate (FDR) calculation to determine regulated GO biological processes.

The Kyoto encyclopedia of genes and genomes (KEGG) mapper v5 was used to identify regulated pathways using the human KEGG database (Kanehisa et al., 2022; Kanehisa & Sato, 2020). KEGG is a knowledge base for biological interpretation of large-scale molecular datasets such as RNA-seq data. Regulated genes with a padj (<0.01) were used to query the KEGG mapper. The top ten regulated pathways with the most regulated genes were extracted for graphing with GraphPad Prism.

The STRING analysis was used to determine protein-protein interactions of inflammatory genes (Szklarczyk et al., 2019, 2021). A list of 148 inflammasome genes was manually curated based on the literature. The genes were compared to the RNA-seq list, and regulated genes with a cutoff padj (<0.01) were extracted. The regulated genes were used to query the STRING analysis software to determine inflammatory pathways that were affected by MPTP treatment.

3.4 Tissue lysis and RNA extraction

For RNA extraction, 30 larvae per genotype (TL; Panx1-KO) and treatment (MPTP; 10µM or 50µM) were pooled. 3 biological replicates (n = 90 larvae per genotype/treatment) were frozen at -80ºC. RNA extraction was performed in 350µM RLT (Qiagen), and 3.5µM βME were added to samples and shaken in the TissueLyser with a metal ball at 50Hz for three minutes. Samples were centrifuged at 13rpm for 2 minutes; the supernatant was collected and centrifuged at 13rpm for three minutes. The lysates were placed in QIAcube for automatic total RNA extraction via RNeasy Plus Mini Kit and Protocol (Qiagen). Obtained RNA samples were measured using a nanometer for concertation at 260/280 wavelength. In addition, samples were visualized on an agarose gel to confirm RNA presence. 1µl of RNA was treated with

formaldehyde (50% of the sample) at 55ºC for 10 minutes, treated with EtBr, and ran under gel electrophoresis at 90V for 20 minutes and visualized via AlphaImager.

3.5 cDNA synthesis

1µg of total RNA was reverse transcribed using the iScript Reverse Transcription Supermix (Bio-Rad Laboratories, Mississauga, Canada) and PCR protocol for cDNA synthesis (**Table 1**).

Table 1. PCR protocol for cDNA synthesis

5 min	25ºC
30 min	42ºC
5 min	85ºC
∞	4ºC

The quality of the cDNA synthesis was confirmed by PCR amplification using 18s_FP 5'-GAGGTGAAATTCTTGGACCGG-3' and 18s_RP 5'- CGAACCTCCGACTTTCGTTCT-3' primers and visualization of 18s products via gel electrophoresis. 1µl of synthesized cDNA was used to amplify the 18s product via Taq polymerase using an Eppendorf Mastercycler® Nexus (**Table 2**). 5µl of the PCR amplification products were mixed with 1µl of a 5x loading dye and separated on an agarose gel containing EtBr at 90V for 20 minutes. PCR products were images using an AlphaImager and contrasted against a 100bp DNA ladder.

Table 2. PCR amplification protocol for 18s product

15 min	95ºC	
30 sec	94ºC	x 17
30 sec	52ºC	
1 min	72ºC	
10 min	72ºC	
∞	4ºC	

3.6 RT-qPCR

The cDNA equivalent of ~133ng generated as described in Section 3.5 was analyzed by quantitative Real Time-PCR using the SsoAdvanced SybrGreen PCR mix and a Bio-Rad CFX96 real-time PCR system as defined by the manufacturer (Bio-Rad). All experiments represent three independent RNA preparations from TL and Panx1-KO lines; each analyzed in triplicate. Each experiment included a melt curve analysis of PCR amplicons generated in each reaction. Comparing theoretical melting points for each amplicon with experimental melt curves served as a control. Raw cycle threshold values (Ct-values) were exported from the CFX Manager Software (Bio-Rad, Canada). Expression ratios were analyzed against their respective controls using the Relative Expression Software Tool (REST-2009) software (Pfaffl et al., 2002). The statistical significance was tested by a Pair Wise Fixed Reallocation Randomisation Test© and plotted using standard error (SE) estimation. All primers (**Table 3 in Section 4.3.1**) were designed using the Real-Time qPCR Assay design tool and were synthesized by the same provider (Integrated DNA Technologies, Toronto, Canada)

3.7 *In vivo* two electrode local field potential electrophysiology

Individual TL and Panx1a-KO larvae (6dpf) were anesthetized with 300µM Pancuronium Bromide (Panc) for 5 minutes or until larvae showed no signs of movement while blood circulation remained robust (**Figure 6**). Each larva was positioned dorsally and immobilized on the experimental stage with 2% noble agar. The stage was placed under a customized Olympus BX 61 upright microscope with a 10x objective. Each larva was checked for viability using heartbeat and blood circulation as indicators. Reference electrodes (2.5-3MΩ resistance) were attached to the glass bottom of the stage with 2% noble agar, and 1ml of E3 medium was topically added to ensure larva survival. The position of the reference electrodes that yielded the largest signal to noise ratio was identified and maintained throughout experiments.

The HC Image Live software was used to visualize larva. An Axon Instruments MultiClamp 700B for amplifying the electrical single and a Digidata 1550A digitizer to reduce background noise were used (both Molecular Devices). The recording electrodes were attached to headstages (MultiClamp 700B Headstage CV-7B) mounted to individual Luigs & Neumann LN Mini 25 micromanipulators controlled by an SM10 remote control unit (Luigs & Neumann). Glass capillaries (1.2mm outer diameter, approximately 1µm tip diameter) were backfilled with 2M NaCl solution. The capillaries were lowered into the E3 medium on top of the fixed larva and reference wire. A check for stable signal and appropriate resistance (2-7MΩ) followed. Once a steady signal of < 0.05mV was established, the setup was ready for insertion of the capillaries into selected brain regions. The insertion of the electrodes was typically completed within 5 min, followed by recording immediately.

3.7.1 Local field potential (LFP) recording in awake larvae

Capillaries were inserted into the right optic tectum (electrode #1) along with either the right dorsomedial (DM) or the right dorsolateral (DL) region of a larvae's telencephalon (forebrain). Local field potentials were recorded in Current-Mode. Recordings were low-pass filtered at 1kHz (-3 dB; eight-pole Bessel), high-pass filtered at 0.1 Hz, digitized at 20kHz, and stored on a PC running pClamp11 software (Axon Instruments). Activities were normalized to baseline activities of each fish to account for the biological variability of individual brains.

Larvae were exposed to either Light-OFF (0 lux) or Light-ON (1000 lux) stimuli for at least five minutes before recording. Baseline activities were recorded for a minimum of three minutes. Images of larvae's heads were taken to document the placement of the electrodes. Drug treatments were applied directly to the larva after baseline recordings. Drugs were applied topically to the larva using published concentrations for PROB (20µM) (Silverman et al., 2008a), bicuculline (BCC) (100µM) (Connaughton et al., 2008), and MK-801 (20µM) (Sison & Gerlai, 2011) (**Figure 6**). Drugs were allowed to incubate with the larva for 30 minutes. The MPTP treatment (50µM) was applied for four hours in the dark at 28ºC. The LFP signal was recorded post-treatment for three minutes after applying the Light-OFF/ON stimuli for a minimum of five minutes.

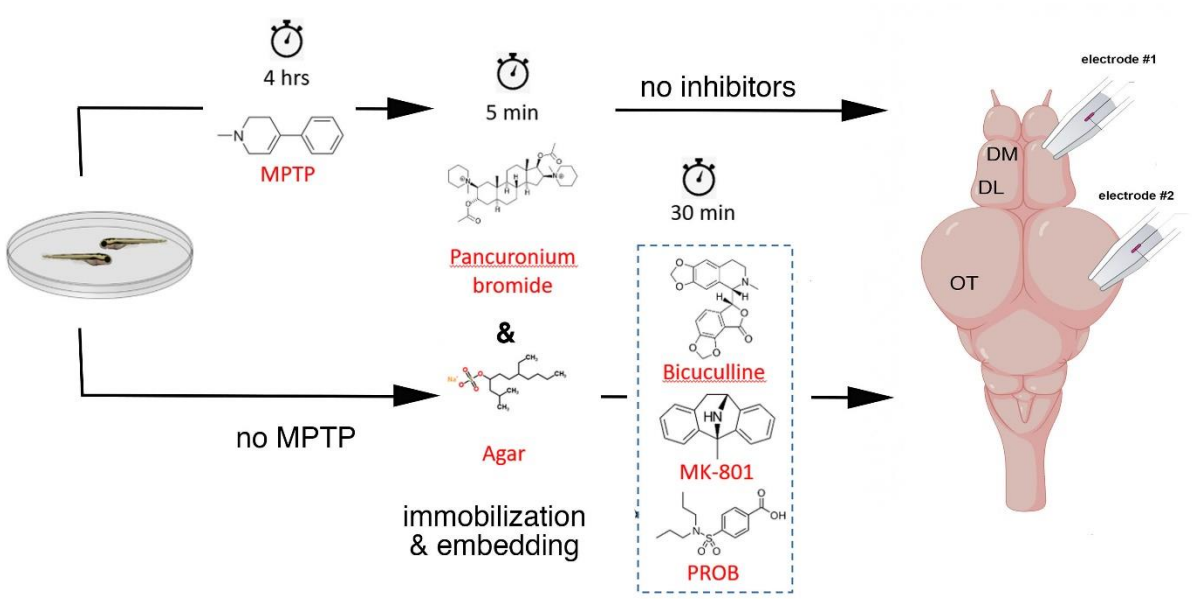

Figure 6. *In vivo* electrophysiology setup. The larva either underwent a four-hour MPTP incubation or no MPTP treatment. After MPTP treatment, the larva was immobilized with pancuronium bromide and embedded with agar. Then the dual local field potential recordings were performed. When no MPTP pre-treatment was done, the larvae were immobilized and fixated immediately. Baseline recordings were conducted from the larvae before a 30-minute incubation with bicuculline, MK-801, or PROB. After drug treatment, another set of recordings was performed from the same larva. (Image generated with BioRender.com).

3.7.2 Post-recording processing of raw LFP data

Raw data were pre-processed using pCLAMP Clampfit 11 (Axon Instruments) and exported to NeuroExplorer 5.0 software (Plexon). A Welsh periodogram method was used to split the data into frequency bins. The raw data files' coherence and power spectral density (PSD) were extracted and exported to Graphpad PRISM 9 for statistical analysis (Whyte-Fagundes et al., 2022). A two-way ANOVA with Tukey's multiple comparison test was applied for the coherence analysis. Based on statistical requirements, the PSD data were analyzed using a paired t-test (BCC, MK-801, and PROB) or a Welch’s t-test (MPTP).

The coherence analysis uses the two variables, X (reference) and Y (target) (Kattla & Lowery, 2010). Fast Fourier transforms of the data segments (after pre-processing) were calculated. Then, individual and cross-densities were calculated:

Equation 1. Individual and cross-densities in coherence analysis

$$\mathrm{Pxx} = \mathrm{FFT(X)} * \mathrm{Conj}\big(\mathrm{FFT(X)}\big),$$

$$\mathrm{Pyy} = \mathrm{FFT(Y)} * \mathrm{Conj}\big(\mathrm{FFT(Y)}\big)$$

$$\mathrm{Pxy} = \mathrm{FFT(X)} * \mathrm{Conj(FFT(Y))}.$$

Here Conj(z) was a complex conjugate of z. Pxx, Pyy, and Pxy values were averaged across all intervals, and coherence values were calculated as:

Equation 2. The equation to calculate coherence

$$\mathrm{Mean(Pxy)} * \mathrm{Mean(Pxy)} \,/\, (\mathrm{Mean(Pxx)} * \mathrm{Mean(Pyy)}).$$

3.8 Behavioral locomotor assay of inflammasome inhibitors

The ZebraBox behavior system and the ZebraLab™ analytical suite were used for automated observation, and video tracking of the locomotor activity of 6dpf zebrafish larvae in clear 48-well plates maintained at 28ºC (ViewPoint Life Technology, Lyon, France). TL and Panx1a-KO larvae (n=16 per group) were treated with drugs alone or in combination with MPTP before recording. The treatment conditions were adenosine (0.1µM), adenosine with MPTP (0.1µM + 10µM), caffeine (100µM), caffeine with MPTP (100µM + 10µM), CY-09 (1µM), CY-09 with MPTP (1µM + 10µM), dexamethasone (1µM), dexamethasone with MPTP (1µM + 10µM), INF39 (1µM and 10µM), INF39 with MPTP (1µM + 10µM and 10µM + 10µM),

MCC950 (1µM), MCC950 with MPTP (1µM + 10µM), and metformin (10µM), metformin with MPTP (10µM + 10µM). Concentrations were chosen based on previous reports (Coll et al., 2015; Cruz et al., 2017; Kamstra et al., 2022; S. Luo et al., 2016; Safarian, 2021; Sandall et al., 2020). The drugs were incubated alone or together with MPTP for four hours. All drugs were dissolved in regular 3M medium. After the incubation period, individual larvae were placed into 48-well plates in the same medium. ZebraLab™ software tracked locomotor activity, and behavioral outputs were automatically generated. After principal component analysis, the behavioral variable "totaldistance" was chosen to examine the larvae's locomotor behavior.

3.8.1 Visual-Motor Response assay

Responsiveness of larvae to changes in light intensity is traditionally measured by the Visual-Motor Response assay (Emran et al., 2008). Typically, the VMR tests focus on the startle response followed by a freeze when switching between Light-OFF/ON conditions. To avoid confounding the behavioral data by the startle response, a light-ramp assay, a variation of the visual-motor response test, was used. Here, individual larvae were placed into wells in a 48-well plate filled with 3M medium. Next, the larvae were moved into the dark (0% light), soundproof ZebraBox chamber for acclimation at 28^{o}C. The larvae were video recorded while returning to a baseline activity level in the dark over 20 minutes. At the 20-minute mark, the light was switched ON to 10% (400 lux) and gradually increased every ten minutes until a final Light-ON stimulus of 40% (1600 lux) was reached.

3.8.2 Statistical analysis of behavioral data

The behavioral data from the ZebraLab™ was exported to Excel and sorted. The data from the "totaldistance" parameter was graphed along with the SEM using Graphpad. For statistical analysis, the total distance moved in the Light-ON condition from 2100-2300 seconds was compared. Between 2100-2300 seconds, larvae are exposed to 800 lux, which is a light intensity evoking consistent swimming activity. The data sets were compared using Welch's t-test along with an estimation plot to determine significance (95% CI).

3.9 Statistics and reproducibility

Statistical analyses were performed in GraphPad Prism 9. A minimum of $N \geq 3$ independent experimental replicates for each analysis were generated. A P-value <0.05 was considered statistically significant, except for the RNA-seq analysis, which had a cut-off P-value of <0.01 applied. A minimum number of n=4 was used for electrophysiological experiments with living animals. For behavioral experiments, a minimum number of n=16 was used. The figure legends indicate all experiments' sample sizes, statistical tests, and P-values. Further statistical details are disclosed in **Supplementary Tables** in the Appendix. The statistical details were excluded from the main results text to increase readability.

4. Materials

4.1 Solutions and Chemicals

4.1.1 Solutions for larvae handling

Solution	Composition	Source
E3 medium	60ppm of Instant Ocean® Sea Salt mixed in RO water (pH 7.2~7.4)	Instant Ocean®

4.1.2 Solutions for molecular biology

Procedure	Solutions	Source
ATP Assay	PBS, ARL-67156, Halt Protease inhibitor, D-Luciferin, Luciferase, Dithiothreitol, Adenosine 5′-triphosphate, 20X Reaction Buffer	Sigma-Aldrich, ThermoFisher Scientific, Life Technologies
Tissue lysis and RNA extraction	RLT Plus Lysis Buffer, βME, RW1 Wash Buffer, RPE Wash Buffer, 70% Ethanol, RNase-free water	QIAGEN (RNeasy plus mini kit)
RNA/DNA visualization	Formaldehyde, Agar, 1x TAE buffer, EtBr, 100bp DNA Ladder	ThermoFisher Scientific
cDNA synthesis	5x iScript Reaction Mix, iScript Reverse Transcriptase, Nuclease-free water	Bio-Rad
18s product PCR	HotStarTaq DNA Polymerase, 1x PCR Buffer, dNTPs, 10mM 18s FP and RP solution, Nuclease-free water	QIAGEN (HotStar Taq Pol Kit)

RT-qPCR	Ssofast™ EvaGreen® Supermix	Bio-Rad

4.1.3 Solutions for electrophysiology

Procedure	**Solutions**	**Source**
Extracellular solution	2M NaCl	internal

4.2 Reagents applied to larvae

Reagent	**In-text appearance**	**Source**
1,1′-[(2β,3*α*,5*α*,16β,17β)-3,17-bis(Acetyloxy)androstane-2,16-diyl]bis(1-methylpiperidinium) dibromide	Pancuronium bromide (Panc)	Tocris cat#P1918
***p*-(Dipropylsulfamoyl)benzoic acid**	Probenecid (PROB)	Sigma cat#P8761
1-methyl-4-phenyl-1,2,3,6-tetrahydropyridine	MPTP	Sigma cat#M0896
(5*S*)-5-[(6*R*)-6,8-Dihydro-8-oxofuro[3,4-*e*]-1,3-benzodioxol-6-yl]-5,6,7,8-tetrahydro-6,6-dimethyl-1,3-dioxolo[4,5-*g*]isoquinolinium iodide	Bicuculline (BCC)	Sigma cat#14343
(5S,10R)-(+)-5-Methyl-10,11-dihydro-5H-dibenzo[a,d] cyclohepten-5,10-imine hydrogen maleate	MK-801	Sigma cat#475878
1,3,7-Trimethylxanthine,	Caffeine	Sigma cat#C0750
9-β-D-Ribofuranosyladenine	Adenosine	Sigma cat#A9251

4-[[4-Oxo-2-thioxo-3-[[3-(trifluoromethyl)phenyl]methyl]-5-thiazolidinylidene]methyl] benzoic acid	CY-09	Sigma cat#SML2465
(11β,16α)-9-Fluoro-11,17,21-trihydroxy-16-methylpregna-1,4-diene-3,20-dione	Dexamethasone	Sigma cat#D4902
Ethyl 2-(2-chlorobenzyl)acrylate	INF-39	Sigma cat#SML2239
MCC950	MCC950	Sigma cat# 5381200001
1,1-Dimethylbiguanide hydrochloride	Metformin	Sigma cat#53183

4.3 Oligonucleotides

4.3.1 Primers for RT-qPCR

Gene sequences were retrieved from NCBI (https://www.ncbi.nlm.nih.gov/nucleotide/) via their accession number. Forward and reverse primer pairs were designed using the IDT software Real-Time qPCR tool (https://www.idtdna.com/scitools/Applications/RealTimePCR/). Primers were purchased from IDT. Each primer pair was confirmed for length, Guanine/Cytosine (GC) content, melting temperature, lack of complementary regions, and location in SnapGene software (https://www.snapgene.com/). Only primer pairs which generated amplicons spanning at least one intron were selected.

Table 3. Summary of primers used for RT-qPCR

Gene Name	Gene Accession Number	Forward Primer (5'-3')	Reverse Primer (5'-3')
ATP5pf	NM_213307	AACTGCAGCGTCTGTATGG	CTCGCGGTCGATGTAAATGA

CFTR	NM_001044883	AGTCAAATACACAGAAGCGGG	TCGCCATCAGTATAAACCAGC
COX4i1	NM_214701	CGGAGACGCTAGAATGTTGG	CGGTCAAAGTATGCAGGGAG
EEF2K	NM_001002740	AAGAACCTCGCTCATAACCAG	CGCTCAGTCTCCATTTCCTC
Ndufa10	NM_199578	TCCCAGCTTTATCCCAGAAATC	GTACCTCACTTCAGCCAGATG
PCK1	NM_214751	GCTGGAAGGTGGAGTGTG	GTTGGTTTTGCTGGAGGTTC
PFKFB3	NM_213397	CCTACTCGCCTATTTCCTTGAC	TTCACTGCCTCCACATTCAG
Uqcrq	NM_001002495	TTGTGGAGGCGATTTAGGTC	GTCATTCTCGAAGTCAGCGG
caspa3	NM_131877	GTTGGAGATGAACGGAGACTG	TGAAGGCATGGGATTGAGG
caspa7	NM_001020607	AAACCTGACCCAAAAGCAATG	AGCCTAAATCTCCCTTTGCG
caspa9	NM_001007404	GTCTTCACTCAGGACATGATCG	ACGCAGGGAATCAAGAAAGG
caspa1	NM_131505	GAGGATCACATCGAGGAACTG	TTTCTTGGCTATCAGAGTCCG
IL-1b	NM_212844	GTTCAGATCCGCTTGCAATG	TGCTTCATTCTGTTCAGGGC
pan-IL16	XM_021477711	AGCGAAGTTAATGGTACAGCC	ATTGCCTCCCGATGAAGCAG
nlrp3	MN088121	GCTGTTACTGGGAGACTGAATGG	GTTTCCAAGCATGCACCTGC
pycard	NM_131495	GCAGTAGCAGATGATCTATTGAGG	CTATCAATTCTTTCCAGTGCTCATCG
Gasdermin E	NM_001001947	ACTCTTCCTGCTCAAATCCTG	ATCGGCTAAAACATCCAGAGC
18s	NR_145818	GAGGTGAAATTCTTGGACCGG	CGAACCTCCGACTTTCGTTCT

4.4 Molecular biology reagents

Procedure	**Kit**
Tissue lysis and RNA extraction	QIAGEN QIAcube RNeasy Plus Mini Kit
cDNA synthesis	Bio-Rad iScript cDNA Synthesis Kit 170-8890
RNA and 18s cDNA visualization	Qiagen HotStar Taq Pol Kit
RT-qPCR	Ssofast™ EvaGreen® Supermix

ATP determination	Molecular Probes® ATP Determination Kit

4.5 Equipment

4.5.1 Equipment for behavioral analysis

Procedure	Equipment	Source
Locomotor activity retrieval; automatically generated outputs and videos	ZebraBox	ViewPoint Behavior Technology, Lyon, France
Incubation of larvae at 28ºC before insertion into ZebraBox	Exo Terra Incubator	Exo Terra, Montreal, Canada

4.5.2 Equipment for ATP assay

Procedure	Equipment	Source
Tissue lysis	TissueLyser LT Adapter, 12-tube	QIAGEN
ATP quantification	Synergy H4 Hybrid Multi-well Plate Reader	Biotek

4.5.3 Equipment for molecular RT-qPCR

Procedure	Equipment	Source
Tissue lysis	TissueLyser LT Adapter, 12-tube	QIAGEN
	Sorvall™ Legend™ Micro 21R Microcentrifuge	Thermo Scientific

RNA extraction	QIAcube	QIAGEN
cDNA PCR	Mastercycler® nexus	Eppendorf, Canada
RNA and cDNA visualization	Nanodrop 2000 Photospectrometer	Thermo Scientific
	Mini-Sub Cell GT System	Bio-Rad
	AlphaImager™ HP System	Alpha Innotech
RT-qPCR	CFX96™ Real-Time PCR Detection System	Bio-Rad

4.5.4 Equipment for electrophysiology

Procedure	**Equipment**	**Source**
Larvae storage	10-140 Analog Incubator	Quincy Lab
Capillary preparation	P-30 Vertical Micropipette Puller	Sutter Instrument
Agar preparation	VWR Analogue Heat Block	VWR Scientific
Embedding of larva	Light Microscope (CKX41)	Olympus
Wire soldering	Weller WES51	Apex Tool Group
Stage and electrode manipulation	Research Control Unit SM7	Luigs & Neumann
Electrode holder	CV-7B Current Clamp and Voltage Clamp Headstage	Axon Instruments
Light/Fluorescence source	Lumen 200 Fluorescence Illumination System	Prior Scientific
Imaging	Femto2D Microscope	Femtonics
LFP signal acquisition	Digidata® 1550A Digitizer	Molecular Devices
LFP signal amplifier	MultiClamp 700B Microelectrode Amplifier	Molecular Devices

4.6 Software

4.6.1 Software for ATP assay

Purpose	Software
Fluorescence Assay	ZEN 2010 (Carl Zeiss Microscopy)
Luminescence Assay	Gen5 Data Analysis Software (BioTek)
Protein Concentration	Nanodrop2000 a280

4.6.2 Software for RT-qPCR

Purpose	Software
Gene sequence retrieval	NCBI – nucleotide
Primer Design	IDT - RealTime qPCR tool
Primer location	SnapGene Viewer 5.3.2
RT-qPCR data acquisition	CFX Manager software™
Relative expression analysis	REST 2009©

4.6.3 Software for RNA-seq

Purpose	Software
Pre-processing of padjusted values (<0.05)	Excel (2016)
Analysis of regulated biological processes	Gene Ontology (GO) Enrichment Analysis
Protein-Protein Interaction Networks Functional Enrichment Analysis	STRING

4.6.4 Software for electrophysiology

Purpose	Software
Recording and visualization of LFP signals	pCLAMP Clampex 11.1
LFP signal amplification	MultiClamp Commander
Microscope control	Olympus BX61 powered by MATLAB®

Larva monitoring and image generation	HCImage Live
Visualization and analysis of LFP signals	pCLAMP Clampfit 11.1
Analysis of the LFP signal	NeuroExplorer ® 5.022
Statistical analysis and figure generation	GraphPad Prism 9.3.1

4.6.5 Software for behavioral assay

Purpose	**Software**
Behavioral tracking	ZebraLab (ViewPoint, Life Technology, Lyon, France)
Processing of ZebraLab output	Fast Data Monitor (ViewPoint Biotechnology)
Statistical analysis and figure generation	GraphPad Prism 9.3.1

5. Results

5.1 The molecular effects of MPTP in 6dpf zebrafish larvae

5.1.1 MPTP treatment induces metabolic stress in TL and Panx1a-KO larvae

To understand how loss of Panx1 changes the expression of genes that are regulated by MPTP treatment a molecular level analysis was performed. At the start of this research, the bioinformatics team at SickKids Centre for Applied Genomics (TCAG) provided a refined transcriptome analysis of a previously completed RNA-seq analysis of MPTP treated and untreated zebrafish larvae (6dpf). The new DESeq2 analysis tested for differential expression by negative binomial generalized linear models (Love et al., 2014). This analysis allowed for

internal normalizations and automatic removal of outliers, which resulted in a more representative analysis of the raw sequencing data than the previously used false discovery rate analysis (FDR). The original raw RNA-seq data identified 58165 protein coding RNA transcripts, including splice variants from > 20,000 genes.

Differentially regulated genes after DESeq2 analysis were identified using the padj-value of $P<0.01$ as the cutoff. After the cutoff, 5087 genes were up-regulated in TL, and 5533 genes were down-regulated. In Panx1a-KO, 3083 genes were up-regulated, and 4253 genes were down-regulated. The improvement over a previous analysis with a less stringent FDR cutoff of $P<0.05$ was immediately evident; the GO biological process analysis for both TL and Panx1a-KO larvae after four hours of treatment with MPTP (50µM) showed an enrichment of genes representing mitochondrial and energy metabolism (**Figure 7a,b**). Most up-regulated biological processes in TL and Panx1a-KO larvae were related to roles in ATP-synthesis and oxidative phosphorylation. Other enrichments were associated with the Golgi apparatus, Golgi vesicle-mediated transport, and glycosyl-phosphatidylinositol (GPI) related processes of the endoplasmic reticulum, indicating modulation of posttranscriptional processes. Down-regulated biological processes enriched in the RNA-seq data were related to the circadian clock, translation, and mRNA processing and splicing. We concluded that four hours of MPTP treatment was sufficient to alter the metabolism of larvae by MPTP/MPP+ inhibition of the mitochondrial Complex I. The induced metabolic crisis was reflected by the up-regulation of biological processes compensating for reduced ATP production, and at the same time, energy-intensive transcription and translation processes were reduced.

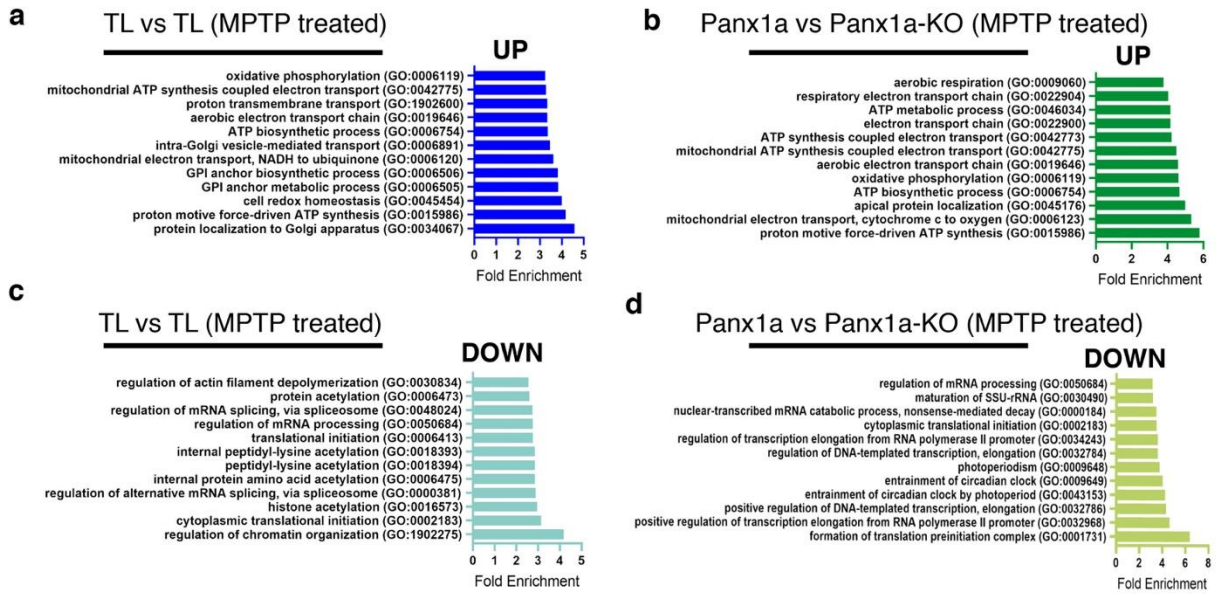

Figure 7. Gene Ontology Analysis. Differentially up-and down-regulated genes with an adjusted P-value (padj-value) of P<0.01 were selected and imported into the Gene Ontology software. Enrichment was determined using Fisher's exact test with the calculation of the false discovery rate (FDR). The top ten enriched GO Biological pathways were exported and graphed. **a,b**) Enrichment of up-regulated genes identified in untreated and MPTP treated TL and Panx1a-KO larvae. **c,d**) Enrichment of down-regulated genes identified in untreated and MPTP treated TL and Panx1a-KO larvae.

5.1.2 MPTP treatment regulates differentially expressed genes associated with disease pathways in TL controls and Panx1a-KO larvae

After the GO biological process analysis, a KEGG pathway analysis was used to search for genes enriched in curated signaling and disease pathways (Kanehisa et al., 2022). The KEGG pathway analysis revealed the regulation of pathways related to metabolism and pathways of neurodegeneration (**Figure 8**). Specifically, genes related to pathways in Parkinson's, Alzheimer's, and Huntington's disease were regulated after MPTP treatment. The regulation of five genes, cytochrome c oxidase subunit 5B (COX5B), mitofusin 1 (MFN1), proteasome 26S subunit ubiquitin receptor, non-ATPase 2 (PSMD2); thioredoxin (TXN), and ubiquitin B (UBB)

stood out as regulated in Parkinson's disease pathways in both TL and Panx1a-KO larvae (**Figure 8b,c**). MPTP treatment also regulated inflammatory and cell death pathways such as MAPK signaling and autophagy. The number of pathways identified in untreated larvae (**Figure 8a**) or when comparing treated TL and Panx1a-KO larvae (**Figure 8d**) was low. Only single genes related to KEGG pathways of Parkinson's disease and metabolic pathways were found. Other regulated pathways were NF-kappa B signaling, MAPK signaling, GABAergic synapses, and metabolic pathways.

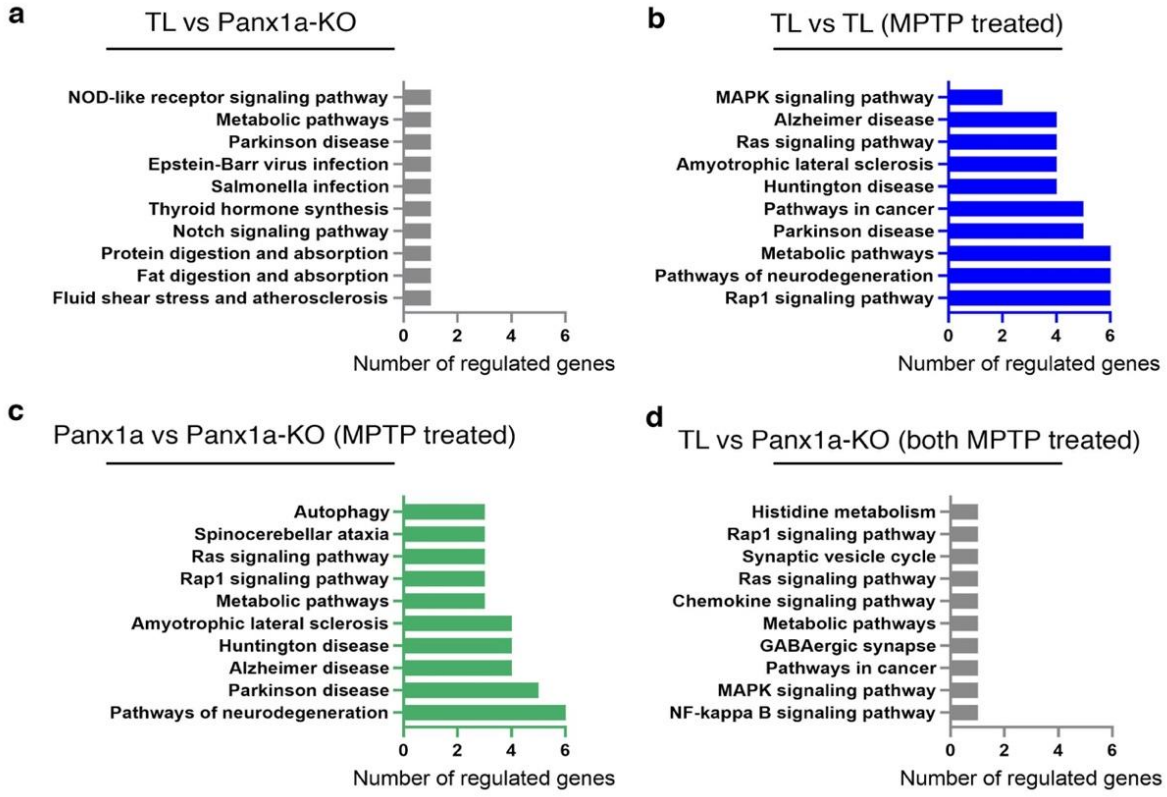

Figure 8. Enriched KEGG pathways before and after MPTP treatment. Regulated genes with a padj-value of P<0.01 were selected and imported into the KEGG Mapper software. The top ten enriched pathways are presented by the number of regulated genes. **a**) The comparison between baseline conditions of TL and Panx1a-KO larvae. **b**) The enriched pathways after MPTP treatment of TL larvae. **c**) The enriched pathways after MPTP treatment of Panx1a-KO larvae. **d**) The differences between TL and Panx1a-KO larvae after MPTP treatment.

5.1.3 STRING analysis revealed inflammatory pathways regulated in the MPTP model

Next, the KEGG Pathway database was used to manually curate a list of 148 mouse and human genes associated with inflammation pathways. Zebrafish orthologs (n=41) of the 148 genes were identified in the RNA-seq data filtered with padjust set to P<0.01. **Figure 9** shows the log2fold expression changes of all 41 genes (**See Supplementary Table S1 for exact values**). The stacked bars indicated that several genes (for example: caspase b, caspb; TGF-beta-activated kinase 1 and MAP3K7-binding protein 2**,** tab2; Inhibitor of nuclear factor kappa B kinase regulatory subunit gamma, ikbkg) responded with a similar up-or down-regulation (see blue/green bars) after MPTP treatment in both genotypes.

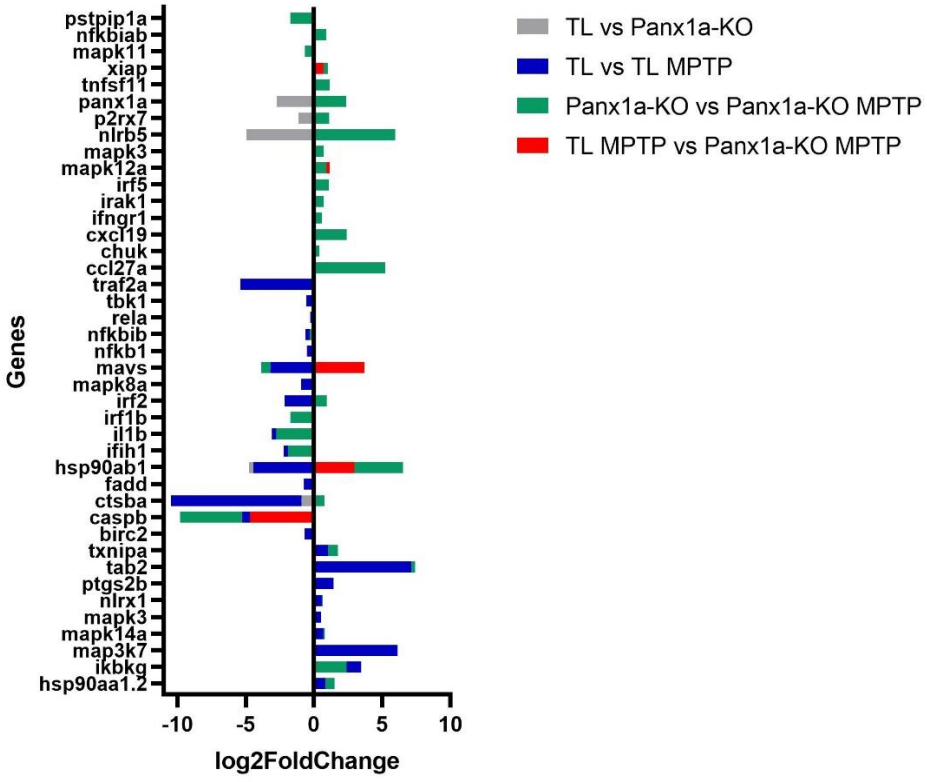

Figure 9. The differential expression of inflammatory genes in the MPTP model. 6dpf TL and Panx1a-KO larvae were treated with MPTP (50μM). The RNA-seq analysis was performed by SickKids (Toronto, ON). The data was analyzed and sorted by extracting genes with an adjusted P value of P<0.01. The log2FoldChange values were graphed using GraphPad Prism.

Regulated inflammatory genes were further analyzed for functional protein association networks using a STRING analysis (Szklarczyk et al., 2019, 2021). The analysis determined three associated clusters related to the NLRP3 inflammasome (**Figure 10**). These clusters represented MAPK, NF-kappa B, and cell death pathways. Taken together, the results of Sections 5.1.1 to 5.1.3 showed that the MPTP/MPP+ model using a four-hour treatment of 6dpf larvae regulated genes and pathways associated with Parkinson's disease and the NLRP3 inflammasome.

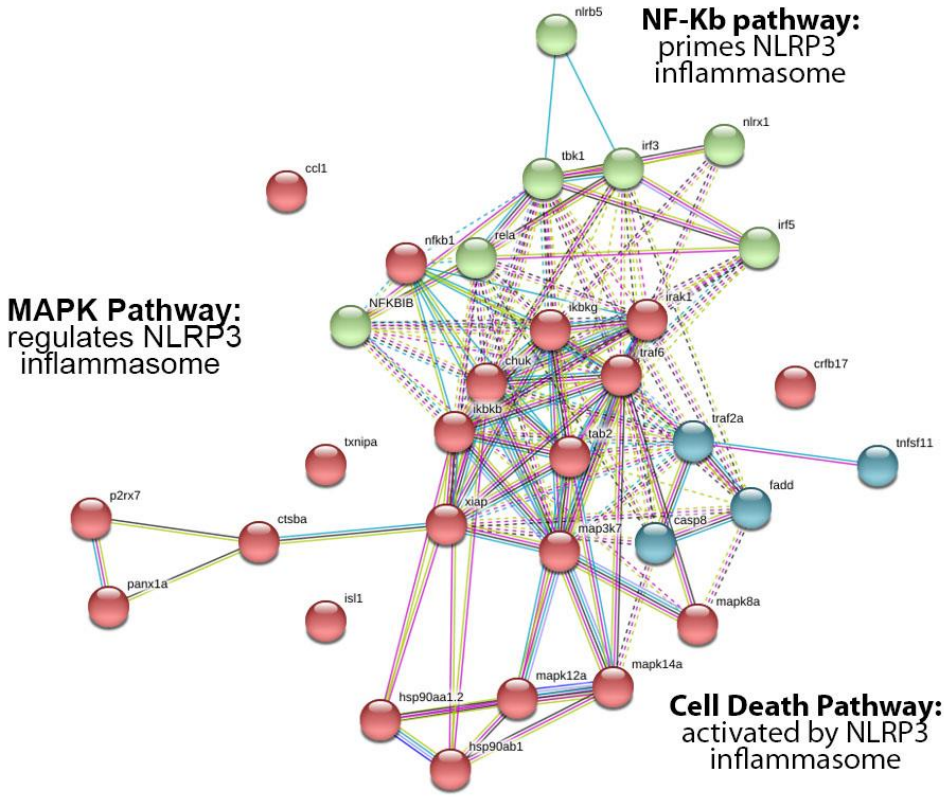

Figure 10. STRING analysis of RNA-seq analysis. Identification of three regulated pathways related to inflammasome activation. Each dot represents a gene that was regulated in the RNA-seq data. The color of the dots represents the pathway to which they belong with MAPK (red), NF-kappa B (green), and general cell death pathways (blue). Lines between the dots represent proteins that interact with one another *in vivo*.

5.1.4 RT-qPCR reveals an up-regulation of inflammasome genes

RT-qPCR was used as an independent method to investigate the regulation of inflammasome genes after MPTP treatment**.** Primer pairs spanning at least one intron were selected to test the expression regulation of 17 genes after treatment with 50µM MPTP in both TL and Panx1a-KO larvae (**Figure 11**). The concentration was chosen since it was previously identified as MPTP's effective upper concentration limit in behavioral experiments.

The treatment with 50µM MPTP in TL caused significant up-regulation of Uqcrq (1.98 fold), CFTR (3.16 fold), and PFKFB3 (2.10 fold) and a down-regulation of Gasdermin E (GSDME) (0.59 fold) (**Statistical information see Supplementary Table S2, 3 in the Appendix**). When Panx1a-KO larvae were treated with 50µM MPTP ATP5pf (1.49 fold), Uqcrq (1.41 fold), CFTR (5.79 fold), EEF2K (1.38 fold), PCK1 (2.71 fold) and PFKFB3 (1.79 fold) were significantly up-regulated. NLRP3 was significantly down-regulated (0.57 fold) in Panx1a-KO larvae. The general trend of MPTP treatment was an up-regulation of inflammatory genes. TL larvae had three genes significantly up-regulated, whereas Panx1a-KO had seven genes up-regulated. Interestingly, core components of the NLRP3 inflammasome (GSDME, NLRP3) were downregulated.

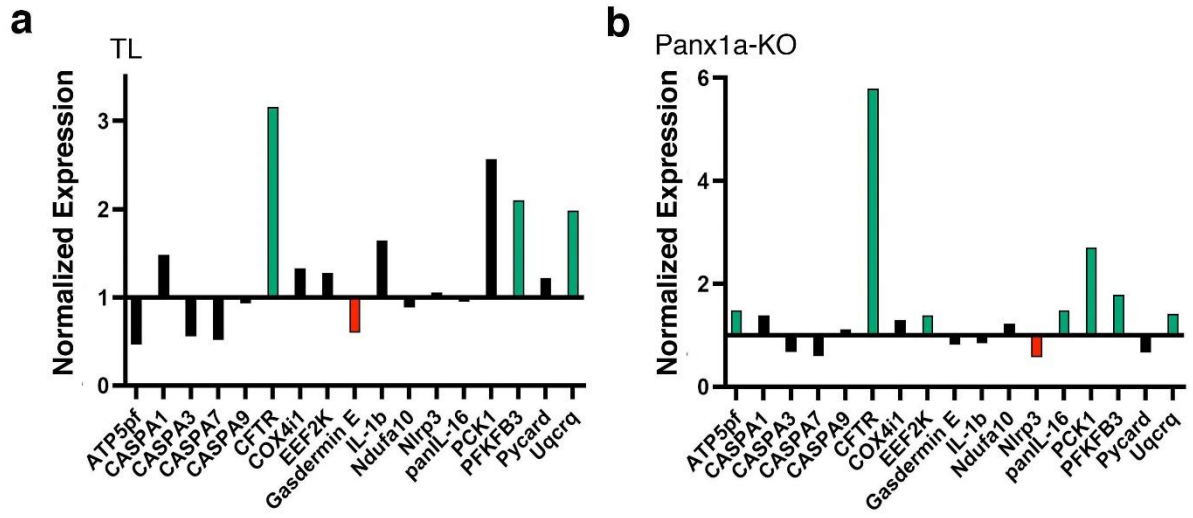

Figure 11. The differential expression of NLRP3 inflammasome genes in TL and Panx1a-KO larvae determined via RT-qPCR. Seventeen genes were selected from the KEGG NOD-like receptor signaling (NLRP3) pathway. **a**) The regulation of genes in TL larvae after 50μM MPTP treatment. The normalized expression is graphed on the left, with gene expression normalized around 1. **b**) The regulation of genes in Panx1a-KO larvae after 50μM MPTP treatment. The normalized expression is graphed on the left, with gene expression normalized to 1 (no change).

5.1.5 MPTP treatment caused a significant decrease of extracellular ATP in TL but not Panx1a-KO larvae

Panx1a channels release ATP, and researchers in the lab recently demonstrated that extracellular ATP was significantly reduced in Panx1a-KO larvae in an experimental model of epilepsy (Whyte-Fagundes et al., 2022). Here, extracellular ATP levels were tested before and after MPTP treatment to confirm the hypothesis that the MPTP/MPP+-induced mitochondrial and energy metabolism crisis translated to low extracellular ATP levels. When the free extracellular ATP concentration was determined in both 6dpf TL and Panx1a-KO larvae before and after MPTP treatment, a baseline ATP concentration of 2.71 nM/μg protein was detected in TL larvae (**Figure 12; Statistical information see Supplementary Table S4 in the Appendix**). The extracellular ATP concentration of TL larvae fell to 0.96 nM/μg protein after treatment with

10µM MPTP. The ATP concentrations of Panx1a-KO larvae pre-treatment (1.06 nM/µg protein) and post-MPTP treatment (0.95 nM/µg protein) were very similar to TL treated with MPTP. This result demonstrated that the Panx1a release of ATP is impaired by MPTP treatment and reduced to very low levels like those found after the loss of Panx1a channel function.

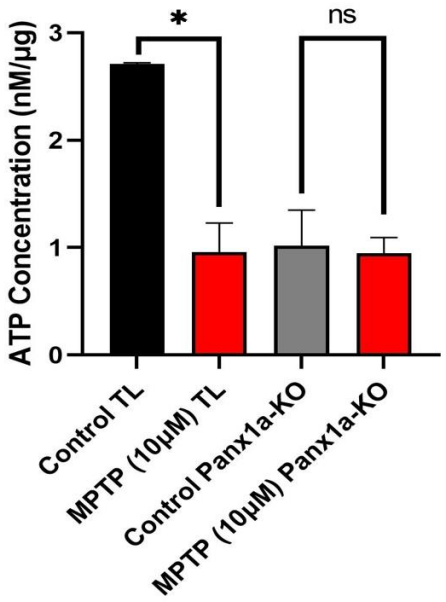

Figure 12. The free extracellular ATP in both TL and Panx1a-KO larvae before and after treatment with MPTP. Free extracellular ATP was extracted from six-day post fertilization larvae. Using a standard firefly luciferase assay, ATP was detected in the nanomolar range (nM) in the supernatants of homogenized larval tissue. ATP concentrations were normalized to protein concentrations (µg) to account for the larvae' bodyweight variability. Tissue samples were prepared from 50x 6dpf larvae. Each data point represents three experimental replicates. Statistics: Welch's t-test: P-values; * (<0.05) and ns (non-significant).

5.2 *In-vivo* electrophysiology of awake zebrafish larvae

5.2.1 The beta- and gamma-frequency bands in local field potential recordings of the zebrafish brain

To understand the effects of loss of Panx1a as well as MPTP treatment on the connectivity of the ascending visual pathway, LFP recordings were conducted. Previous studies

from our lab have shown prominent activity peaks of the gamma-band in awake zebrafish LFP recordings (Safarian et al., 2020). Here, the rationale for analyzing the gamma- and beta-bands was based on reports implicating changes of both bands in other models of Parkinson's disease and human patients (Jackson et al., 2019; Swann et al., 2016). The PSD analysis of raw data determined power distribution into frequency components composing that signal. In both TL and Panx1a-KO larvae, a prominent peak around 40Hz in the gamma-band range was detected (**Figure 13**). The beta-band did not show major peaks, but smaller peaks at the 12Hz and 30Hz ends of the beta-band.

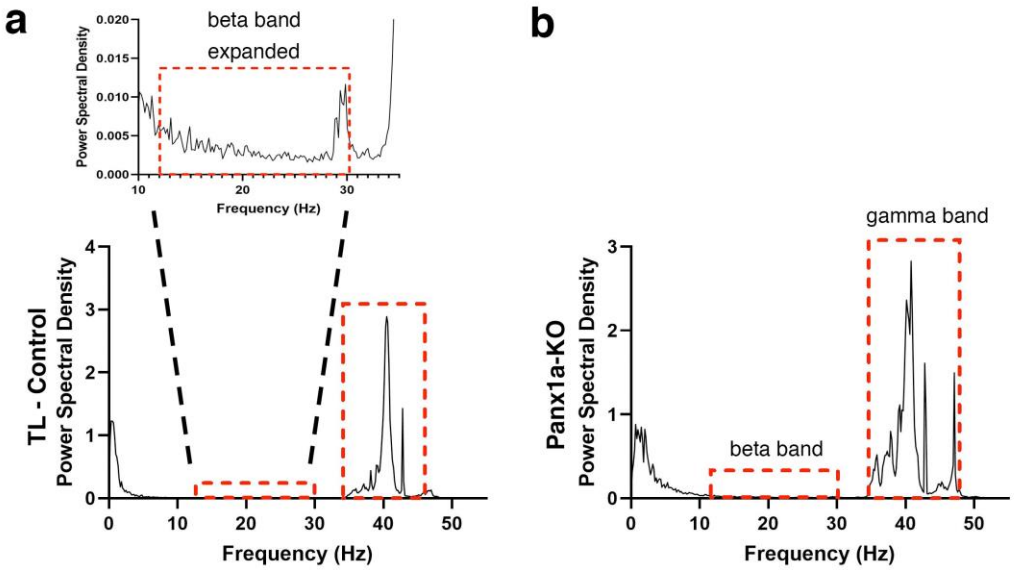

Figure 13. Examples of the power spectral density analysis for TL and Panx1a-KO larvae. A bandpass filter extracted traces ranging from 0 to 55 hertz (Hz) from raw data, collecting continuous signals ranging up to 20 kilohertz (kHz). Baseline PSDs represent **a**) untreated TL and **b**) Panx1a-KO zebrafish. The boxed areas represent the frequency ranges selected for data analysis.

5.2.2 Baseline activities in the ascending visual pathway showed no response to light changes but distinct power spectral density peaks

Initial studies determined the responses of three brain regions, DM, DL, and OT, to Light-ON (1000 lux) and Light-OFF (0 lux) conditions. In the gamma-band range (35-45 Hz), overlapping power spectral densities were detected in TL and Panx1a-KO larvae in both Light-ON and Light-OFF conditions **(Figure 14a-d).** No significant differences were detected in the maximum power of the gamma band in all regions of TL and Panx1a-KO larvae (**Figure 14e,f**). However, in both genotypes, a shift of the maximum peak PSD power spike was observed **(Figure 14g,h)**, with the spike maximum (MAX) detected in DM and DL regions in the 38-39Hz range and the OT spike at around 41Hz. The Light-ON/OFF stimuli did not affect the shift to a higher gamma band frequency in the OT. We speculated that the shift in the PSD peak reflected intrinsic properties of the brain region we had recorded from.

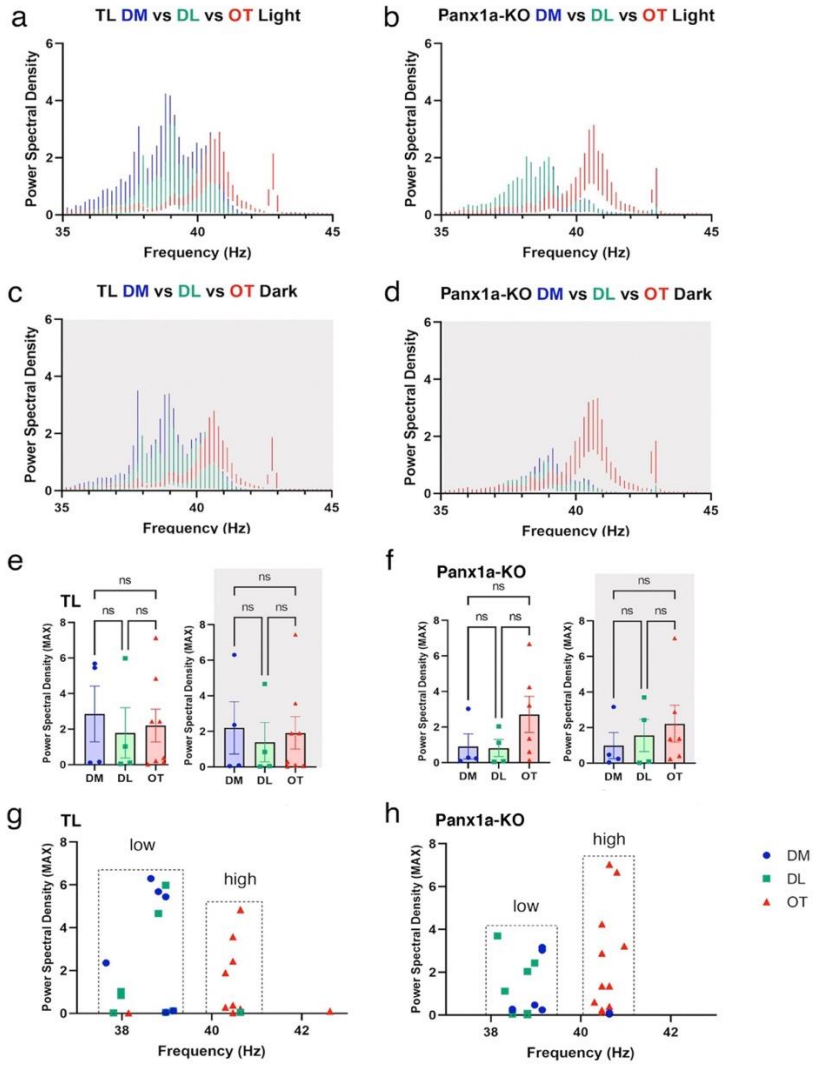

Figure 14. Baseline activities of the brain regions DM, DL, and OT region in the 6dpf zebrafish larvae.

a-d) The power spectrum of the PSD analysis of the gamma-band (35-45 Hz). The PSDs were color coded for DM (blue), DL (green), and OT (red). The data were binned using the Welch periodogram method. Each bar represents the average PSD across four individual larvae ± SEM at that frequency.

e-f) The maximum power of the PSD analysis was determined from the gamma-band quantification and plotted for each TL and Panx1a-KO larva in Light-ON (white background) and Light-OFF (grey background) conditions. No significant differences were observed between the peak power (MAX) of the three regions tested.

g-h) The maximum power of DM (blue), DL (green), and OT (red) at their respective frequency. A distinct shift can be seen in the boxed areas between the frequencies of DM/DL and OT in both the TL and Panx1a-KO. The OT peak was shifted by ≈ two hertz (low to high).

In a-h) PSD units are in Nanoampere/Hertz

Statistics: A Kruskal-Wallis test was used to calculate significance. NS means no significant differences were found (P-value = >0.05). n = 4 for TL DM and DL, n = 8 for TL OT, n = 4 for Panx1a-KO DM and DL, and n = 4 for Panx1a-KO OT.

5.2.3 Beta-band activities in TL and Panx1a-KOs showed complex responses to pharmacological blocking of NMDA- and $GABA_A$-receptors, Panx1 channels, and MPTP treatment

Pharmacological treatments were used to investigate how the loss of Panx1a function affected the activities of the three regions, OT, DM, and DL. PROB is a blocker of Panx1 channels (Silverman et al., 2008b). The $GABA_A$ receptor antagonist BCC and the NMDA receptor blocker MK-801 were selected to block GABAergic inhibitory and the NMDAR mediated component of glutamatergic excitatory transmission (Johnston, 2013; Song et al., 2018). MPTP is a prodrug, which, when converted to the neurotoxin MPP^+ causes permanent symptoms of Parkinson's disease by destroying dopaminergic neurons. **Figure 15** outlines how PROB, BCC, and MK-801 were expected to affect neuronal networks' excitation – inhibition balance.

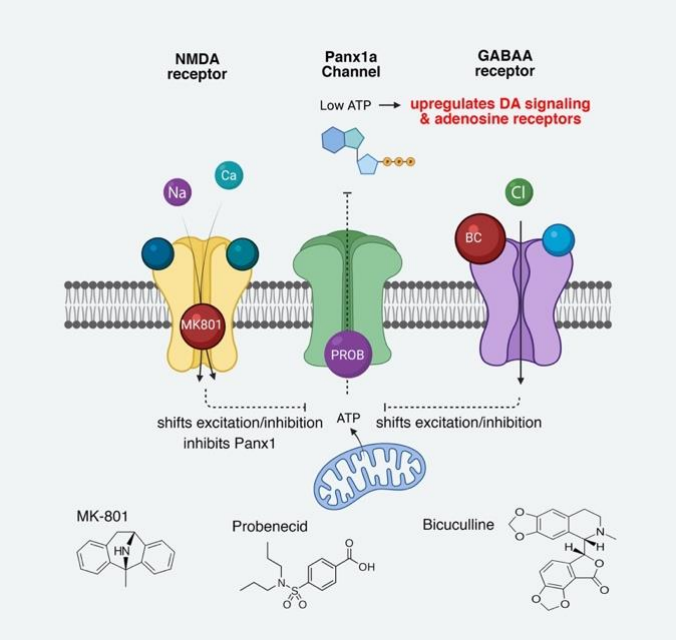

Figure 15. Overview of the predicted actions caused by interventions with selected drugs. Three types of drugs were tested. Probenecid blocks Panx1a channels. The inhibition of Panx1a channels blocks the release of ATP into the synaptic cleft, causing reduced levels of ATP in the extracellular space. The reduction of ATP is known to up-regulate D2 dopaminergic receptors and adenosine receptors (Safarian et al., 2020). Bicuculline acts on $GABA_A$ receptors, causing an inhibition of the movement of chloride through the channel. MK-801 is an uncompetitive antagonist of the N-Methyl-D-aspartate receptor (NMDAR). The inhibition of $GABA_A$ and NMDA receptors was expected to shift neurons' excitation/inhibition balance. The blockage of $GABA_A$ reduces the receptors frequency of opening, shifting the balance to increased excitation. The blockage of NMDA receptors causes a shift to more inhibition. (Image generated with BioRender.com)

Here, we focused first on the PSD analysis of the beta-band. In the three regions, OT, DM, and DL, the peak power of the beta-band (range 12 to 30 Hz) were unaffected by PROB and light in TL **(Figure 16; Statistical information see Supplementary Tables S5-8 in the Appendix)**.

BCC caused a significant decrease in the OT and DL of Panx1a-KO larvae in both the Light-ON and Light-OFF conditions ($P< 0.05, 0.01, 0.01$, and 0.01). BCC treatment of TL larvae did not cause significant changes in peak power.

MK-801 treatment caused a significant decrease in peak power of the beta band of Panx1a-KO larvae's OT region in both Light-ON and OFF conditions ($P < 0.02$ and 0.02). In TL larvae, MK-801 treatment caused a significant decrease in peak power of the DM region in the Light-ON condition only ($P < 0.05$).

MPTP was the only drug causing a significant increase in the peak power of Panx1a-KO larvae in the OT region ($P < 0.04$ and 0.04). The beta band peak power from other regions of the Panx1a-KO larvae and all regions of the TL larvae tested were not significantly affected by MPTP treatment.

Next, an Average Power analysis was used as a second method to compare beta-band power before and after drug treatment. Estimation plots (**Figure 17A-D**) present the magnitude of the drug effects, along with a visual representation of its precision (95% confidence interval (C.I.)). When Panx1 channels were blocked by PROB treatment, the DM region of TL larvae showed a significant increase in overall beta-band power, whereas both OT and DL regions had an opposite, significant decrease in average beta power (**Figure 17A; Statistical information see Supplementary Tables S13-16 in the Appendix**). In Panx1a-KO larvae, the PROB treatment caused an increase in the average beta-band power across all three regions tested.

The general trend observed in the average beta band power of TL larvae after BCC treatment was a decrease in the OT, DM, and DL in Light-OFF conditions, whereas beta-band power increased in the OT and DM in the Light-ON condition (**Figure 17B**). The Panx1a-KO larvae have lost the response to Light-ON. A significant decrease in average beta-band power was detected across OT, DM, and DL in both Light-ON and Light-OFF stimuli.

The TL larvae's beta band was significantly affected by the MK-801 treatment. In the OT region, MK-801 treatment caused a significant increase in the average beta-band power, while in both the DM and DL regions, a significant decrease in average beta power was observed (**Figure 17C**). In the Panx1a-KO, the general trend was a decreased average beta-band power for all regions.

The MPTP treatment significantly affected the beta-band in both TL and Panx1a-KO larvae. The OT of TL larvae showed a significant decrease in the average power of the beta-band (**Figure 17D**). The DM and DL regions showed a significant increase in beta-band power. In the Panx1a-KO larvae, MPTP treatment caused a significant increase in average beta-band power in OT and DL in Light-OFF conditions and during Light-ON conditions in the DM. In the Light-OFF condition, the DM region had a significant decrease in the average beta power. Taken together, the analysis showed complex responses to the different drugs and light stimuli used, and that the loss of Panx1a led to an increase in average and peak beta-band power after MPTP treatment.

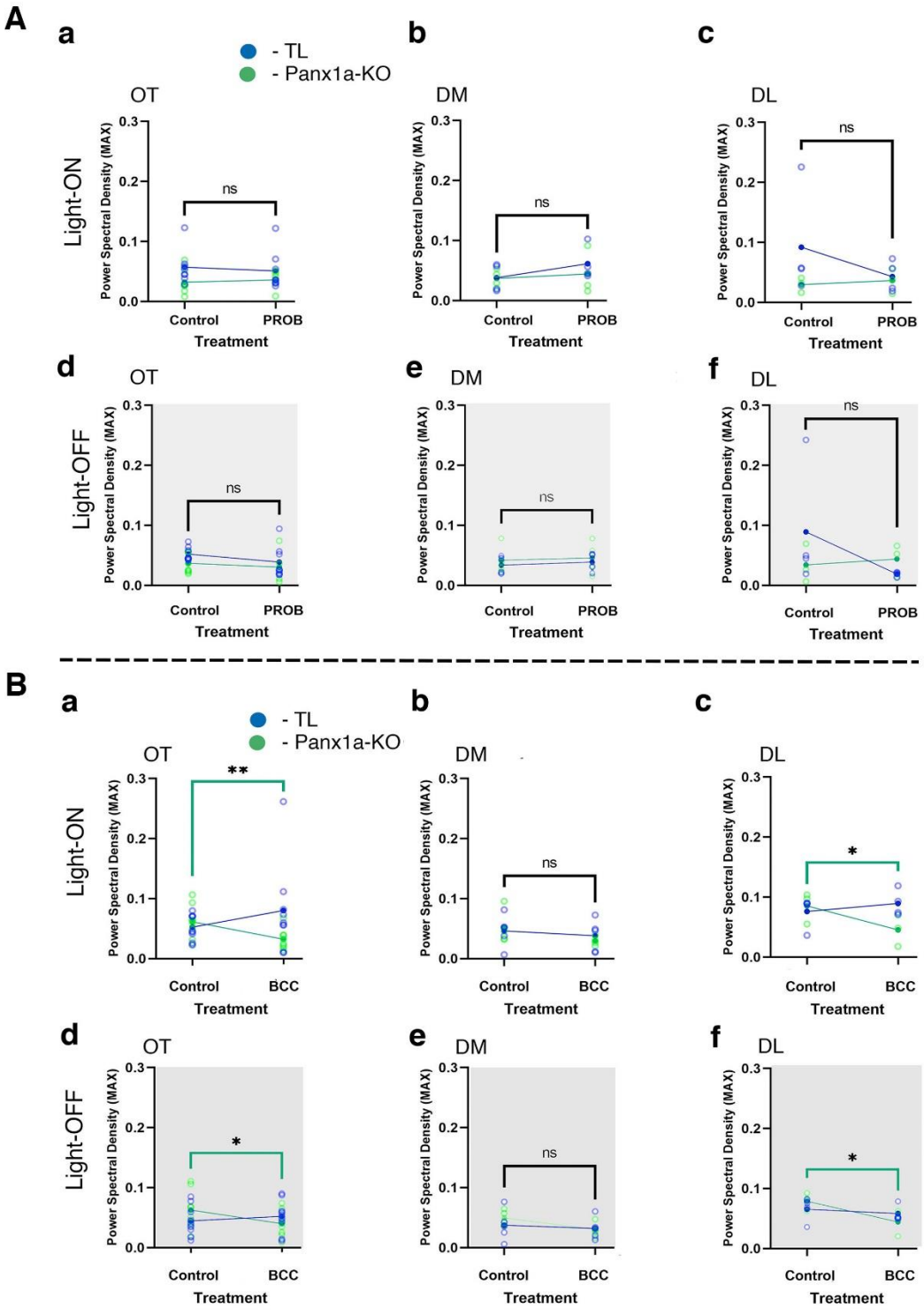
A
a
b
c
- TL
- Panx1a-KO
OT
DM
DL
Light-ON
Power Spectral Density (MAX)
ns
Control
PROB
Treatment
d
e
f
Light-OFF
B
**
*
BCC

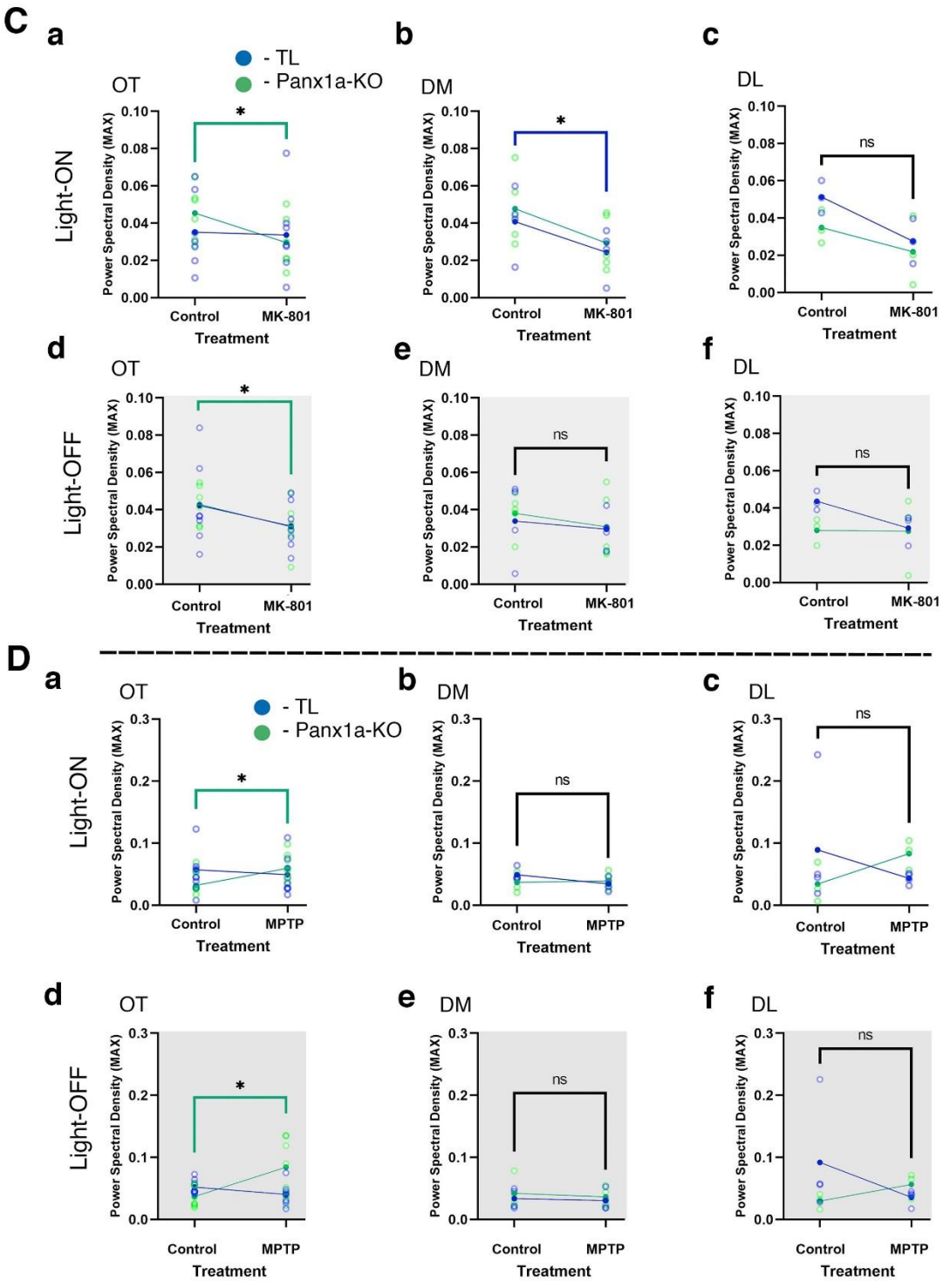
C
a
b
c
- TL
- Panx1a-KO
OT
DM
DL
Light-ON
Power Spectral Density (MAX)
0.10
0.08
0.06
0.04
0.02
0.00
*
ns
Control
MK-801
Treatment
d
e
f
Light-OFF
D
0.3
0.2
0.1
0.0
MPTP

Figure 16 A-D. The analysis of maximum beta-band power after drug treatments. Local field potentials were recorded from the visual ascending pathway of six days post fertilization TL and Panx1a-KO *Danio rerio* larvae. Three regions were recorded, the optic tectum (OT), amygdala (DM), and hippocampus (DL). Drug treatments were for 30 minutes before recording. The concentrations used: Probenecid (PROB; 20μM), bicuculline (BCC; 100μM), and MK-801 (20μM). Each larva was recorded in Light-ON/OFF conditions. MPTP treatment (50μM) was for four hours before recording. The beta-band was extracted and analyzed with the power spectral density (PSD) analysis. Units of PSD is Nanoampere/Hertz. The peak power values of each recording were averaged before and after treatment. The peak power values of individual larvae before (Control) and after treatment were graphed in open circles in light blue (TL) and light green (Panx1a-KO). Significance was calculated using paired t-tests. The average of the peak powers was graphed in filled circles in dark blue (TL) or dark green (Panx1a-KO). Significance: (****) indicates a P-value less than 0.0001, (***) indicates a P-value of less than 0.001, (**) indicates a P-value of less than 0.01, (*) indicates a P-value of less than 0.05 and (ns) refers to no significant differences (P-value > 0.05).

A - Probenecid. The treatment with PROB had no significant effects on the peak power frequency of the beta-band peak in both TL and Panx1a-KO larvae. The number of larvae tested: TL DM (n = 4), TL DL (n = 4), TL OT (n = 8), Panx1a-KO DM (n = 4), Panx1a-KO DL (n = 3) and Panx1a-KO OT (n = 5).

B - Bicuculline. BCC treatment caused a significant decrease in beta-band peak power in the OT and DL regions of Panx1a-KO larvae. No other regions were significantly affected by the BCC treatment. The number of larvae tested: TL DM (n = 5), TL DL (n = 4), TL OT (n = 9), Panx1a-KO DM (n = 4), Panx1a-KO DL (n = 3) and Panx1a-KO OT (n = 7).

C - MK-801. After treatment with MK-801, a significant decrease in TL DM beta-band peak power in the light-ON region. The beta-band peak power of the OT region of Panx1a-KO larvae was significantly decreased in both the light-ON/OFF conditions. No other regions were significantly affected by MK-801 treatment. The number of larvae tested: TL DM (n = 4), TL DL (n = 3), TL OT (n = 6), Panx1a-KO DM (n = 5), Panx1a-KO DL (n = 3) and Panx1a-KO OT (n = 7).

D - MPTP. The beta-band peak power of Panx1a-KO larvae in the OT region was significantly increased after MPTP treatment. No other regions were significantly affected after MPTP treatment. Significance was calculated using a Welch's t-test and visualized using estimation plots. The number of larvae tested: TL DM (n = 4), TL DL (n = 4), TL OT (n = 8), Panx1a-KO DM (n = 4), Panx1a-KO DL (n = 3) and Panx1a-KO OT (n = 7).

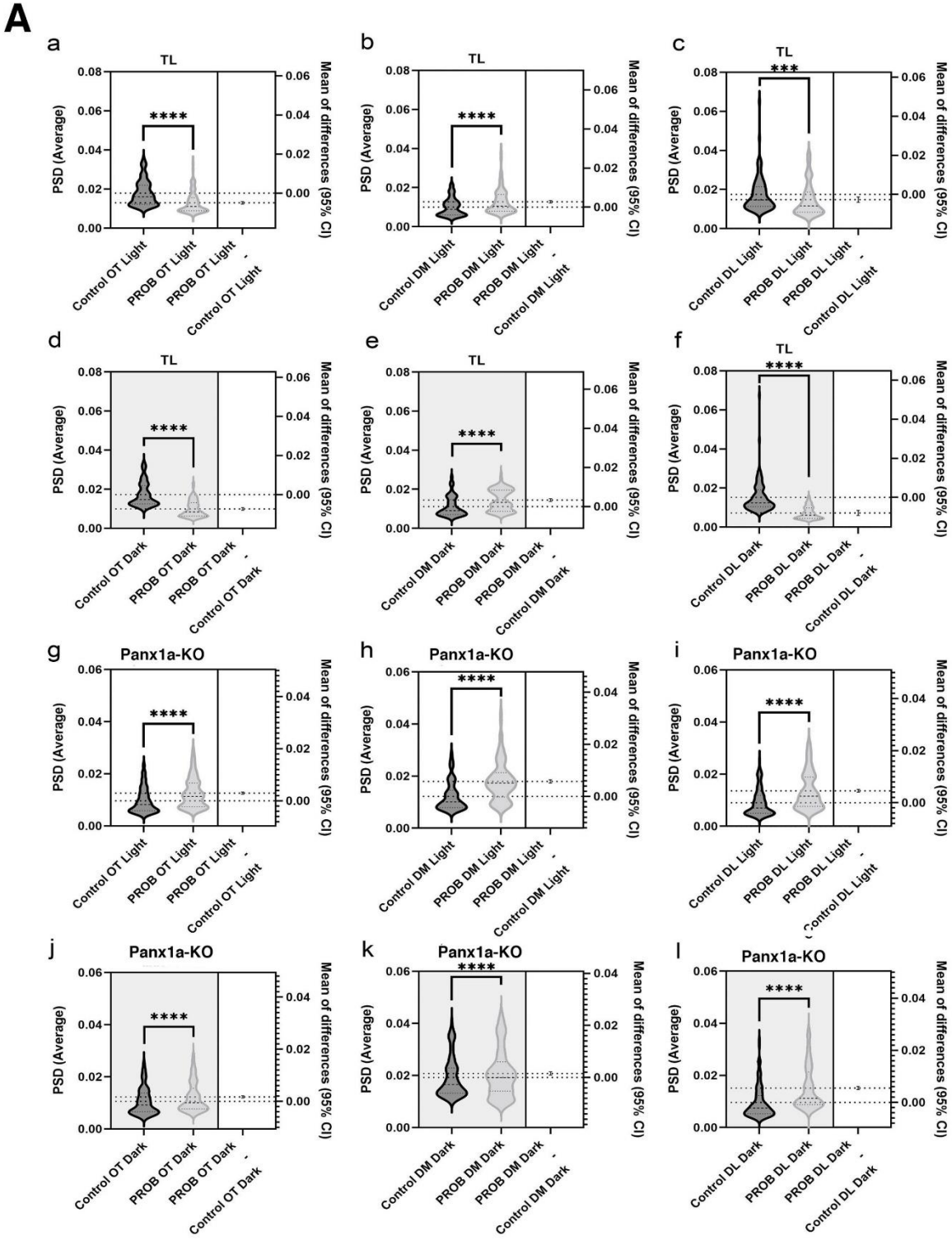
A
a
TL
PSD (Average)
Mean of differences (95% CI)
****
Control OT Light
PROB OT Light
PROB OT Light
Control OT Light
b
TL
****
Control DM Light
PROB DM Light
PROB DM Light
Control DM Light
c
TL
***
Control DL Light
PROB DL Light
PROB DL Light
Control DL Light
d
TL
****
Control OT Dark
PROB OT Dark
PROB OT Dark
Control OT Dark
e
TL
****
Control DM Dark
PROB DM Dark
PROB DM Dark
Control DM Dark
f
TL
****
Control DL Dark
PROB DL Dark
PROB DL Dark
Control DL Dark
g
Panx1a-KO
****
Control OT Light
PROB OT Light
PROB OT Light
Control OT Light
h
Panx1a-KO
****
Control DM Light
PROB DM Light
PROB DM Light
Control DM Light
i
Panx1a-KO
****
Control DL Light
PROB DL Light
PROB DL Light
Control DL Light
j
Panx1a-KO
****
Control OT Dark
PROB OT Dark
PROB OT Dark
Control OT Dark
k
Panx1a-KO
****
Control DM Dark
PROB DM Dark
PROB DM Dark
Control DM Dark
l
Panx1a-KO
****
Control DL Dark
PROB DL Dark
PROB DL Dark
Control DL Dark

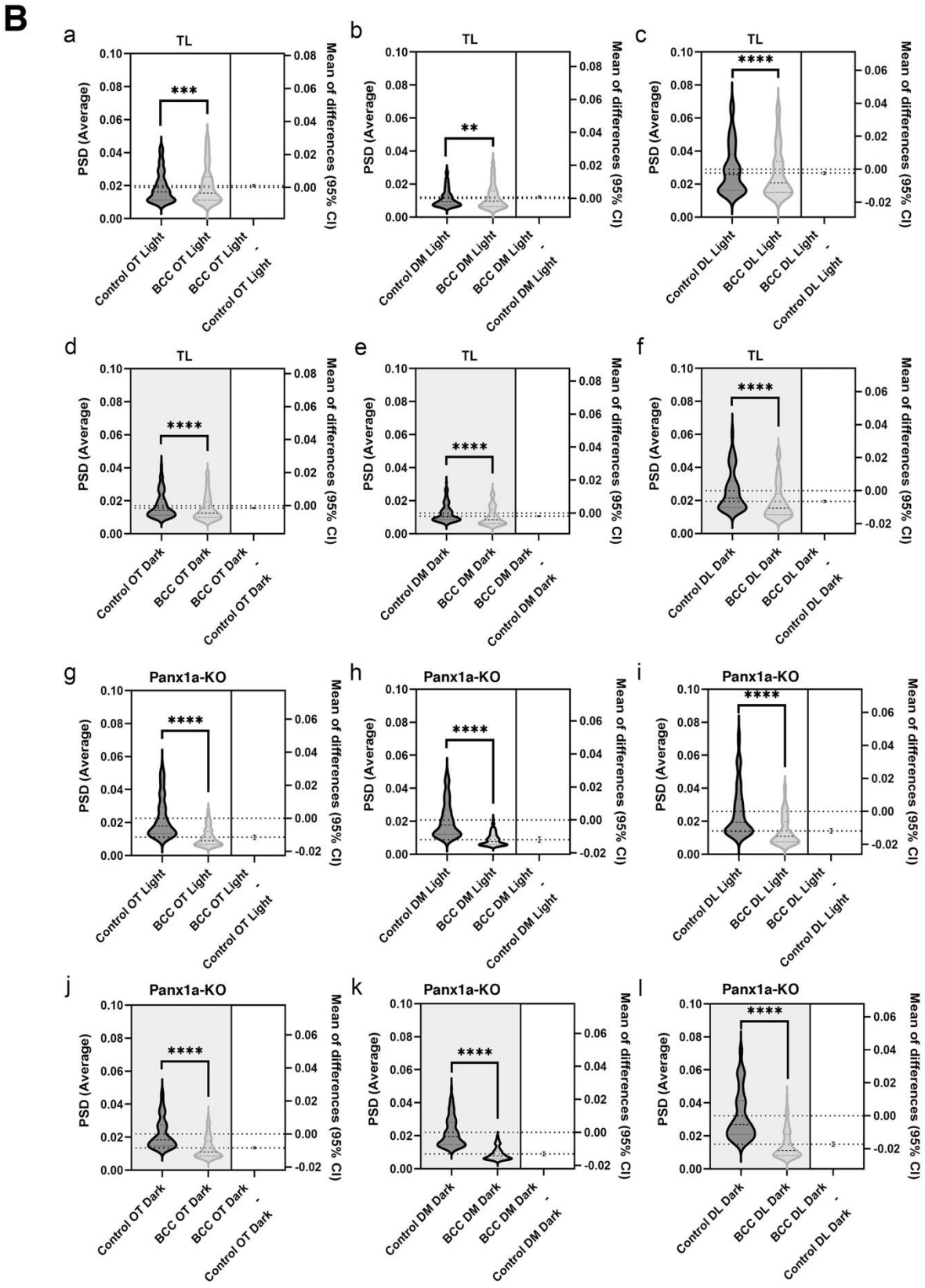
B
a
TL
***
PSD (Average)
Mean of differences (95% CI)
Control OT Light
BCC OT Light
BCC OT Light - Control OT Light
b
TL
**
Control DM Light
BCC DM Light
BCC DM Light - Control DM Light
c
TL
****
Control DL Light
BCC DL Light
BCC DL Light - Control DL Light
d
TL
****
Control OT Dark
BCC OT Dark
BCC OT Dark - Control OT Dark
e
TL
****
Control DM Dark
BCC DM Dark
BCC DM Dark - Control DM Dark
f
TL
****
Control DL Dark
BCC DL Dark
BCC DL Dark - Control DL Dark
g
Panx1a-KO
****
Control OT Light
BCC OT Light
BCC OT Light - Control OT Light
h
Panx1a-KO
****
Control DM Light
BCC DM Light
BCC DM Light - Control DM Light
i
Panx1a-KO
****
Control DL Light
BCC DL Light
BCC DL Light - Control DL Light
j
Panx1a-KO
****
Control OT Dark
BCC OT Dark
BCC OT Dark - Control OT Dark
k
Panx1a-KO
****
Control DM Dark
BCC DM Dark
BCC DM Dark - Control DM Dark
l
Panx1a-KO
****
Control DL Dark
BCC DL Dark
BCC DL Dark - Control DL Dark

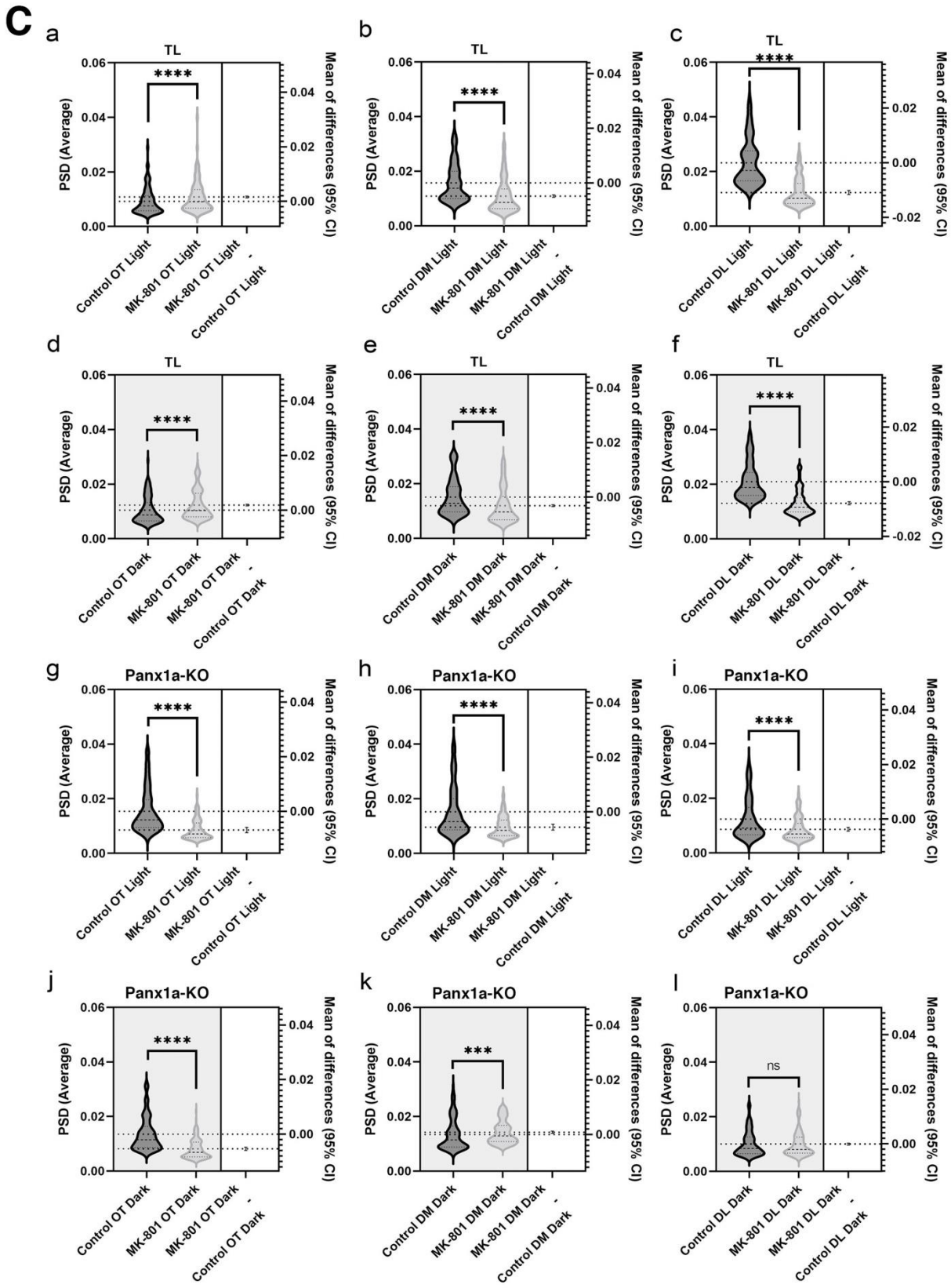
C
a
TL
****
PSD (Average)
Mean of differences (95% CI)
Control OT Light
MK-801 OT Light
MK-801 OT Light - Control OT Light
b
TL
****
Control DM Light
MK-801 DM Light
MK-801 DM Light - Control DM Light
c
TL
****
Control DL Light
MK-801 DL Light
MK-801 DL Light - Control DL Light
d
TL
****
Control OT Dark
MK-801 OT Dark
MK-801 OT Dark - Control OT Dark
e
TL
****
Control DM Dark
MK-801 DM Dark
MK-801 DM Dark - Control DM Dark
f
TL
****
Control DL Dark
MK-801 DL Dark
MK-801 DL Dark - Control DL Dark
g
Panx1a-KO
****
h
Panx1a-KO
****
i
Panx1a-KO
****
j
Panx1a-KO
****
k
Panx1a-KO
***
l
Panx1a-KO
ns

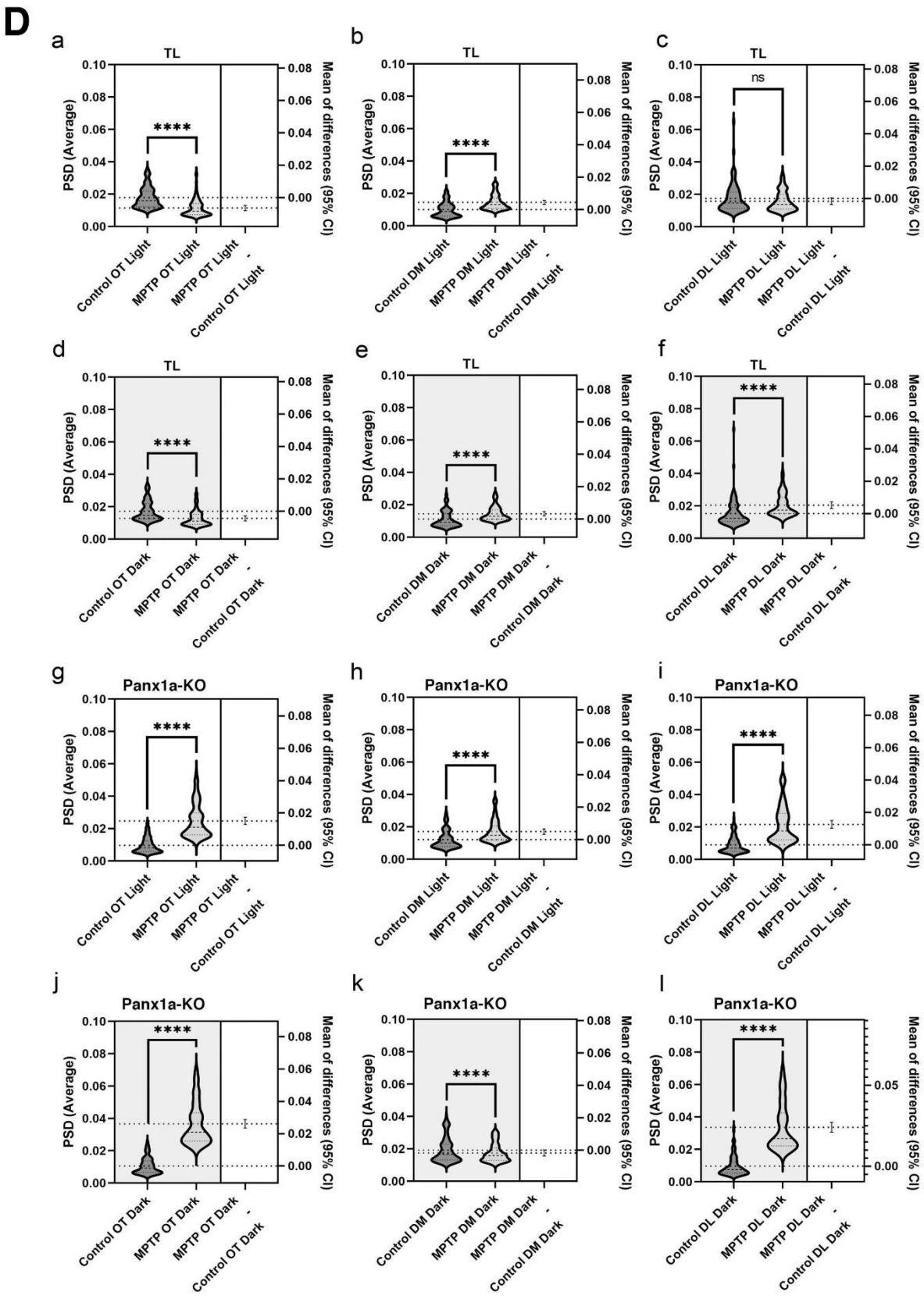
D
a
TL
****
PSD (Average)
Mean of differences (95% CI)
Control OT Light
MPTP OT Light
MPTP OT Light - Control OT Light
b
TL
****
Control DM Light
MPTP DM Light
MPTP DM Light - Control DM Light
c
TL
ns
Control DL Light
MPTP DL Light
MPTP DL Light - Control DL Light
d
TL
****
Control OT Dark
MPTP OT Dark
MPTP OT Dark - Control OT Dark
e
TL
****
Control DM Dark
MPTP DM Dark
MPTP DM Dark - Control DM Dark
f
TL
****
Control DL Dark
MPTP DL Dark
MPTP DL Dark - Control DL Dark
g
Panx1a-KO
****
h
Panx1a-KO
****
i
Panx1a-KO
****
j
Panx1a-KO
****
k
Panx1a-KO
****
l
Panx1a-KO
****

Figure 17 A-D. The analysis of average beta-band power after drug treatment. The average beta-band power analysis used the identical raw data for quantifying the maximum beta band power. Each beta-band recording was averaged over multiple trials and analyzed using a paired t-test or a Welch's t-test for MPTP. Using GraphPad Prism, an estimation statistics analysis calculated the 95% confidence interval (CI). The final plots show Estimation plots presented as violin plots (for >100 data points) with differences between means (error bars = 95% CI). The shaded grey color indicated Light-OFF. Dotted lines indicate the means for each condition. Significances are indicated with a (*) where (****) indicates a P-value less than 0.0001, (***) indicates a P-value of less than 0.001, (**) indicates a P-value of less than 0.01, (*) indicates a P-value of less than 0.05 and (ns) means no significant differences were observed (P-value > 0.05). Units of PSD is Nanoampere/Hertz.

A - Probenecid. The general trend observed was a decrease in average band power in the OT and DL and an increase in TL. In Panx1a-KO larvae, the PROB treatment caused an increase in the average power of all three regions. The number of larvae tested: TL DM (n = 4), TL DL (n = 4), TL OT (n = 8), Panx1a-KO DM (n = 4), Panx1a-KO DL (n = 3) and Panx1a-KO OT (n = 5).

B - Bicuculline. BCC treatment in general caused a decrease in the average beta frequency power. The number of larvae tested: TL DM (n = 5), TL DL (n = 4), TL OT (n = 9), Panx1a-KO DM (n = 4), Panx1a-KO DL (n = 3) and Panx1a-KO OT (n = 7).

C - MK-801. MK-801 treatment caused a significant decrease in the beta band power in the DM and DL but caused an increase in the OT of TL. In Panx1a-KO larvae, the average band power decreased. The number of larvae tested: TL DM (n = 4), TL DL (n = 3), TL OT (n = 6), Panx1a-KO DM (n = 5), Panx1a-KO DL (n = 3) and Panx1a-KO OT (n = 7).

D - MPTP. MPTP treatment caused an increase in the DM and DL, as well as decreased the average beta power of the OT in TL. In Panx1a-KO larvae, the MPTP treatment generally increased beta band power. The number of larvae tested was TL DM (n = 4), TL DL (n = 4), TL OT (n = 8), Panx1a-KO DM (n = 4), Panx1a-KO DL (n = 3) and Panx1a-KO OT (n = 7).

5.2.4 Gamma-band activities in TL and Panx1a-KOs showed complex responses to pharmacological blocking of NMDA- and $GABA_A$-receptors, Panx1 channels, and MPTP treatment

As shown in the previous chapter, the gamma-band (35-45 Hz) was extracted from the PSD analysis. The treatment with PROB did not affect the peak power of the gamma-band of both TL and Panx1a-KO larvae in all conditions tested (**Figure 18A, a-f**; **Statistical information see Supplementary Tables S9-12 in the Appendix)**.

BCC treatment caused a significant increase in the OT region of Panx1a-KO larvae in the Light-ON condition (**Figure 18B, d**). Otherwise, BCC did not significantly affect TL larvae or Panx1a-KO larvae.

The third drug, MK-801, just like PROB, did not cause any significant changes in the peak power of the gamma-band in TL and Panx1a-KO larvae (**Figure 18C, a-f**).

The last drug MPTP caused a significant increase in peak gamma power in the OT of TL larvae in both Light-ON and OFF conditions (**Figure 18D, a,d**). MPTP did not cause any other significant difference.

The PSD data were also analyzed for the changes in the average gamma-band power. In both the OT and DM of TL larvae, the treatment with PROB treatment caused a significant increase in the overall power of the gamma-band in Light-ON and Light-OFF conditions (**Figure 19A; Statistical information see Supplementary Tables S17-20 in the Appendix**). However, the DL region had the opposite effect of causing a decrease in average gamma power in the Light-ON condition. In the Panx1a-KO larvae, PROB treatment caused a significant decrease in both the DM and OT regions, while the DL region gamma power was significantly increased.

When larvae were treated with BCC, it generally caused decreases in gamma-band power of TL larvae, whereas the effect was the opposite in Panx1a-KO larvae (**Figure 19B**).

In the gamma-band, the MK-801 treatment caused a significant decrease in the average gamma power of TL in the OT and a significant increase in the DM (**Figure 19C**). Under the Light-ON condition, a significant increase of gamma power in the DL was observed and a significant decrease in the Light-OFF condition. The average power of Panx1a-KO was increased in the OT region and significantly decreased in the DL. Under the Light-ON stimulus,

the DM region of Panx1a-KO larvae showed a decrease in average power and an increase with the Light-OFF stimulation.

Lastly, MPTP treatment in TL larvae caused a significant increase in the average gamma power in the OT, whereas the DM and DL regions had a significant decrease in average power (**Figure 19D**). In the Panx1a-KO larvae, the OT, DM, and DL regions observed a significant decrease in average gamma power for the Light-ON condition. A significant increase in average gamma power was observed in the Light-OFF condition for the DL region. Overall, the gamma-band activities showed opposite responses to light stimuli across multiple brain regions with significant differences between genotypes.

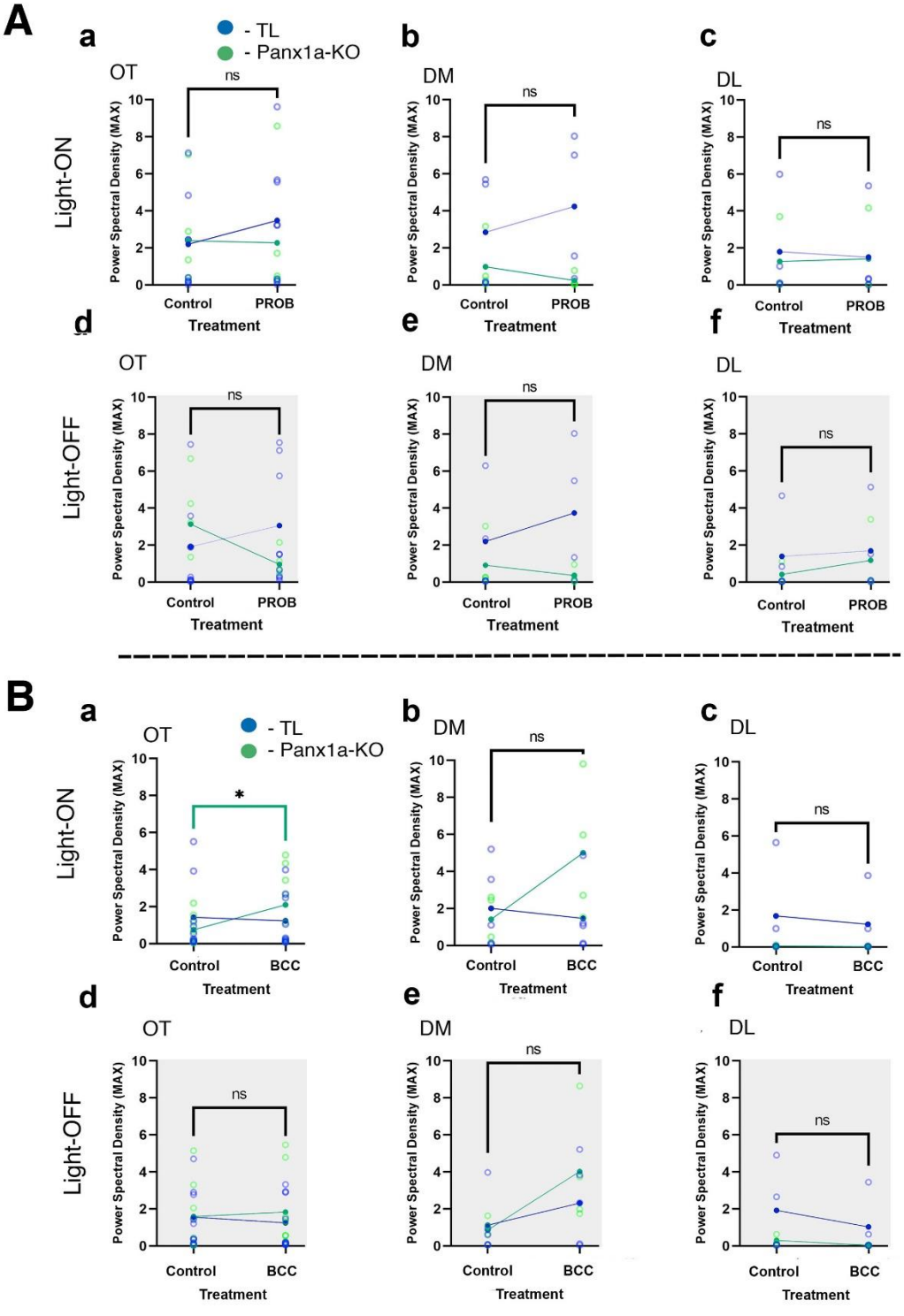
A
a
b
c
- TL
- Panx1a-KO
OT
DM
DL
ns
Power Spectral Density (MAX)
Control
PROB
Treatment
Light-ON
d
e
f
Light-OFF
B
*
BCC

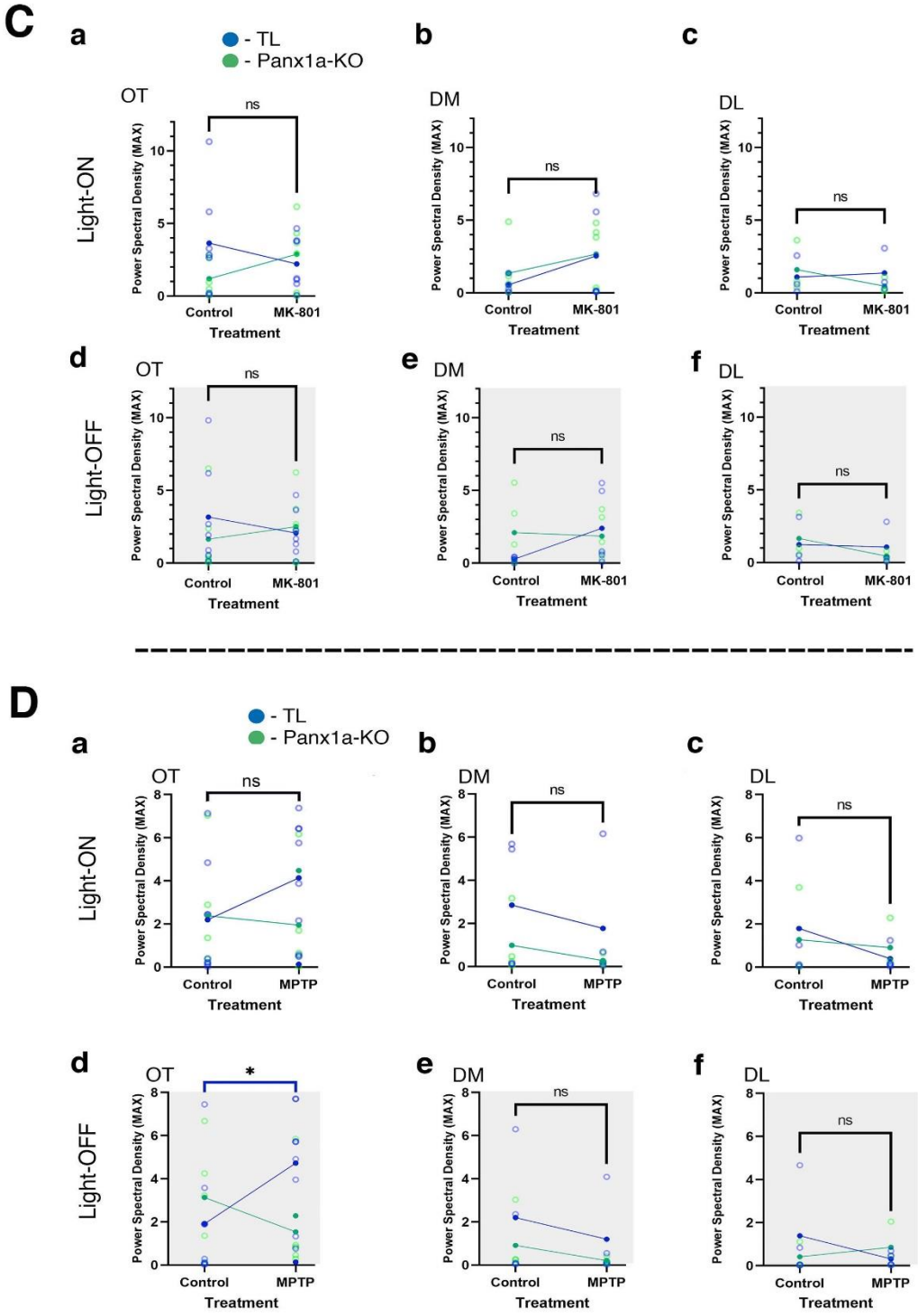
C
a
- TL
- Panx1a-KO
OT
ns
Light-ON
Power Spectral Density (MAX)
Control
MK-801
Treatment
b
DM
c
DL
d
Light-OFF
e
f
D
MPTP
*

Figure 18 A-D. The analysis of maximum gamma-band power after drug treatments. Local field potentials were recorded from the visual ascending pathway of six days post fertilization TL and Panx1a-KO *Danio rerio* larvae. Three regions were recorded, the optic tectum (OT), amygdala (DM), and hippocampus (DL). Drug treatments were for 30 minutes before recording. The concentrations used were Probenecid (PROB; 20μM), bicuculline (BCC; 100μM), and MK-801 (20μM). Each larva was recorded in Light-ON/OFF conditions. MPTP treatment (50μM) was for four hours before recording. The gamma band was extracted and analyzed for power spectral density (PSD). Units of PSD is Nanoampere/Hertz. The peak power values of each recording were averaged before and after treatment. The peak power values of individual larvae before (Control) and after treatment were graphed in open circles in light blue (TL) and light green (Panx1a-KO). Significance was calculated using paired t-tests. The average of the peak powers was graphed in filled circles in dark blue (TL) or dark green (Panx1a-KO). Significance: (****) indicates a P-value less than 0.0001, (***) indicates a P-value of less than 0.001, (**) indicates a P-value of less than 0.01, (*) indicates a P-value of less than 0.05 and (ns) refers to no significant differences (P-value > 0.05).

A - Probenecid. No significant differences were observed in the peak power of TL and Panx1a-KO larvae after PROB treatment in the three regions tested. Significance was calculated using a paired t-test and visualized using estimation plots. The number of larvae tested: TL DM (n = 4), TL DL (n = 4), TL OT (n = 8), Panx1a-KO DM (n = 4), Panx1a-KO DL (n = 3) and Panx1a-KO OT (n = 5).

B - Bicuculline. The treatment with BCC caused a significant increase in gamma-band power of Panx1a-KO larvae of the OT region in the light-ON condition. No other region of the Panx1a-KO larvae or any of the TL larvae had a significant change in the peak gamma frequency. The number of larvae tested: TL DM (n = 5), TL DL (n = 4), TL OT (n = 9), Panx1a-KO DM (n = 4), Panx1a-KO DL (n = 3) and Panx1a-KO OT (n = 7).

C - MK-801. No significant differences were observed in the peak power of TL and Panx1a-KO larvae after MK-801 treatment in the three regions tested. The number of larvae tested: TL DM (n = 4), TL DL (n = 3), TL OT (n = 6), Panx1a-KO DM (n = 5), Panx1a-KO DL (n = 3) and Panx1a-KO OT (n = 7).

D - MPTP. The treatment with MPTP caused a significant increase in the OT region's gamma-band power of TL larvae in the light-ON/OFF condition. No other region of the TL larvae or any of the Panx1a-KO larvae had a significant change in the peak gamma frequency. Significance was calculated using a Welch's t-test and visualized using estimation plots. The number of larvae tested: TL DM (n = 4), TL DL (n =4), TL OT (n = 8), Panx1a-KO DM (n = 4), Panx1a-KO DL (n = 3) and Panx1a-KO OT (n = 7).

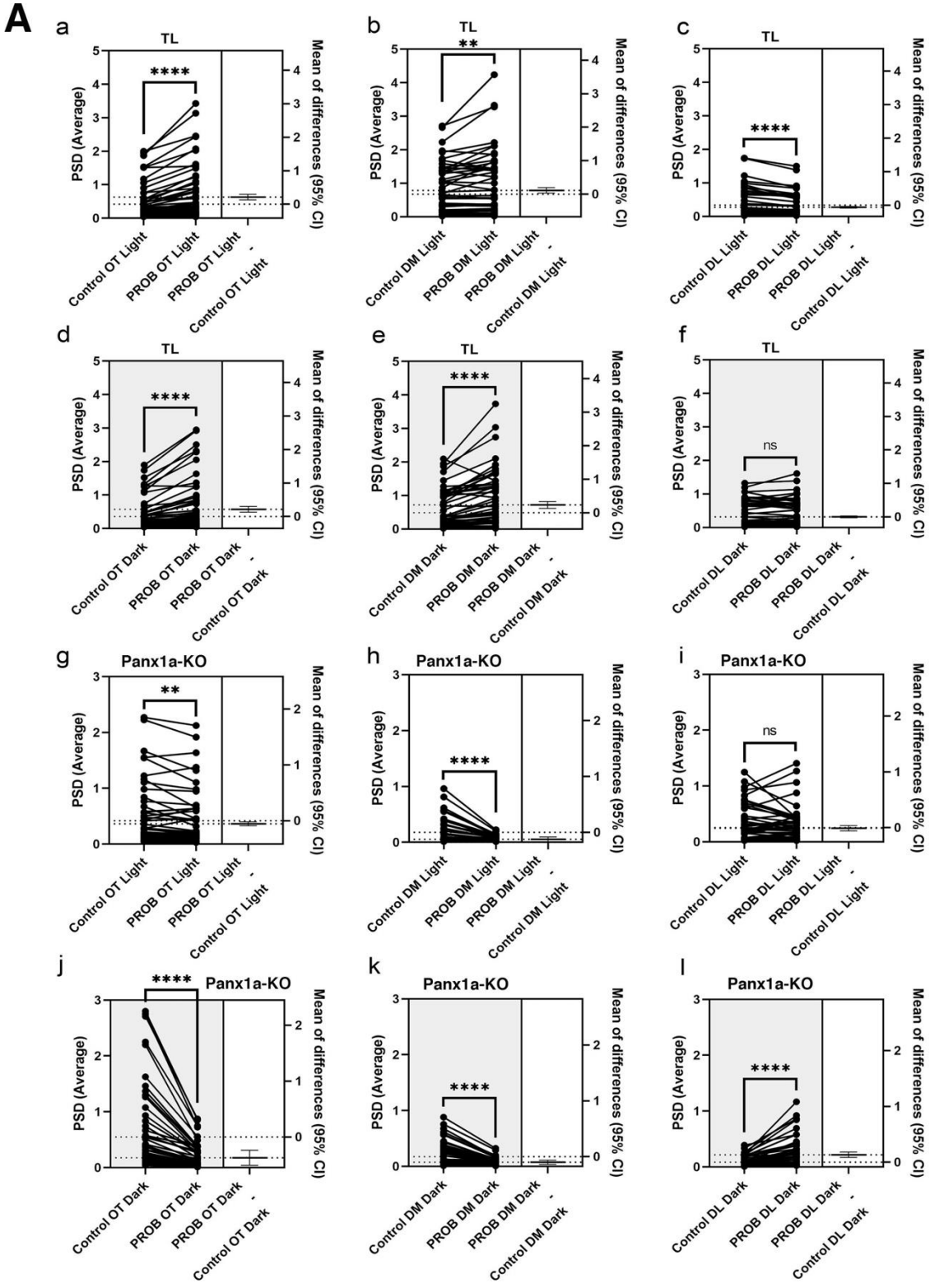
A
a
TL
****
PSD (Average)
Mean of differences (95% CI)
Control OT Light
PROB OT Light
PROB OT Light - Control OT Light
b
TL
**
Control DM Light
PROB DM Light
PROB DM Light - Control DM Light
c
TL
****
Control DL Light
PROB DL Light
PROB DL Light - Control DL Light
d
TL
****
Control OT Dark
PROB OT Dark
PROB OT Dark - Control OT Dark
e
TL
****
Control DM Dark
PROB DM Dark
PROB DM Dark - Control DM Dark
f
TL
ns
Control DL Dark
PROB DL Dark
PROB DL Dark - Control DL Dark
g
Panx1a-KO
**
h
Panx1a-KO
****
i
Panx1a-KO
ns
j
****
Panx1a-KO
k
Panx1a-KO
****
l
Panx1a-KO
****

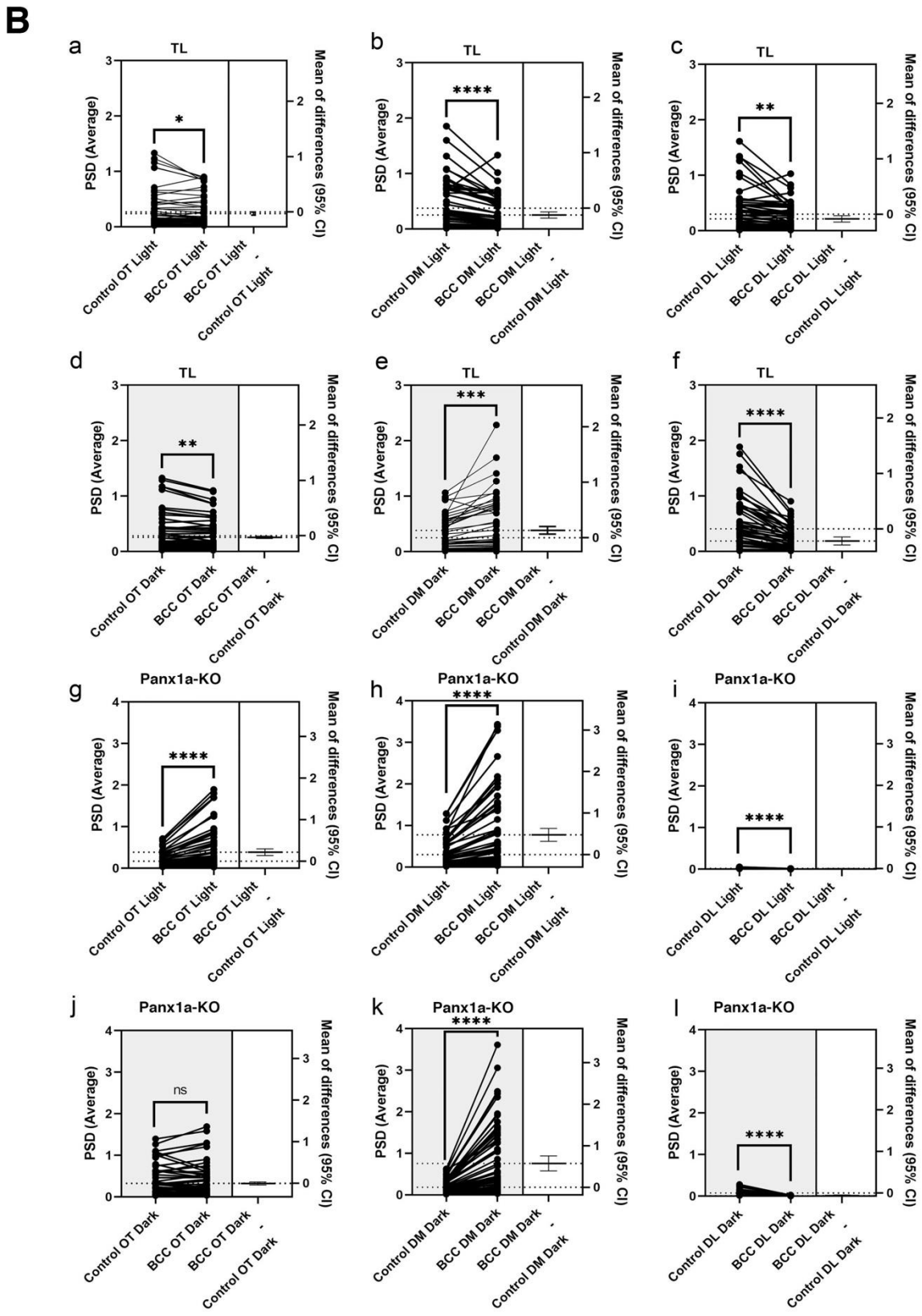
B
a
TL
*
PSD (Average)
Mean of differences (95% CI)
Control OT Light
BCC OT Light
BCC OT Light - Control OT Light
b
TL
****
Control DM Light
BCC DM Light
BCC DM Light - Control DM Light
c
TL
**
Control DL Light
BCC DL Light
BCC DL Light - Control DL Light
d
TL
**
Control OT Dark
BCC OT Dark
BCC OT Dark - Control OT Dark
e
TL
***
Control DM Dark
BCC DM Dark
BCC DM Dark - Control DM Dark
f
TL
****
Control DL Dark
BCC DL Dark
BCC DL Dark - Control DL Dark
g
Panx1a-KO
****
h
Panx1a-KO
****
i
Panx1a-KO
****
j
Panx1a-KO
ns
k
Panx1a-KO
****
l
Panx1a-KO
****

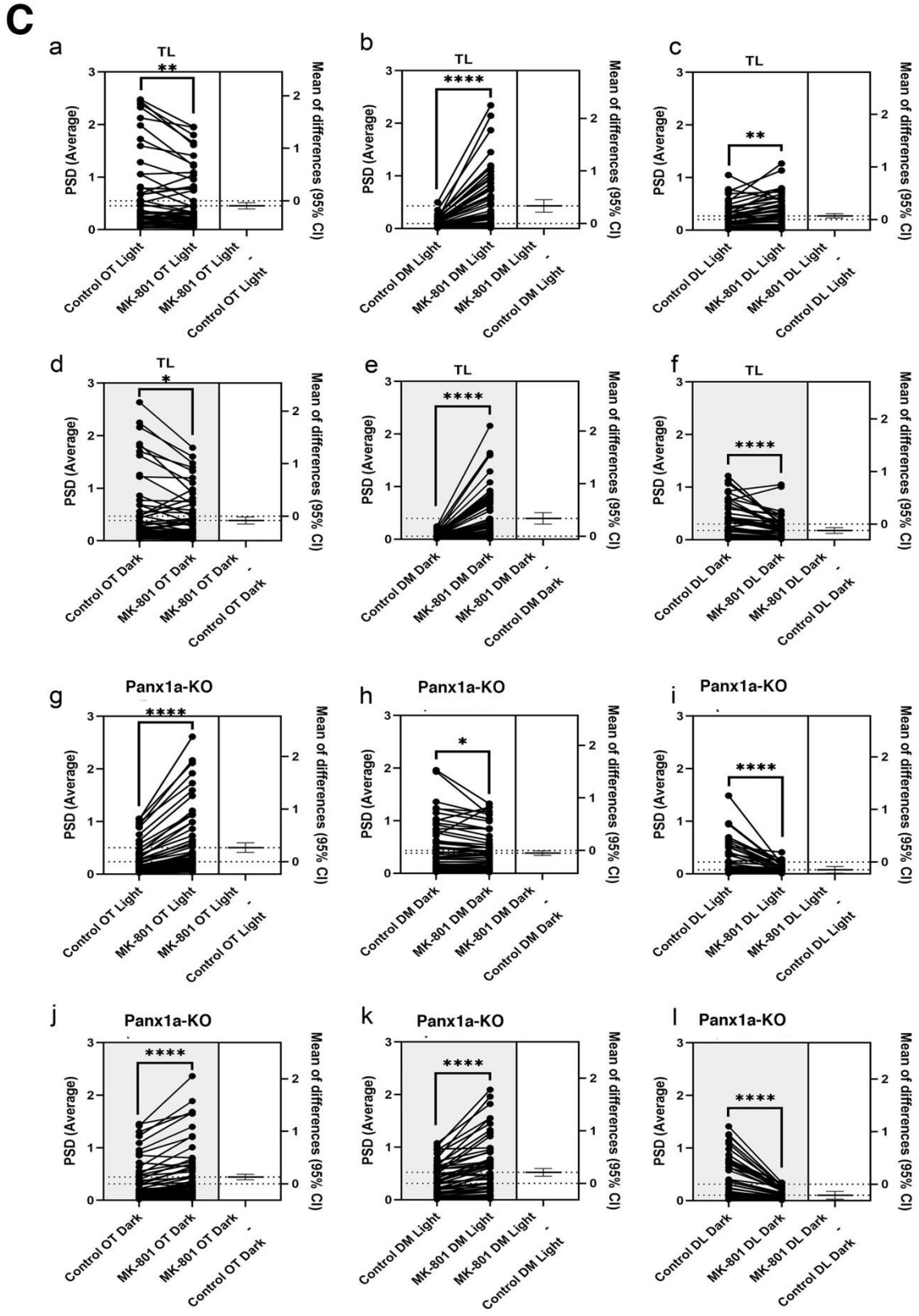
C
a
TL
**
PSD (Average)
Mean of differences (95% CI)
Control OT Light
MK-801 OT Light
MK-801 OT Light
Control OT Light
b
TL
****
Control DM Light
MK-801 DM Light
MK-801 DM Light
Control DM Light
c
TL
**
Control DL Light
MK-801 DL Light
MK-801 DL Light
Control DL Light
d
TL
*
Control OT Dark
MK-801 OT Dark
MK-801 OT Dark
Control OT Dark
e
TL
****
Control DM Dark
MK-801 DM Dark
MK-801 DM Dark
Control DM Dark
f
TL
****
Control DL Dark
MK-801 DL Dark
MK-801 DL Dark
Control DL Dark
g
Panx1a-KO
****
Control OT Light
MK-801 OT Light
MK-801 OT Light
Control OT Light
h
Panx1a-KO
*
Control DM Dark
MK-801 DM Dark
MK-801 DM Dark
Control DM Dark
i
Panx1a-KO
****
Control DL Light
MK-801 DL Light
MK-801 DL Light
Control DL Light
j
Panx1a-KO
****
Control OT Dark
MK-801 OT Dark
MK-801 OT Dark
Control OT Dark
k
Panx1a-KO
****
Control DM Light
MK-801 DM Light
MK-801 DM Light
Control DM Light
l
Panx1a-KO
****
Control DL Dark
MK-801 DL Dark
MK-801 DL Dark
Control DL Dark

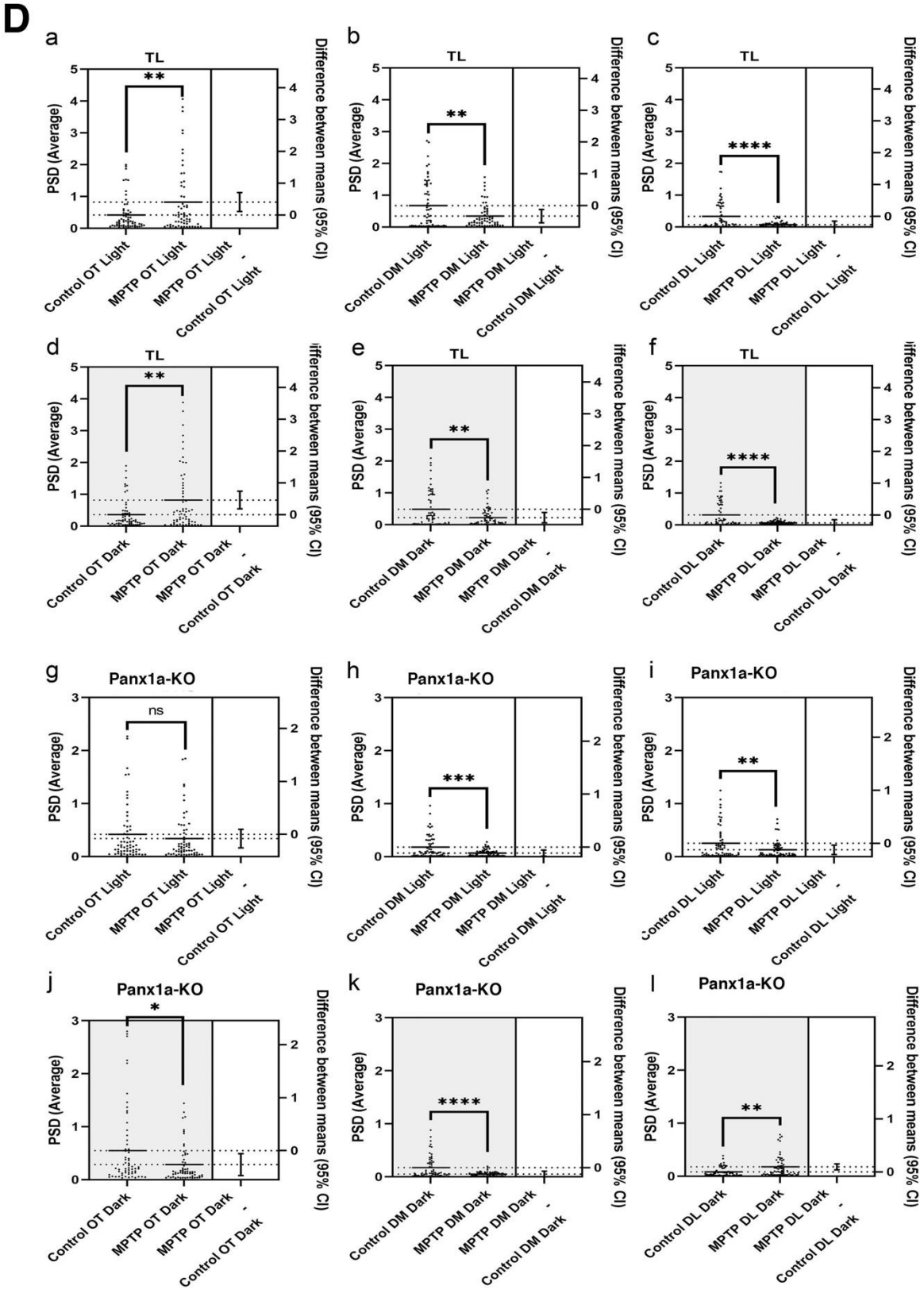
D
a
TL
**
PSD (Average)
Difference between means (95% CI)
Control OT Light
MPTP OT Light
MPTP OT Light
Control OT Light
b
TL
**
PSD (Average)
Difference between means (95% CI)
Control DM Light
MPTP DM Light
MPTP DM Light
Control DM Light
c
TL
****
PSD (Average)
Difference between means (95% CI)
Control DL Light
MPTP DL Light
MPTP DL Light
Control DL Light
d
TL
**
PSD (Average)
Difference between means (95% CI)
Control OT Dark
MPTP OT Dark
MPTP OT Dark
Control OT Dark
e
TL
**
PSD (Average)
Difference between means (95% CI)
Control DM Dark
MPTP DM Dark
MPTP DM Dark
Control DM Dark
f
TL
****
PSD (Average)
Difference between means (95% CI)
Control DL Dark
MPTP DL Dark
MPTP DL Dark
Control DL Dark
g
Panx1a-KO
ns
PSD (Average)
Difference between means (95% CI)
Control OT Light
MPTP OT Light
MPTP OT Light
Control OT Light
h
Panx1a-KO
***
PSD (Average)
Difference between means (95% CI)
Control DM Light
MPTP DM Light
MPTP DM Light
Control DM Light
i
Panx1a-KO
**
PSD (Average)
Difference between means (95% CI)
Control DL Light
MPTP DL Light
MPTP DL Light
Control DL Light
j
Panx1a-KO
*
PSD (Average)
Difference between means (95% CI)
Control OT Dark
MPTP OT Dark
MPTP OT Dark
Control OT Dark
k
Panx1a-KO
****
PSD (Average)
Difference between means (95% CI)
Control DM Dark
MPTP DM Dark
MPTP DM Dark
Control DM Dark
l
Panx1a-KO
**
PSD (Average)
Difference between means (95% CI)
Control DL Dark
MPTP DL Dark
MPTP DL Dark
Control DL Dark

Figure 19 A-D. The analysis of average gamma-band power after drug treatment. The average gamma-band power analysis used the identical raw data used for the quantification of the maximum beta band power. The gamma band was averaged and analyzed using a paired t-test. Using GraphPad Prism, an estimation statistics analysis calculated the 95% confidence interval (CI). The final plots show Estimation plots with differences between means (error bars = 95% CI). The shaded grey color indicated Light-OFF. Dotted lines indicate the means for each condition. Significances are indicated with a (*) where (****) indicates a P-value less than 0.0001, (***) indicates a P-value of less than 0.001, (**) indicates a P-value of less than 0.01, (*) indicates a P-value of less than 0.05 and (ns) means no significant differences were observed (P-value > 0.05). Units of PSD is Nanoampere/Hertz.

A - Probenecid. PROB treatment caused an increase in the average gamma-band power of the DM and OT region and decreased average power in the DL of TL larvae. The general trend after PROB treatment was a decrease in average band power in the DM and OT and an increase in the DL of Panx1a-KO larvae. The number of larvae tested was TL DM (n = 4), TL DL (n = 4), TL OT (n = 8), Panx1a-KO DM (n = 4), Panx1a-KO DL (n = 3) and Panx1a-KO OT (n = 5).

B - Bicuculline. BCC treatment caused a general decrease in the gamma-band power of TL and an increase in Panx1a-KO larvae. The number of larvae used was TL OT (n = 9), TL DM (n = 5), TL DL (n = 4), Panx1a-KO OT (n = 7), Panx1a-KO DM (n = 4) and Panx1a-KO DL (n = 3).

C - MK-801. MK-801 treatment caused an increase in average gamma-band power in the DM, a decrease in the OT, and differential regulation of the DL in TL. MK-801 treatment caused an increase in average gamma-band power in the OT, a decrease in the DL, and differential regulation of the DM in Panx1a-KO. The number of larvae used was TL OT (n = 7), TL DM (n = 4), TL DL (n = 3), Panx1a-KO OT (n = 6), Panx1a-KO DM (n = 5) and Panx1a-KO DL (n = 3).

D - MPTP. The gamma band was averaged over multiple trials, analyzed using a Welch's t-test, and graphed as an estimation plot using GraphPad Prism. MPTP treatment caused an increase in average gamma-band power in the DM and DL, as well as the decreased average power of the OT region in TL larvae. Generally, average gamma-band power was decreased after MPTP treatment in Panx1a-KO larvae. The number of larvae used was TL OT (n = 8), TL DM (n = 4), TL DL (n = 4), Panx1a-KO OT (n = 7), Panx1a-KO DM (n = 4) and Panx1a-KO DL (n = 3).

5.2.5 The comparison of the regulation of the beta- and gamma-band frequencies of TL and Panx1a-KOs revealed a complex relationship with drug treatments and light responses

The average band power of the beta- and gamma-bands shown in **Figures 17 and 19** were compared. The rationale for presenting this comparison as a heat map was to visualize increases, decreases, or nonsignificant differences in average band power in a simplified graph. Arbitrary values of 0, 1, and 2 were assigned for significant decrease (green), no change (black), or increase (red) based on the P-values shown in (**Figure 17A-D**) and (**Figure 19A-D**).

MPTP treatment generally caused a down-regulation of the beta-band and an up-regulation of the gamma-band in both TL and Panx1a-KO (**Figure 20**). The OT region of TL and Panx1a-KO larvae appeared to have the opposite regulation after MPTP treatment.

Treatment with BCC overall caused a decrease in average beta-band power in TL and Panx1a-KO larvae. TL larvae showed a decrease in average power in the gamma-band, whereas, in Panx1a-KO larvae, average power increased in the OT and DM regions.

MK-801 treatment generally caused a decrease in average beta-band power in both TL and Panx1a-KO larvae. The OT region of TLs was differentially regulated compared to Panx1a-KO larvae, where MK-801 treatment caused an increase. Each region was differentially regulated when the gamma-band was analyzed after MK-801 treatment.

PROB treatment caused an overall decrease of beta-band power in TL larvae and an increase in Panx1a-KO larvae. In the gamma-band, there was a flip from the beta-band trend. The TL larvae generally had an increase in average gamma-band power, and Panx1a-KO larvae had a decrease in power. Overall, the DM and DL regions of TL and Panx1a-KO larvae had similar regulations. The OT region of TL and Panx1a-KO larvae showed more opposite regulations than the two other regions.

Overall, the OT region showed the most differences between TL and Panx1a-KO larvae. For example, MPTP treatment reduced beta-band power in the OT of TL and an opposite increase in Panx1a-KO. When Panx1a was present, both the beta- and gamma-band showed opposite responses after treatment with PROB, BCC, MK-801, and MPTP. The DM and DL regions showed no distinct patterns with the drugs tested in both TL and Panx1a-KO larvae.

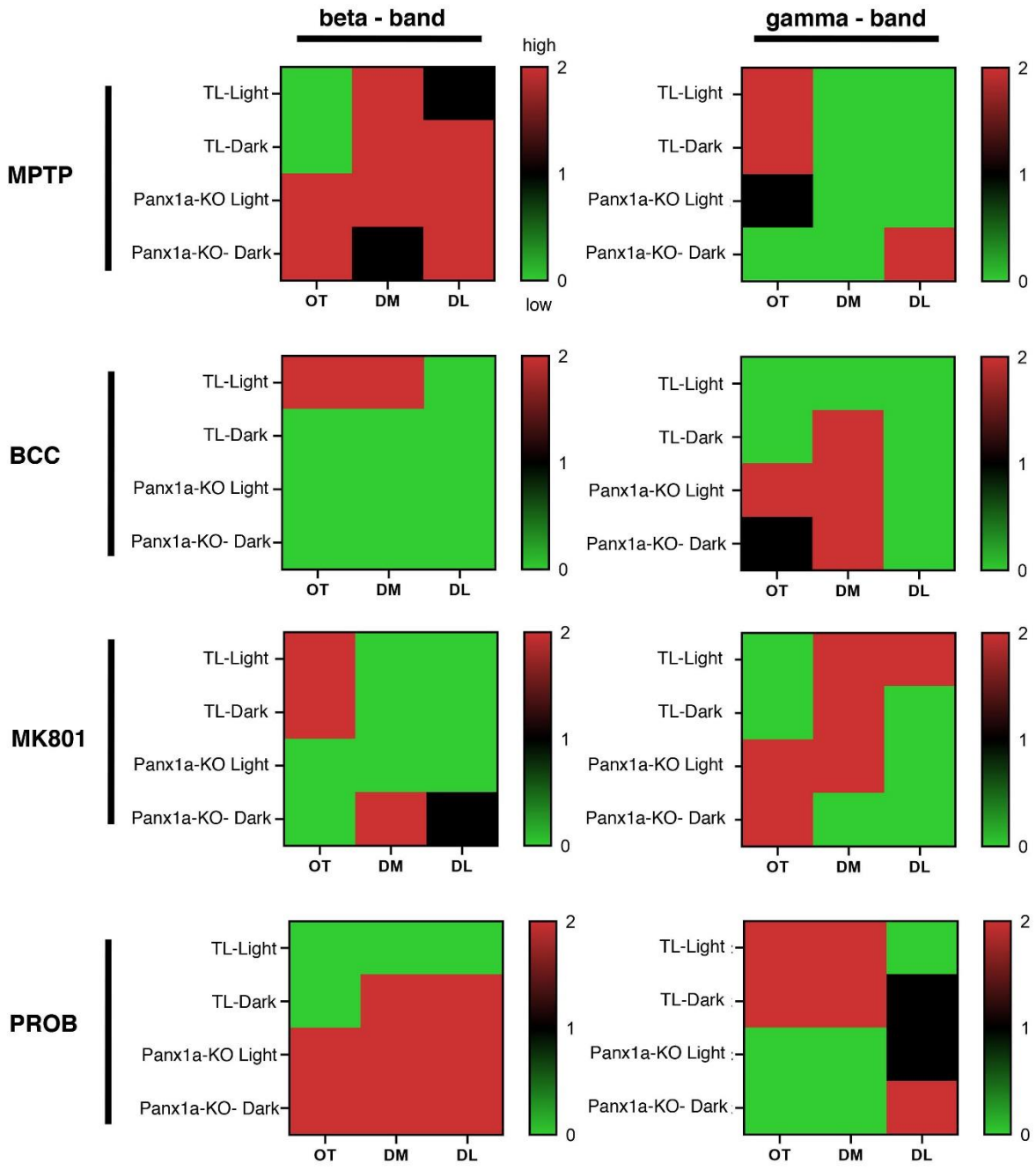

Figure 20. The comparison of the average power of the beta- and gamma-bands. When average power significantly increased after treatment, a value of two was assigned that was graphed as red in the heat map. When average power significantly decreased, a value of zero was given that was graphed as green in the heat map. When no significant differences were observed post-treatment, a value of one was assigned, which appears as black on the heat map. The assignment of values derived from the P-values is shown in Sections 5.2.3 and 5.2.4. Scale bars reference the colors assigned to the values 0, 1, and 2.

5.2.6 A Coherence Analysis showed that light and drug treatment affected the relationship between OT, DM, and DL in the ascending visual pathway

General trends observed in the previous result sections suggested complex responses, often with opposite or mixed trends, were induced by blocking GABAergic (BCC), glutamatergic (MK-801), or ATP-mediated purinergic signaling (PROB). Here, we took advantage of the two-electrode recording setup and performed a coherence analysis which allowed testing the relation between data sets recorded simultaneously from two regions of the zebrafish brain. Since coherence determines the relationship between two continuously recorded data sets, a higher coherence was expected, indicating a greater relationship and vice versa.

The coherence between the pallium represented by the DL and DM, and the OT was determined from simultaneous recordings. Treatment with PROB had little effect on the coherence between the DM and OT regions of TL larvae, only causing an increase in the gamma frequency in the Light-OFF condition (**Figure 21; Statistical information see Supplementary Tables S21-24 in the Appendix**). When the DL and OT regions were analyzed, there were significant increases in coherence across all frequencies in TL larvae. In Panx1a-KO larvae, the PROB treatment changed the coherence in the beta- and gamma-bands with little effect in the lower frequency range.

BCC treatment caused an increase in coherence in TL and a decrease in coherence in Panx1a-KO larvae. All regions except for DM and OT in the Light-OFF condition changed coherence significantly.

MK-801 treatment in TL significantly increased coherence between the DM and OT in the Light-OFF condition but not in the Light-ON condition. This response was opposite to the

response detected in Panx1a-KO larvae, which showed a significant decrease in the Light-ON condition when comparing the DM and OT regions. When the DL and OT regions were compared, coherence in TL larvae was increased, whereas Panx1a-KO larvae showed a decrease in the lower frequency bands. No differences in the gamma-band of Panx1a-KO larvae in DL and OT recordings were observed.

MPTP treatment had a unique effect on both TL and Panx1a-KO larvae. The treatment with MPTP caused a significant decrease in coherence in TL larvae but increased coherence in Panx1a-KO larvae across the entire frequency range.

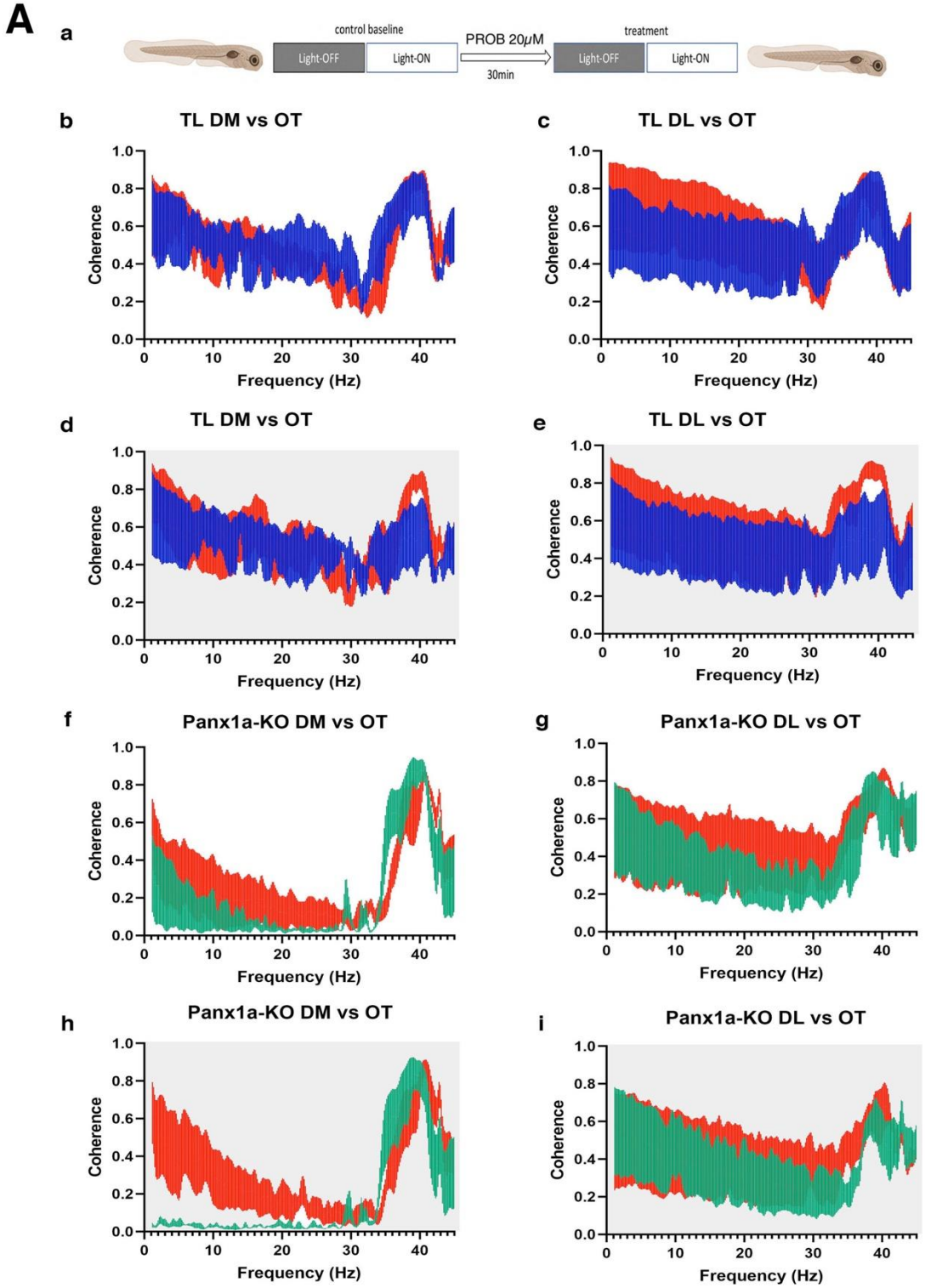
A
a
control baseline
Light-OFF
Light-ON
PROB 20μM
30min
treatment
Light-OFF
Light-ON
b
TL DM vs OT
c
TL DL vs OT
d
TL DM vs OT
e
TL DL vs OT
f
Panx1a-KO DM vs OT
g
Panx1a-KO DL vs OT
h
Panx1a-KO DM vs OT
i
Panx1a-KO DL vs OT
Coherence
Frequency (Hz)

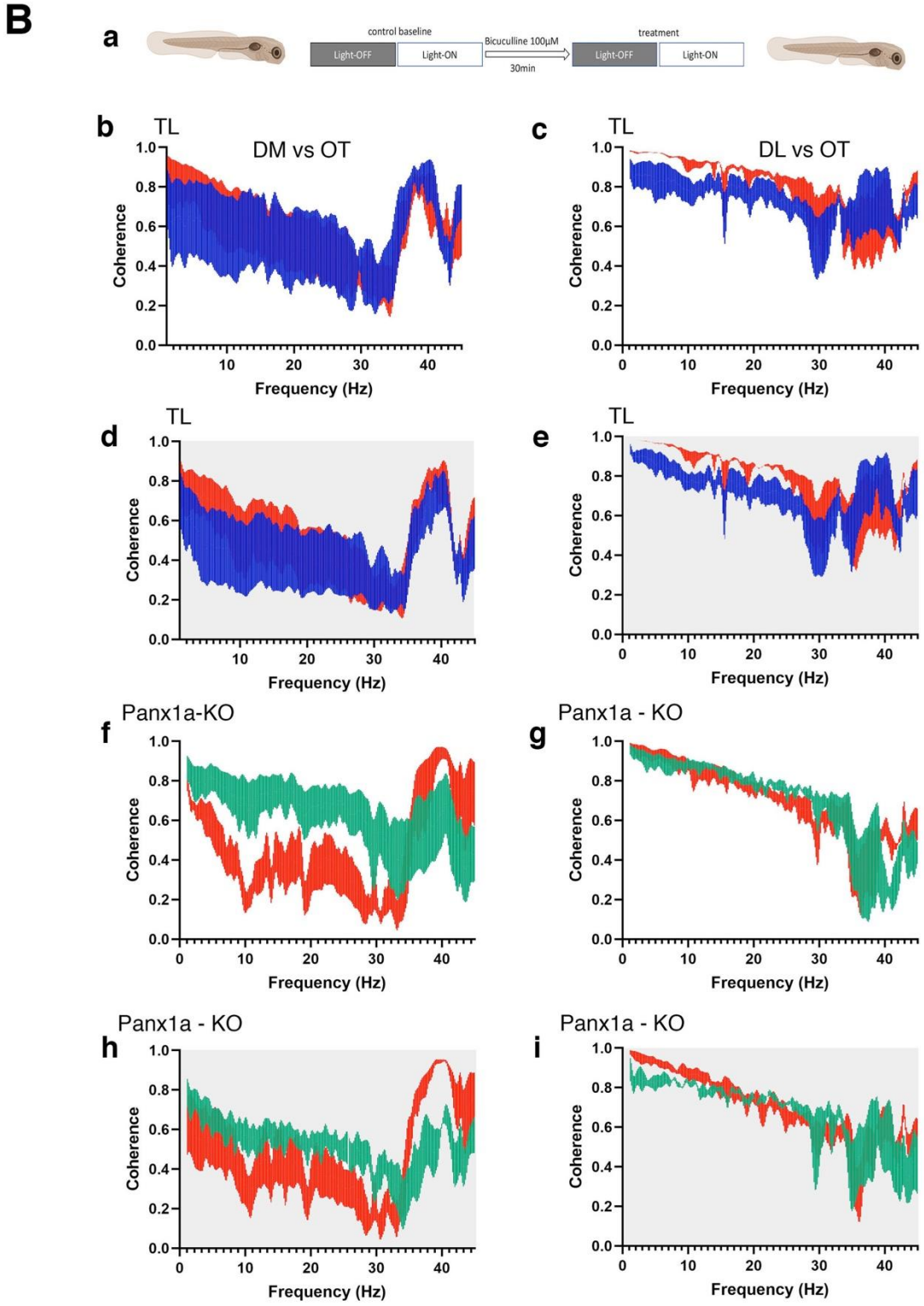
B
a
control baseline
Light-OFF
Light-ON
Bicuculline 100µM
30min
treatment
Light-OFF
Light-ON
b
TL
DM vs OT
c
TL
DL vs OT
d
TL
e
TL
f
Panx1a-KO
g
Panx1a - KO
h
Panx1a - KO
i
Panx1a - KO
Coherence
Frequency (Hz)

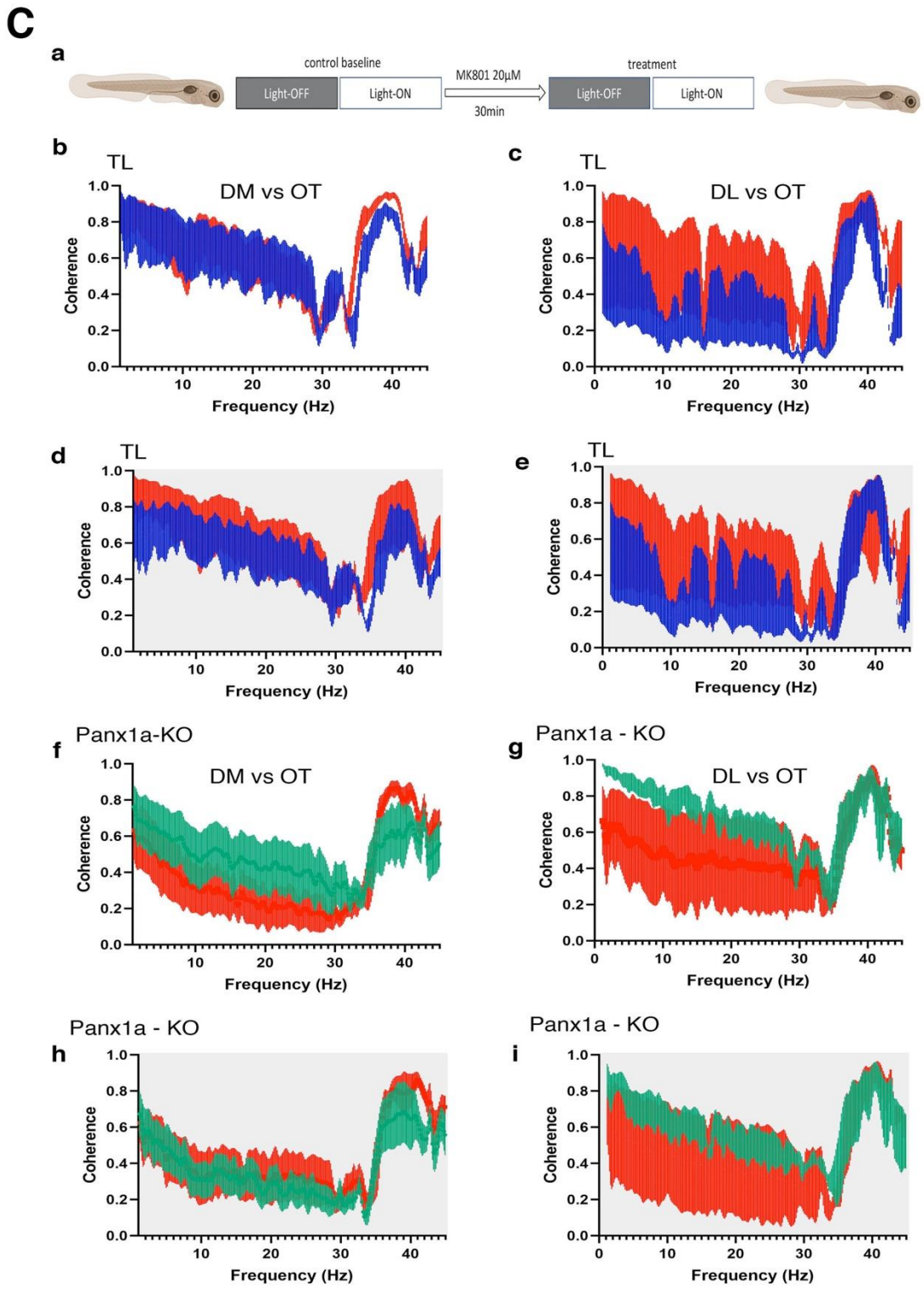
C
a
control baseline
Light-OFF
Light-ON
MK801 20µM
30min
treatment
Light-OFF
Light-ON
b
TL
DM vs OT
c
TL
DL vs OT
d
TL
e
TL
f
Panx1a-KO
DM vs OT
g
Panx1a - KO
DL vs OT
h
Panx1a - KO
i
Panx1a - KO
Coherence
Frequency (Hz)

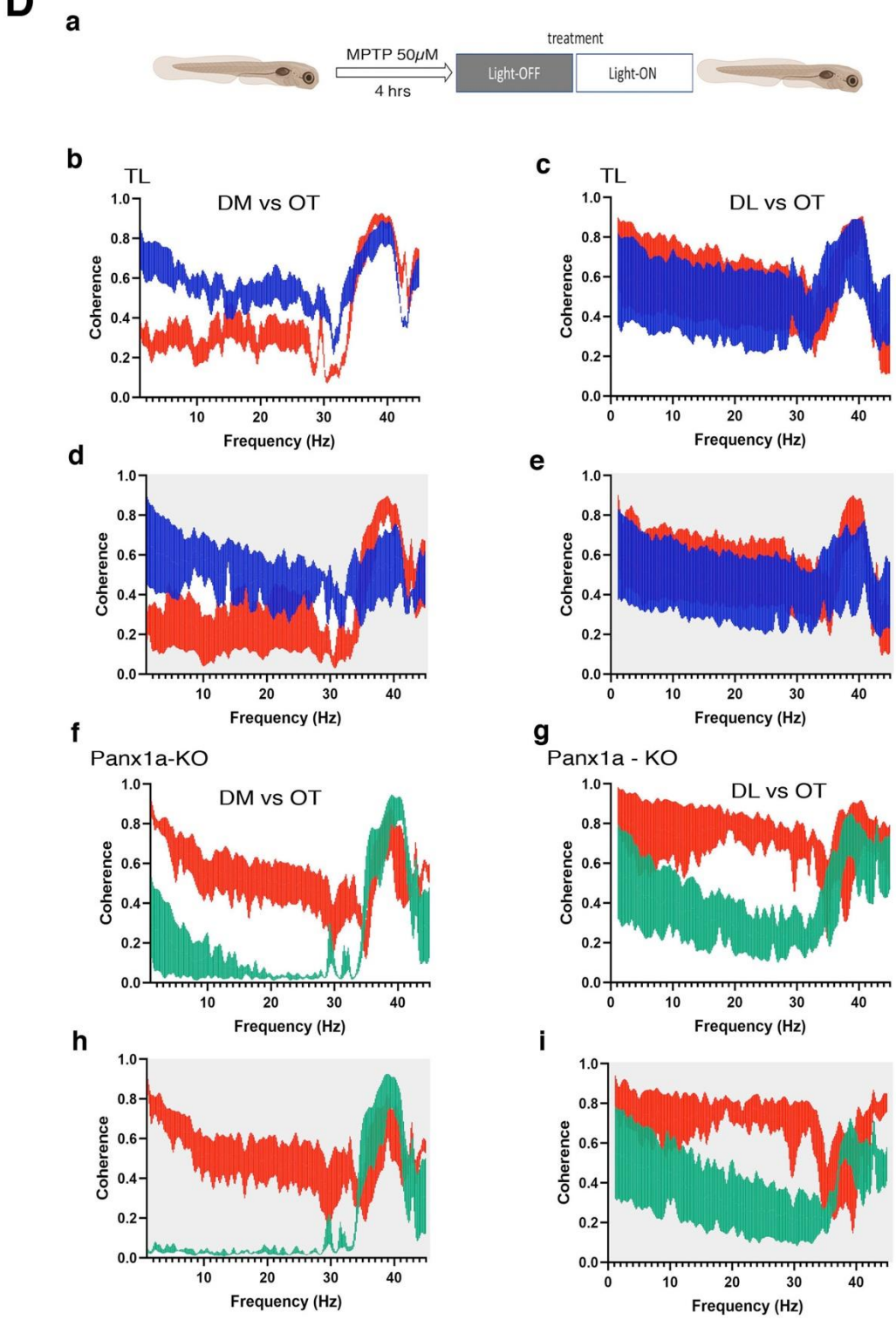
D
a
MPTP 50μM
4 hrs
treatment
Light-OFF
Light-ON
b
TL
DM vs OT
c
TL
DL vs OT
Coherence
Frequency (Hz)
d
e
f
Panx1a-KO
DM vs OT
g
Panx1a - KO
DL vs OT
h
i

Figure 21 A-D. Coherence analysis between the pallium and the optic tectum in the visual ascending pathway. *Danio rerio* larvae were tested between five to seven days old. The cartoons in A-D **a**) indicate the experimental paradigms used (Image generated with BioRender). Baseline (control) activities of larvae were recorded using Light-ON/OFF conditions followed by treatment for 30 minutes with probenecid (20µM), bicuculline (100µM), and MK-801 (20µM). After 30min, larvae were exposed again to Light-ON/OFF conditions. In the case of MPTP treatment, the larvae were incubated for four hours in the dark before recording. The coherence analysis shows DM and OT on the left (**b**, **d**, **f**, **h**) and DL and OT on the right (**c**, **e**, **g**, **i**). Baseline recordings are presented in blue/green, and post-drug treatments in red. The traces show average ± SEM.

A - Probenecid. **b-e**) Probenecid appears to have little effect on coherence in TL larvae in the lower frequencies. However, probenecid shows a trend of increasing coherence in the gamma band of TL larvae in the dark. **f-i**) Panx1a-KO larvae show a consistent effect of having increased coherence at lower frequencies but little incoherence in the gamma band**.** Statistics: n = 4 for TL and n = 4 for Panx1a-KO.

B - Bicuculline. **b-e**) BCC increased coherence in TL larvae in the lower frequencies. However, BCC treatment showed little coherence changes in TL larvae's gamma band. **f-i**) Panx1a-KO larvae show an opposite effect of having decreased coherence at lower frequencies and greater coherence in the gamma band**.** Statistics: n = 4 for TL, n = 4 for Panx1a-KO DM, and n = 3 for Panx1a-KO DL.

C - MK-801. **b-e**) MK-801 appears to have little effect on coherence in the DM/OT region in the lower frequencies, whereas in the DL/OT, larger changes are observed. MK-801 shows a trend of increasing coherence in the gamma band of TL larvae in the DM/OT region. **f-i**) MK-801 treatment generally caused a decrease in coherence in the lower frequency bands of the DM/OT and DL/OT. MK-801 increased coherence in the DM/OT region in the gamma band. Statistics: n = 4 for TL DM, n = 3 for TL DL, n = 5 for Panx1a-KO DM and n = 3 for Panx1a-KO DL.

D - MPTP. **b-e**) MPTP causes a significant decrease in coherence at the lower frequencies of the DM/OT. The coherence between DL/OT was only slightly increased post MPTP treatment at lower frequencies. MPTP causes an increase in the coherence of the gamma band **f-i**). Overall, MPTP treatment of Panx1a-KOs caused increased coherence at lower frequencies in all regions tested. The gamma-band appears to decrease after MPTP treatment generally. Statistics: n = 4 for TL and n = 4 for Panx1a-KO.

5.2.7 The comparison of coherence in TL and Panx1a-KOs revealed a complex relationship with drug treatments and light responses

The results of the coherence analysis were complex again, with each drug revealing distinct relationships between genotypes, light conditions, and tissues of interest. The coherence traces were split into the delta, theta, alpha, beta, and gamma frequencies to extract patterns. The extracted data were further analyzed using a 2-way ANOVA followed by Tukey's multiple comparisons. The P-values from this 2-way ANOVA were graphed as heat maps to visualize

whether stimuli and drugs had significant effects on coherence in the brain regions tested (**Figure 22; Statistical information see Supplementary Tables S21-24 in the Appendix**).

In the control and PROB-treated larvae, there were no significant changes in the coherence of the DM/OT of both TL and Panx1a-KO and the DL/OT of Panx1a-KO. The DL/OT of TL larvae showed more variability than the DM/OT both before and after treatment.

When TL and Panx1a-KO larvae were treated with BCC, the coherence between Light-ON and Light-OFF stimuli became more similar in the DM/OT regions. The coherence between the DL/OT regions became more different compared to the control conditions. MK-801 showed the opposite effect, where after treatment, coherence became more similar in the DL/OT region and less similar in the DM/OT regions.

MPTP treatment, in general, caused a significant difference in coherence compared to pre-treatment levels between the DM/OT and DL/OT regions of both TL and Panx1a-KO larvae.

We concluded that the genotypes did not determine the responses to BCC and MK-801 since both TL and Panx1a-KO larvae showed similar trends. However, the opposite trends in response to light stimuli caused by blocking GABAergic versus glutamatergic signaling suggested differences in the balance between excitation and inhibition in both DM and DL regions. In contrast, MPTP treatment was disruptive and caused decreases in the beta-band coherence of TL. MPTP treatment in Panx1a-KO caused increases in beta-band coherence.

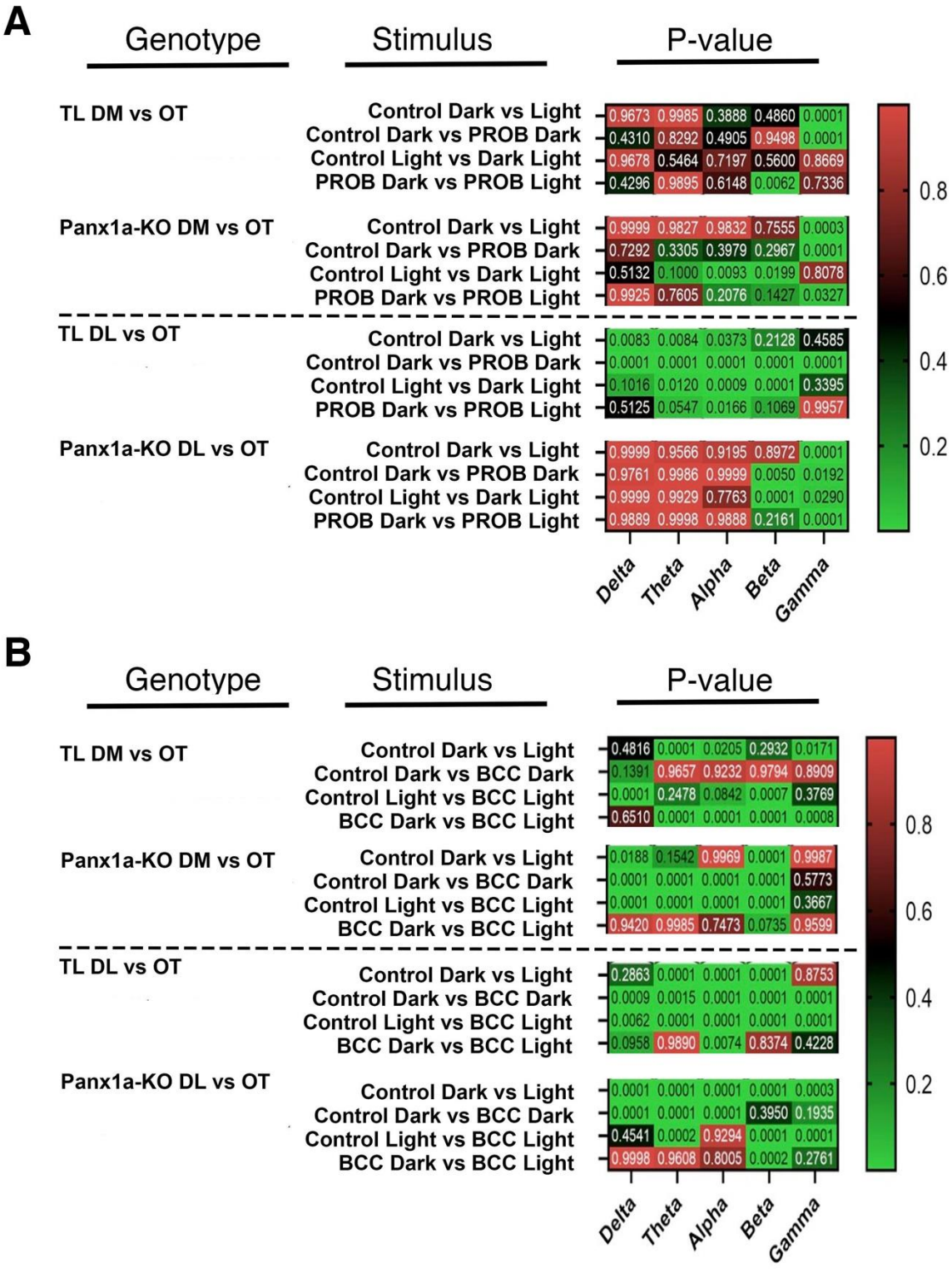
A
Genotype
Stimulus
P-value
TL DM vs OT
Control Dark vs Light 0.9673 0.9985 0.3888 0.4860 0.0001
Control Dark vs PROB Dark 0.4310 0.8292 0.4905 0.9498 0.0001
Control Light vs Dark Light 0.9678 0.5464 0.7197 0.5600 0.8669
PROB Dark vs PROB Light 0.4296 0.9895 0.6148 0.0062 0.7336
Panx1a-KO DM vs OT
Control Dark vs Light 0.9999 0.9827 0.9832 0.7555 0.0003
Control Dark vs PROB Dark 0.7292 0.3305 0.3979 0.2967 0.0001
Control Light vs Dark Light 0.5132 0.1000 0.0093 0.0199 0.8078
PROB Dark vs PROB Light 0.9925 0.7605 0.2076 0.1427 0.0327
TL DL vs OT
Control Dark vs Light 0.0083 0.0084 0.0373 0.2128 0.4585
Control Dark vs PROB Dark 0.0001 0.0001 0.0001 0.0001 0.0001
Control Light vs Dark Light 0.1016 0.0120 0.0009 0.0001 0.3395
PROB Dark vs PROB Light 0.5125 0.0547 0.0166 0.1069 0.9957
Panx1a-KO DL vs OT
Control Dark vs Light 0.9999 0.9566 0.9195 0.8972 0.0001
Control Dark vs PROB Dark 0.9761 0.9986 0.9999 0.0050 0.0192
Control Light vs Dark Light 0.9999 0.9929 0.7763 0.0001 0.0290
PROB Dark vs PROB Light 0.9889 0.9998 0.9888 0.2161 0.0001
Delta
Theta
Alpha
Beta
Gamma
0.8
0.6
0.4
0.2
B
Genotype
Stimulus
P-value
TL DM vs OT
Control Dark vs Light 0.4816 0.0001 0.0205 0.2932 0.0171
Control Dark vs BCC Dark 0.1391 0.9657 0.9232 0.9794 0.8909
Control Light vs BCC Light 0.0001 0.2478 0.0842 0.0007 0.3769
BCC Dark vs BCC Light 0.6510 0.0001 0.0001 0.0001 0.0008
Panx1a-KO DM vs OT
Control Dark vs Light 0.0188 0.1542 0.9969 0.0001 0.9987
Control Dark vs BCC Dark 0.0001 0.0001 0.0001 0.0001 0.5773
Control Light vs BCC Light 0.0001 0.0001 0.0001 0.0001 0.3667
BCC Dark vs BCC Light 0.9420 0.9985 0.7473 0.0735 0.9599
TL DL vs OT
Control Dark vs Light 0.2863 0.0001 0.0001 0.0001 0.8753
Control Dark vs BCC Dark 0.0009 0.0015 0.0001 0.0001 0.0001
Control Light vs BCC Light 0.0062 0.0001 0.0001 0.0001 0.0001
BCC Dark vs BCC Light 0.0958 0.9890 0.0074 0.8374 0.4228
Panx1a-KO DL vs OT
Control Dark vs Light 0.0001 0.0001 0.0001 0.0001 0.0003
Control Dark vs BCC Dark 0.0001 0.0001 0.0001 0.3950 0.1935
Control Light vs BCC Light 0.4541 0.0002 0.9294 0.0001 0.0001
BCC Dark vs BCC Light 0.9998 0.9608 0.8005 0.0002 0.2761
Delta
Theta
Alpha
Beta
Gamma
0.8
0.6
0.4
0.2

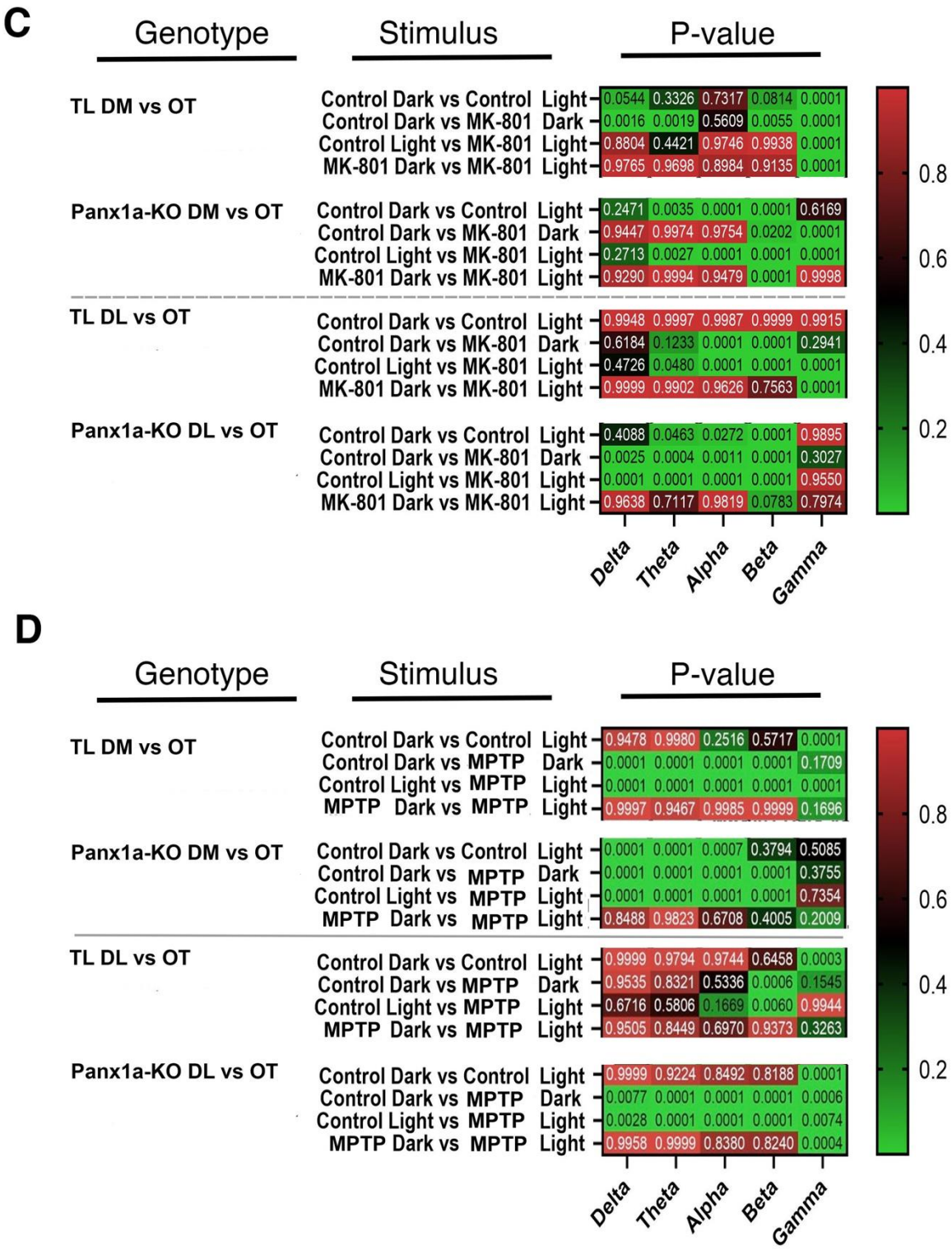
C
Genotype
Stimulus
P-value
TL DM vs OT
Control Dark vs Control Light 0.0544 0.3326 0.7317 0.0814 0.0001
Control Dark vs MK-801 Dark 0.0016 0.0019 0.5609 0.0055 0.0001
Control Light vs MK-801 Light 0.8804 0.4421 0.9746 0.9938 0.0001
MK-801 Dark vs MK-801 Light 0.9765 0.9698 0.8984 0.9135 0.0001
Panx1a-KO DM vs OT
Control Dark vs Control Light 0.2471 0.0035 0.0001 0.0001 0.6169
Control Dark vs MK-801 Dark 0.9447 0.9974 0.9754 0.0202 0.0001
Control Light vs MK-801 Light 0.2713 0.0027 0.0001 0.0001 0.0001
MK-801 Dark vs MK-801 Light 0.9290 0.9994 0.9479 0.0001 0.9998
TL DL vs OT
Control Dark vs Control Light 0.9948 0.9997 0.9987 0.9999 0.9915
Control Dark vs MK-801 Dark 0.6184 0.1233 0.0001 0.0001 0.2941
Control Light vs MK-801 Light 0.4726 0.0480 0.0001 0.0001 0.0001
MK-801 Dark vs MK-801 Light 0.9999 0.9902 0.9626 0.7563 0.0001
Panx1a-KO DL vs OT
Control Dark vs Control Light 0.4088 0.0463 0.0272 0.0001 0.9895
Control Dark vs MK-801 Dark 0.0025 0.0004 0.0011 0.0001 0.3027
Control Light vs MK-801 Light 0.0001 0.0001 0.0001 0.0001 0.9550
MK-801 Dark vs MK-801 Light 0.9638 0.7117 0.9819 0.0783 0.7974
Delta
Theta
Alpha
Beta
Gamma
0.8
0.6
0.4
0.2
D
Genotype
Stimulus
P-value
TL DM vs OT
Control Dark vs Control Light 0.9478 0.9980 0.2516 0.5717 0.0001
Control Dark vs MPTP Dark 0.0001 0.0001 0.0001 0.0001 0.1709
Control Light vs MPTP Light 0.0001 0.0001 0.0001 0.0001 0.0001
MPTP Dark vs MPTP Light 0.9997 0.9467 0.9985 0.9999 0.1696
Panx1a-KO DM vs OT
Control Dark vs Control Light 0.0001 0.0001 0.0007 0.3794 0.5085
Control Dark vs MPTP Dark 0.0001 0.0001 0.0001 0.0001 0.3755
Control Light vs MPTP Light 0.0001 0.0001 0.0001 0.0001 0.7354
MPTP Dark vs MPTP Light 0.8488 0.9823 0.6708 0.4005 0.2009
TL DL vs OT
Control Dark vs Control Light 0.9999 0.9794 0.9744 0.6458 0.0003
Control Dark vs MPTP Dark 0.9535 0.8321 0.5336 0.0006 0.1545
Control Light vs MPTP Light 0.6716 0.5806 0.1669 0.0060 0.9944
MPTP Dark vs MPTP Light 0.9505 0.8449 0.6970 0.9373 0.3263
Panx1a-KO DL vs OT
Control Dark vs Control Light 0.9999 0.9224 0.8492 0.8188 0.0001
Control Dark vs MPTP Dark 0.0077 0.0001 0.0001 0.0001 0.0006
Control Light vs MPTP Light 0.0028 0.0001 0.0001 0.0001 0.0074
MPTP Dark vs MPTP Light 0.9958 0.9999 0.8380 0.8240 0.0004
Delta
Theta
Alpha
Beta
Gamma
0.8
0.6
0.4
0.2

Figure 22 A-D. The comparison of changes in coherence between the DM/OT region and DL/OT region after drug treatment. The coherence between the DM/OT and DL/OT was analyzed using NeuroExplorer. The delta (0.5-3Hz), theta (3-7Hz), alpha (7-12Hz), beta (12-30Hz), and gamma (30-45Hz) frequency bands were separated and analyzed before and after treatment. Differences and significances were calculated using GraphPad Prism using a 2-Way ANOVA with Tukey's multiple comparison analysis. Heat maps were created in GraphPad Prism based on P-values. Scale bars indicate no significance (red) to high significance (green).

A - Probenecid. Statistics: n = 4 for TL and n = 4 for Panx1a-KO.

B - Bicuculline. Statistics: n = 4 for TL, n = 4 for Panx1a-KO DM, and n = 3 for Panx1a-KO DL.

C - MK-801. Statistics: n = 4 for TL DM, n = 3 for TL DL, n = 5 for Panx1a-KO DM and n = 3 for Panx1a-KO DL.

D - MPTP. Statistics: n = 4 for TL and n = 4 for Panx1a-KO.

5.3 Behavioral phenotyping of zebrafish larvae

5.3.1 Inhibition of the NLRP3 inflammasome improves the MPTP-induced zebrafish swimming behavior

The effects of MPTP treatment and loss of Panx1a on the behavioral phenotype were investigated using behavioral assays. In Sections 5.1.3 and 5.1.4, we showed evidence that the NLRP3 inflammasome was regulated in the acute MPTP zebrafish model. As shown in **Figure 23a**, the NLRP3 inflammasome assembly triggers caspase activation and interleukin-1β (IL-1β) signaling, eventually leading to cell death. Indirect activation pathways via NF-kB and MAPK signaling or canonical and non-canonical activation are known. The drugs CY-09, INF39, MCC950, and dexamethasone are inhibitors that target these pathways. Here they were used in the context of effects on behavioral phenotypes. When the visual system was stimulated, the evoked swimming behavior was quantified by automatic locomotion tracking. We exploited that in a modified VMR test during a period of 20 minutes in a Light-OFF phase (0 lux), the swimming behavior of larvae was reduced to a minimum. When light intensity was ramped up

stepwise from 0 to 1600 lux during a Light-ON phase, larvae resumed swimming without showing a startle and freeze response, as demonstrated by Safarian et al. (2020).

In untreated larvae, the TL moved 25.57 ± 0.48mm and the Panx1a-KO moved 21.12 ± 0.45mm. As shown by Estimation Plots (**Figure 23**), the application of the drugs CY-09 (TL = 14.12 ± 0.46mm; Panx1a-KO = 14.58 ± 0.44mm), INF39 (TL = 21.76 ± 0.95mm; Panx1a-KO = 7.028 ± 0.59mm), and dexamethasone (Panx1a-KO = 16.54 ± 0.78mm) to TL and Panx1a-KO larvae caused a significant decrease in the total distance travelled (**Statistical information see Supplementary Tables S27-30 in the Appendix**). MCC950 significantly (P-value = 0.0002) improved the behavioral phenotype of TL larvae compared to untreated conditions (TL control = 25.57 ± 0.48 mm; TL-MCC950 28.89 ± 0.90mm; per 10 seconds).

MPTP treatment reduced swimming behavior in both TL and Panx1a-KO larvae (TL = 14.29 ± 0.74mm; Panx1a-KO = 8.84 ± 0.70mm). INF-39, in combination with MPTP, caused a significant rescue (18.57 ± 0.49mm) of the MPTP-induced phenotype in TL larvae (**Figure 23c**). The average distance significantly increased when INF-39 was combined with MPTP. In Panx1a-KO larvae, the INF-39 treatment combined with MPTP did not cause any significant improvement.

Combination treatments with MPTP and CY-09, MCC950, or dexamethasone did not significantly improve swimming behavior (**Figure 23b,d-f,h,i**). These drugs either worsened the behavioral phenotype or had no significant effect compared to larvae treated only with MPTP. Some drugs, like dexamethasone (Panx1a-KO = 10.34 ± 0.48mm), MCC950 (TL = 15.84 ± 0.69mm) and CY-09 (9.52 ± 0.34mm) increased the distance travelled, but the effect was not statistically significantly.

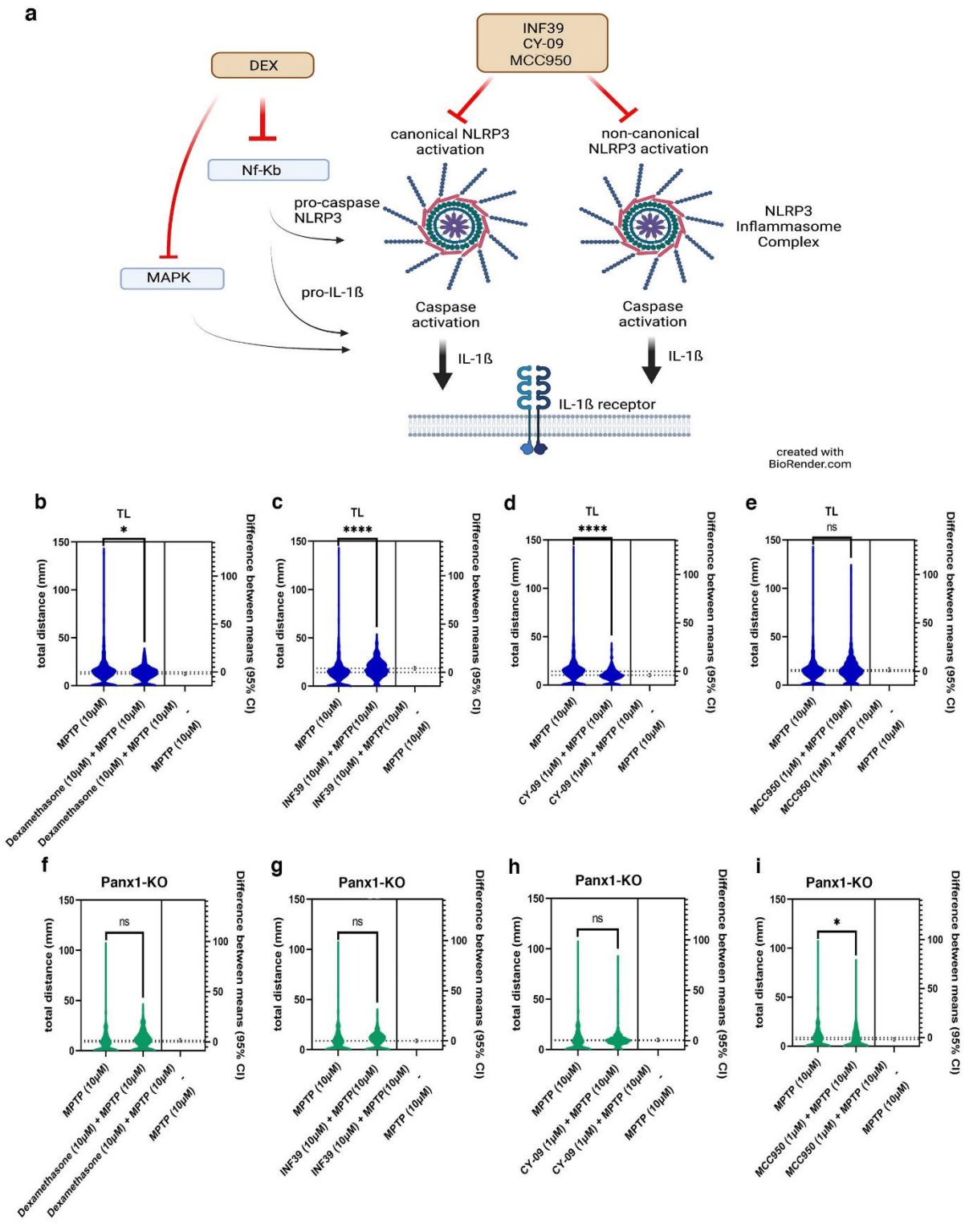
a
INF39
CY-09
MCC950
DEX
canonical NLRP3 activation
non-canonical NLRP3 activation
Nf-Kb
pro-caspase NLRP3
NLRP3 Inflammasome Complex
MAPK
pro-IL-1ß
Caspase activation
Caspase activation
IL-1ß
IL-1ß
IL-1ß receptor
created with BioRender.com
b
TL
*
c
TL
****
d
TL
****
e
TL
ns
total distance (mm)
Difference between means (95% CI)
MPTP (10µM)
Dexamethasone (10µM) + MPTP (10µM)
INF39 (10µM) + MPTP(10µM)
CY-09 (1µM) + MPTP (10µM)
MCC950 (1µM) + MPTP (10µM)
f
Panx1-KO
ns
g
Panx1-KO
ns
h
Panx1-KO
ns
i
Panx1-KO
*

Figure 23. The effect of inflammasome inhibitors on the swimming behavior of MPTP treated larvae.

a) Overview of the activation of the NLRP3 inflammasome. The NLRP3 inflammasome formation leads to caspase activation. Caspase activation leads to the secretion of pro-inflammatory cytokines such as IL-1β. IL-1β binds receptors on the cell surface, which leads to cell death. INF-39, CY-09, and MCC950 inhibit the formation of the NLRP3 inflammasome. Dexamethasone inhibits the MAPK and NF-kB pathways which play a role in NLRP3 complex formation and IL-1β signaling.

b-i) Zebrafish larvae were incubated with MPTP and inflammasome inhibitors (Dexamethasone, INF-39, CY-09, and MCC950) for four hours prior to testing. During this period, larvae were placed in a 48-well plate and incubated at 28ºC in the water-heated chamber of the Zebrabox. Larvae were exposed to the "light ramp" assay, where they were exposed to a 0% light stimulus (Light-OFF) condition for 20 minutes. Afterward, the light was ramped up by 10% (400 lux) every 10 minutes up to a maximum of 40% (1600 lux). The total distance traveled by each larva was video recorded and quantified in millimeters (mm) with the help of the Fast Data Monitor software (ViewPoint). TL larvae are at the top in blue and Panx1a-KO larvae are at the bottom in green. The distance traveled was determined between 2100-2300 seconds. In this period, larvae are exposed to a light intensity of 800 lux before swimming behavior starts to plateau at 1200 lux. Significance was calculated using a Welch's t-test, estimation analysis (95% CI), and visualized by estimation plots. Ns stands for no significant differences. The number of larvae tested for each genotype and drug treatment were: MPTP (n=20), dexamethasone (n=16), INF-39 (n=20), CY-09 (n=20) and MCC950 (n=16). Untreated controls (n=20).

5.3.2 Compounds with anti-inflammatory activity did not improve the MPTP-induced phenotype

Compounds with anti-inflammatory activity were tested using the light ramp assay in combination with the MPTP model (**Figure 24**). After MPTP treatment, the larvae were treated with metformin, caffeine, and adenosine to determine whether anti-inflammatory drugs could improve the behavioral phenotype. Metformin has been shown to exhibit anti-inflammatory actions in addition to the known antihyperglycemic effects (Nasri & Rafieian-Kopaei, 2014). Caffeine and adenosine have been reported to diminish inflammation. In the experimental paradigm, all drugs did not improve the MPTP-induced swimming behavior in both TL or

Panx1a-KO larvae. Caffeine (9.84 ± 0.23mm) was the only compound that increased the behavioral phenotype, but the effect was not statistically significant in Panx1a-KO larvae (**Statistical information see Supplementary Tables S25, 26 and 31 in the Appendix**).

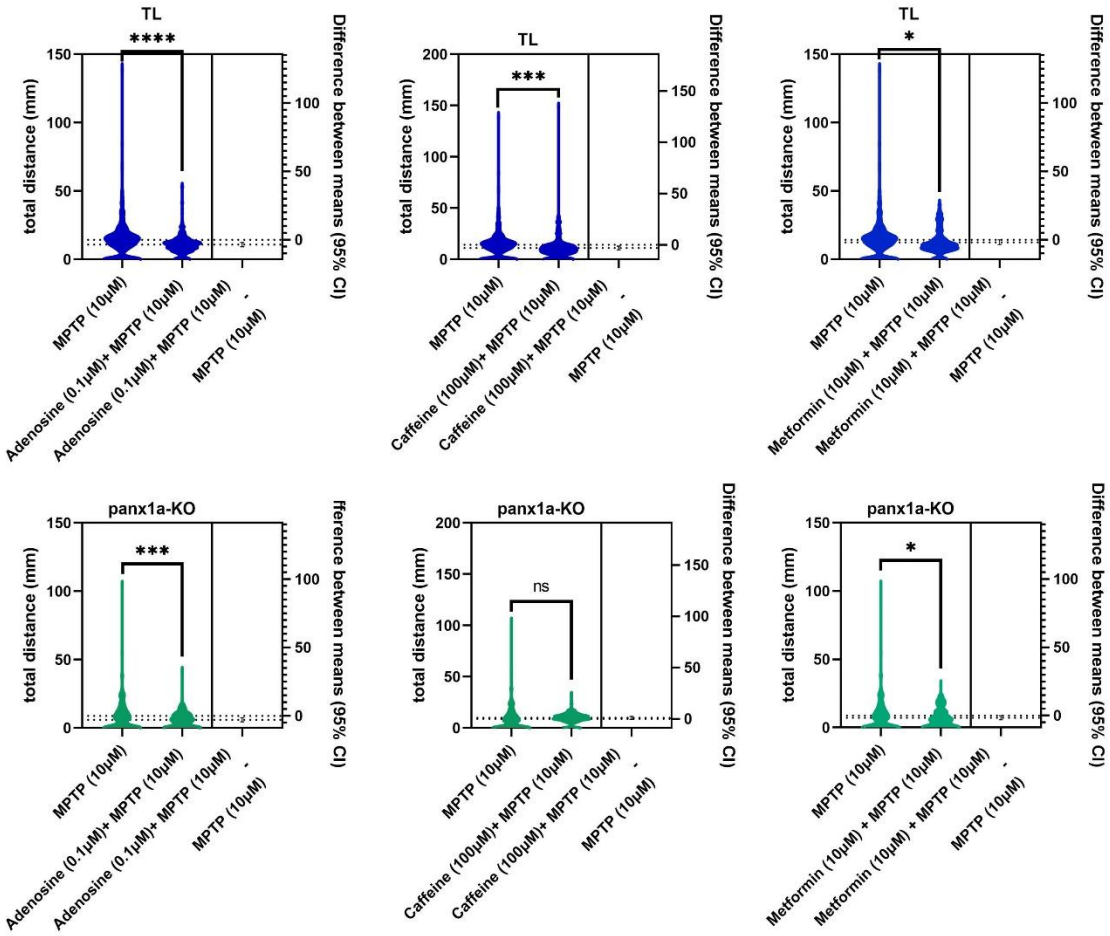

Figure 24. The effect of general inflammation inhibitors on the MPTP-induced phenotype. Zebrafish larvae were incubated with MPTP and inflammation inhibitors (Adenosine, caffeine, and metformin) for four hours prior to testing. The larvae were placed in 48-well plates and inserted into the water-heated chamber of the Zebrabox. Larvae were exposed to a light ramp assay where they were exposed to a 0% light stimulus (Light-OFF) condition for 20 minutes. Afterward, the light was ramped up by 10% for every 10 minutes up to a maximum of 40%. The total distance traveled by the larvae was quantified in millimeters (mm) with the help of Fast Data Monitor (ViewPoint). TL larvae are at the top in blue and Panx1a-KO larvae are at the bottom in green. The distance traveled was determined between 2100-2300 seconds. In this period, larvae are exposed to a light intensity of 800 lux, which is favorable for swimming behavior. Significance was calculated using a Welch's t-test and visualized with estimation plots. Ns stands for no significant differences. N=20 for all treatment conditions.

6. Discussion

A role of Panx1 channels in Parkinson's disease has been proposed, but the evidence is limited to very few reports. To address this knowledge gap, molecular, electrophysiological, and behavioral changes of wild-type TL and Panx1a-KO zebrafish larvae were tested after acute treatment with MPTP. A transcriptome analysis validated a broad regulation of metabolic processes, including those affecting mitochondrial health or causing inflammation. Using a two-electrode protocol, the simultaneous recording of local field potentials in separate brain regions showed that acute MPTP treatment caused dissonance in the visual ascending pathway. Finally, we found evidence that Panx1a is not a risk factor for the early stages of Parkinson's disease. Therefore, the evidence presented in this thesis disproved our initial hypothesis. Instead, the loss of function of this ATP-release channel enhances the severity of the MPTP induced phenotype.

6.1 MPTP treatment induces metabolic stress and causes inflammation in the acute MPTP model of Parkinson’s

Panx1 expression and action have been closely tied to ATP release. MPTP treatment selectively affects ATP production in animal models by binding Complex I of the ETC (Aras et al., 2014; Richardson et al., 2007). The typical experimental models use MPTP for chronic administration, from 24 hours to several months (Bashirzade, Cheresiz, Belova, Drobkov, Korotaeva, Azizi-Arani, et al., 2022; Muñoz-Manchado et al., 2016). Acute models of MPTP exposure for four hours have been used in cell culture and a mouse model (Di et al., 2019; Nyitrai et al., 1997). However, to our knowledge, acute MPTP models in zebrafish have not been reported. Therefore, showing that the acute treatment with MPTP affected larvae causing a PD-like phenotype was a critical proof of principle requirement.

We demonstrate that treatment with MPTP for four hours caused significant changes on a molecular level. MPTP treatment caused the expected effects of metabolic stress in the RNA-seq data due to its inhibition of the ETC. Furthermore, the expression of genes regulated in PD pathways were significantly regulated in both TL and Panx1a-KO larvae after acute MPTP treatment. The ATP assay also highlighted the effect of MPTP as ATP levels in the extracellular space were significantly reduced in TL larvae. This reduction was similar to the reduction caused by loss of Panx1a channel function alone, as well as the reduction found in an epilepsy model (Whyte-Fagundes et al., 2022). This suggests that a lower limit for extracellular ATP concentration exists, which can be induced by affecting ATP production through MPTP treatment or ATP release by blocking Panx1. Since this limit was within the detection range of our ATP assay, we concluded that this result was not due to technical constraints.

In addition to metabolic stress, the MPTP treatment also modulated inflammatory pathways. The STRING analysis highlighted the regulation of the MAPK, NF-κB, and cell death pathways. MPTP treatment also caused significant up-regulation of inflammasome genes tested by RT-qPCR. The regulated genes represented modulators of the inflammasome. The activation of the NLRP3 inflammasome is highly regulated by both MAPK and NF-κB pathways (Bauernfeind et al., 2009; Boaru et al., 2015; D. Li et al., 2018). The NLRP3 inflammasome is activated by external triggers such as mitochondrial dysfunction and reactive oxygen species (Kelley et al., 2019). Regulation of the NLRP3 inflammasome has also been linked to PD as it was up-regulated in PD patients (Anderson et al., 2021).

Among the downregulated genes found by RT-qPCR was GSDME. This gene is a member of the gasdermin protein family, which mediates programmed cell death, including apoptosis and pyroptosis (Wang et al., 2021). GSDME mediated pyroptosis contributes to tissue

damage and pathological inflammations. Therefore, inhibiting GSDME mediated pyroptosis is discussed as a potential target for ameliorating inflammatory conditions (Liao et al., 2022; G. Luo et al., 2022). Here, GSDME was down-regulated in the RT-qPCR data of TL larvae. In conditions with low GSDME expression, only cytokine release happens. High GSDME levels lead to cell death and cytokine release (Zhou & Abbott, 2021). Therefore, the observed down-regulation of GSDME might represent a neuroprotective mechanism protecting neurons from cell death in TL, but not Panx1a-KO larvae.

When looking past the molecular level, the larvae also showed an altered behavioral phenotype when acute MPTP treatment caused a significant decrease in the distance traveled by zebrafish larvae. A similarly reduced locomotion phenotype has also been reported in chronic MPTP models (Abolarin et al., 2022; Kalyn & Ekker, 2021). Together results of the study provide evidence for the validity of the acute MPTP protocol to investigate neuroinflammation and early stages of PD in zebrafish larvae.

6.2 MPTP treatment causes dissonance in the visual ascending pathway

Previous PD work showed that a prominence map in the intermediate layer of the superior colliculus couples action and perception through modulation of attention (Pretegiani et al., 2019). A failure of this network increases abnormal basal ganglia output and can cause visual and visual-motor deficits observed in PD. PD also has effects on the amygdala and hippocampus; PD patients show reduced amygdala volume and increased anxiety and hippocampal dysfunctions (Camicioli et al., 2003; Diederich et al., 2020; Dissanayaka et al., 2014; Tanner et al., 2017).

LFP recordings have been used to shed light on the pathophysiology of movement disorders and they may lead to the discovery or refinement of treatments (Thompson et al., 2014). Here, the gamma-band was selected for analysis as it is the fastest frequency below 100Hz and produces a distinct peak in the zebrafish larva during single-electrode LFP recordings (Safarian et al., 2020). Gamma waves represent the firing of different nerve cells to execute cognitive or motor actions (Satapathy et al., 2019). Disorders such as Parkinson's, Alzheimer's, and epilepsy have modulations in the gamma-band (Hughes, 2008; van Deursen et al., 2008). Usually, a decrease in gamma-band power, as well as coherence, have been affected in PD patients (Cao & Hu, 2016; Muthuraman et al., 2020).

This study showed a decrease in average gamma-band power in TL and Panx1a-KO larvae which is typical in PD patients. The only region that had an increase in average gamma band power, as well as an increase in peak frequency, was the OT of TL larvae. This increase may reflect that dopaminergic neurons, the cell type most responsive to MPTP, are present in the DM and DL regions but not the OT (Du et al., 2016). Therefore, the MPTP treatment may not affect the OT as much as in the other two regions. Other research also suggests that increasing gamma-band oscillations may act as compensatory mechanisms, improving the PD symptoms such as bradykinesia and restoring plasticity in the motor cortex (Guerra et al., 2020; Muralidharan et al., 2017; Muthuraman et al., 2020). In humans, this is achieved using external manipulation through deep brain stimulation, which has been shown to be very effective in improving motor function (Krack et al., 2003; Limousin et al., 1998).

The beta-band has also been ascribed an important role in PD as it is modulated in human patients (Bronte-Stewart et al., 2009; Little & Brown, 2014; Timmermann & Florin, 2012). Upregulation of the beta-band in PD has been linked to bradykinesia and rigidity. The degree of

beta-band suppression has been correlated with improvements in motor symptoms of PD patients (Tinkhauser et al., 2017).

Aside from the well-studied effect of PD on motor systems, there is a paucity of data investigating the cognitive deficits seen in PD patients. In healthy study participants, beta power decreases when episodic memory is formed (MacDonald et al., 2019). This episodic memory formation is inhibited in PD patients, which correlated with increases in beta power. In this study, zebrafish larvae had increased beta-band activity after MPTP treatment in both the DM and DL of TL and all three regions of Panx1a-KO.

In the zebrafish, the anterior DL region is considered a hippocampus-like anatomical structure of the pallium, the fish's forebrain, because this region displays high spontaneous neural activity embedded with fast ripple oscillations (above 100Hz) in the adult (Vargas et al., 2012). Zebrafish display episodic-like memory as they remember what object they saw, where they saw it, and on which occasion it was presented (Hamilton et al., 2016). In humans, episodic memory is associated with the hippocampus and large-scale networks, a property that is diminished in PD patients.

The DM region is located in the dorsomedial portion of the zebrafish pallium and considered as the homolog of the basolateral/lateral mammalian amygdala (Maximino et al., 2013). The structure is relevant for processing fear-related stimuli in the fish (Assad et al., 2020; Lal & Kawakami, 2022; von Trotha et al., 2014). Anxiety is frequent in PD patients and has a negative impact on disease symptoms and quality of life. The underlying mechanisms remain largely unknown, but evidence for alterations to the volume, shape, and texture of the amygdala, the cortical thickness as well as the functional connectivity (FC) of the fear circuit in PD patients with and without clinically relevant anxiety has been noted (Carey et al., 2021). Based on the

data presented here and the known roles of DM and DL, we propose to test in the future the hypothesis that an increase in beta-band power during memory encoding would be diminished in the acute MPTP model and that this would interfere with episodic memory formation and anxiety in the fish.

Consistently, we found that the OT region of TL had an opposite effect after MPTP treatment compared to the two other brain regions, where there was a decrease in average beta-band activity. In both the gamma- and beta-band, the presence of Panx1a in wild-type larvae appeared to make a difference in how the OT reacted to the metabolic stress induced by MPTP. We can only speculate about the underlying mechanisms. It is well documented that the optic tectum of larval zebrafish plays essential roles in processes by which tectal circuits receive and process retina-derived visual information (Heap et al., 2018; Suzuki et al., 2019). It is also worth noting that different from the DL and DM regions, both visual-motor and visual-sensory processes converge at the OT. The complex connections of the OT with deeper brain structures such as the thalamus and hypothalamus, as well as distinct molecular and cellular compositions of each region most likely contribute to the distinct responses seen in the OT after MPTP treatment.

Coherence between different brain regions is also affected in PD. PD patients have increased beta-band synchronization compared to healthy controls (Ahn et al., 2019; George et al., 2013; Schwerdt et al., 2022). Dopaminergic activity, which is lost in PD patients, usually limits uncontrolled beta-band synchronization (Mallet et al., 2008). MPTP treatment selectively initiates processes that destroy dopaminergic neurons. This effect was prominent in TL larvae which showed a decrease in the coherence of the beta-band between the DM/OT and an increase

between DL/OT. In Panx1a-KO, both the DM/OT and DL/OT had increased beta-band synchronization after MPTP treatment.

TL, which express Panx1a, performed better and had increased gamma- and decreased beta-band activity in the OT as well as a decreased beta-band coherence between the DM and OT regions. The characterization of the visual-sensory system should be followed up in the future using a similar approach to investigate the coherence between OT and the visuomotor system. It will be interesting to introduce more complex stimuli, such as moving gratings or prey/predator stimuli to evoke robust electrophysiological responses and locomotion.

6.3 Panx1a is not a risk factor for the early stages of Parkinson's disease

Pannexin1 has been ascribed roles in inflammation, PD, and other neurodegenerative disorders (Crespo et al., 2017; Frederiksen et al., 2019; Ortiz & Puebla, 2020). The role of Panx1 in PD appears to be due to the channels' involvement in inflammatory processes, most likely by sending "find-me" signals when ATP is released where neurons undergo apoptosis or forms of lytic cell death such as "pyroptosis" (Chekeni et al., 2010; Chen et al., 2020).

It has been recently demonstrated that mouse Panx1 and zebrafish Panx1a are risk factors for the severity of epileptic seizures (Aquilino et al., 2020; Whyte-Fagundes et al., 2022). The loss of Panx1, Panx1a, or the pharmacological inhibition of Panx1 channels in mice and fish with probenecid reduced seizure activities. Due to the detrimental role of Panx1a in epilepsy and other diseases, Panx1a was considered a risk factor for PD (Frederiksen et al., 2019). However, in this research, the opposite was found; Panx1a-KO larvae performed worse than wild-type TL in all categories tested, from molecular to systems, to behavior. This difference may be due to Panx1a's role in inflammation. Panx1 promotes the activation of inflammatory processes, such as

the activation of the NLRP3 inflammasome (Chen et al., 2020). The NLRP3 inflammasome has been identified as a player in the pathogenesis of PD and a potential target for treatment (Haque et al., 2020; Holbrook et al., 2021; Yan et al., 2020). In this thesis, the NLRP3 inflammasome was inhibited with several drugs to rescue the MPTP-induced phenotype. INF39, a selective NLRP3 inflammasome inhibitor, was able to rescue the MPTP-induced behavioral phenotype in TL larvae, but not Panx1a-KO (Shi et al., 2021). This difference may be due to the presence of Panx1a channels and the selective inhibition of the NLRP3 inflammasome protecting the TL larvae that INF39 alone cannot do.

The lack of rescue of the MPTP-induced phenotype by the other inflammasome blockers is interesting. MCC950 has been reported to alleviate canonical and non-canonical NLRP3 inflammasome activation of the inflammatory response *in vitro* and improves functional recovery in the acute mouse model of spinal cord injury (Jiao et al., 2020). Another research group determined that CY-09 is an effective and direct inhibitor of NLRP3, which showed significant inhibition of NLRP3 inflammasome *in vivo* in mice models and *ex vivo* in human cells (Jiang et al., 2017). Why do these blockers not show any rescue effect despite the effectiveness of these drugs on the NLRP3 inflammasome? Since the blockers target different domains of the NLRP3 inflammasome, it is possible that the drug efficacy of some blockers is affected by the molecular interaction of Panx1a with the inflammasome.

6.4 Points of consideration and limitations of this study

This thesis shows that the presence of Panx1a was beneficial in early stages of an MPTP induced PD-like phenotype. The opposite happens in zebrafish and mouse models of epileptic seizures where loss of Panx1 reduced seizures (Penuela et al., 2014; Whyte-Fagundes et al.,

2022). It is noteworthy that in humans, PD patients rarely have epilepsy, whereas epilepsy patients rarely have PD (Feddersen et al., 2014; Son et al., 2016). Future studies will have to address the molecular and cellular mechanisms which cause the opposite effects. The question is timely since Panx1 is considered a viable drug target, with some Panx1 blockers approved for clinical trials (https://www.clinicaltrials.gov), or promoted by PANNEX Therapeutics (https://pannextherapeutics.com/) as the target for the development of life-saving pain therapies (Crocetti et al., 2021; Dahl & Keane, 2012; Navis et al., 2020). The evidence provided in this thesis suggests that drug discovery targeting Panx1 should be re-evaluated and approached with caution.

Some limitations of the present study need to be acknowledged. No evidence was collected on whether dopaminergic neurons die within four hours of MPTP incubation in zebrafish larvae, which needs to be investigated. To address this question. I have generated transgenic fish lines expressing AnnexinV for *in-vivo* cell-death studies in zebrafish larvae using previously reported protocols (van Ham et al., 2010).

Although we are excited about the LFP analysis, the method has its limitations. LFPs reflect the highly dynamic flow of information across neural networks, but as a composite signal that receives contributions from multiple neural sources its significance is limited by several confounding factors and technical limitations (Oscar Herreras, 2016). One technical limitation is that electrodes were placed to the best of our abilities using a vision-guided approach. Nevertheless, electrode placement is inherently coarse, affecting the reproducibility from larva to larva. To tackle this problem, I have generated transgenic zebrafish lines which express the green-fluorescent calcium-sensor GCaMP6f (Chen et al., 2013). These lines will allow targeting regions of interest or individual cells with greater precision, or the readout of neuronal activity

through calcium-induced fluorescence changes. However, due to the pandemic shutdowns and refurbishment of the animal facility, the studies' use of the transgenic lines is delayed, and preliminary data was not included.

The transcriptome analysis of whole larva is most likely obscuring important molecular changes which occur only in a small number of cells. Unfortunately, the dissection of brains from 6dpf larvae is not practical and single cell RNA sequencing technology is unavailable. In addition, the transcriptome analysis highlighted that the acute treatment with MPTP activated differential expression of genes associated with other diseases such as Alzheimer's disease, Huntington's disease, and amyotrophic lateral sclerosis. How these different brain disorders intersect with Panx1 functions must be investigated in the future.

A final limitation of the study was that there was not sufficient time to test INF39, the selective NLRP3 inflammasome inhibitor, which was able to rescue the MPTP-induced behavioral phenotype in TL larvae, but not Panx1a-KO, in more detail at molecular and systems levels.

6.4 Summary and Conclusion

The technical innovations of this thesis are the proof of concept of an acute MPTP model using zebrafish larvae and the implementation of a two-electrode local field potential setup and analysis strategy to study outcomes at systems level. The innovations were the foundation to study the roles of Panx1a channels using an interdisciplinary molecular, systems, and behavioral approach in zebrafish larvae.

The strategy chosen in this thesis led to results which were opposite to the initial hypothesis that loss of Panx1a would alleviate the PD phenotype. Instead, the presence of

Panx1a reduced the expression of a key inflammation biomarker, caused a better outcome in LFP recordings, and improved the behavioral phenotype in the acute MPTP model. It was concluded that Panx1a channels help to maintain homeostasis in the zebrafish under conditions of metabolic stress induced by MPTP. The loss of function of Panx1a contributes to the severity of outcomes in the MPTP model of inflammation and early Parkinson's disease. The role of Panx1a in inflammation found here opens avenues to explore whether inflammation is a shared mechanism with other neurodegenerative disease models like Alzheimer’s disease and Amyotrophic lateral sclerosis.

7. References

Abhang, P. A., Gawali, B. W., & Mehrotra, S. C. (2016). *Chapter 2 - Technological Basics of EEG Recording and Operation of Apparatus* (P. A. Abhang, B. W. Gawali, & S. C. B. T.-I. to E. S.-B. E. R. Mehrotra (eds.); pp. 19–50). Academic Press. https://doi.org/https://doi.org/10.1016/B978-0-12-804490-2.00002-6

Abolaji, A. O., Adedara, A. O., Adie, M. A., Vicente-Crespo, M., & Farombi, E. O. (2018). Resveratrol prolongs lifespan and improves 1-methyl-4-phenyl-1,2,3,6-tetrahydropyridine-induced oxidative damage and behavioural deficits in Drosophila melanogaster. *Biochemical and Biophysical Research Communications*, *503*(2), 1042–1048. https://doi.org/10.1016/j.bbrc.2018.06.114

Abolarin, P. O., Nafiu, A. B., Oyewole, A. L., Amin, A., Ogundele, O. M., & Owoyele, B. V. (2022). Selenium reduces nociceptive response in acute 1-methyl-4-phenyl-1, 2, 3, 6-tetrahydropyridine (MPTP)-induced neurotoxicity. *IBRO Neuroscience Reports*, *12*, 1–11. https://doi.org/https://doi.org/10.1016/j.ibneur.2021.11.001

Ahmadian, E., Eftekhari, A., Samiei, M., Maleki Dizaj, S., & Vinken, M. (2019). The role and therapeutic potential of connexins, pannexins and their channels in Parkinson's disease. *Cellular Signalling*, *58*, 111–118. https://doi.org/https://doi.org/10.1016/j.cellsig.2019.03.010

Ahn, S., Park, C., & Rubchinsky, L. L. (2019). Neural Synchronization in Parkinson's Disease on Different Time Scales. *Multiscale Models of Brain Disorders*, 57–65.

Ahrens, M. B., Orger, M. B., Robson, D. N., Li, J. M., & Keller, P. J. (2013). Whole-brain functional imaging at cellular resolution using light-sheet microscopy. *Nature Methods*, *10*(5), 413–420. https://doi.org/10.1038/nmeth.2434

Anderson, F. L., von Herrmann, K. M., Andrew, A. S., Kuras, Y. I., Young, A. L., Scherzer, C. R., Hickey, W. F., Lee, S. L., & Havrda, M. C. (2021). Plasma-borne indicators of inflammasome activity in Parkinson's disease patients. *Npj Parkinson's Disease*, *7*(1), 2. https://doi.org/10.1038/s41531-020-00147-6

Anichtchik, O. V, Kaslin, J., Peitsaro, N., Scheinin, M., & Panula, P. (2004). Neurochemical and behavioural changes in zebrafish Danio rerio after systemic administration of 6-hydroxydopamine and 1-methyl-4-phenyl-1,2,3,6-tetrahydropyridine. *Journal of Neurochemistry*, *88*(2), 443–453. https://doi.org/10.1111/j.1471-4159.2004.02190.x

Antony, P. M. A., Diederich, N. J., Krüger, R., & Balling, R. (2013). The hallmarks of Parkinson's disease. *The FEBS Journal*, *280*(23), 5981–5993. https://doi.org/https://doi.org/10.1111/febs.12335

Aquilino, M. S., Whyte-Fagundes, P., Lukewich, M. K., Zhang, L., Bardakjian, B. L., Zoidl, G. R., & Carlen, P. L. (2020). Pannexin-1 Deficiency Decreases Epileptic Activity in Mice. In *International Journal of Molecular Sciences* (Vol. 21, Issue 20). https://doi.org/10.3390/ijms21207510

Aras, S., Tanriover, G., Aslan, M., Yargicoglu, P., & Agar, A. (2014). The role of nitric oxide on visual-evoked potentials in MPTP-induced Parkinsonism in mice. *Neurochemistry International*, *72*, 48–57. https://doi.org/10.1016/j.neuint.2014.04.014

Ardiles, A. O., Flores-Muñoz, C., Toro-Ayala, G., Cárdenas, A. M., Palacios, A. G., Muñoz, P., Fuenzalida, M., Sáez, J. C., & Martínez, A. D. (2014). Pannexin 1 regulates bidirectional hippocampal synaptic plasticity in adult mice . In *Frontiers in Cellular Neuroscience* (Vol. 8). https://www.frontiersin.org/article/10.3389/fncel.2014.00326

Armstrong, R. A. (2011). Visual Symptoms in Parkinson's Disease. *Parkinson's Disease*, *2011*, 908306. https://doi.org/10.4061/2011/908306

Assad, N., Luz, W. L., Santos-Silva, M., Carvalho, T., Moraes, S., Picanço-Diniz, D. L. W., Bahia, C. P., Oliveira Batista, E. de J., da Conceição Passos, A., Oliveira, K. R. H. M., & Herculano, A. M. (2020). Acute Restraint Stress Evokes Anxiety-Like Behavior Mediated by Telencephalic Inactivation and GabAergic Dysfunction in Zebrafish Brains. *Scientific Reports*, *10*(1), 5551. https://doi.org/10.1038/s41598-020-62077-w

Baranova, A., Ivanov, D., Petrash, N., Pestova, A., Skoblov, M., Kelmanson, I., Shagin, D., Nazarenko, S., Geraymovych, E., Litvin, O., Tiunova, A., Born, T. L., Usman, N., Staroverov, D., Lukyanov, S., & Panchin, Y. (2004). The mammalian pannexin family is homologous to the invertebrate innexin gap junction proteins. *Genomics*, *83*(4), 706–716. https://doi.org/10.1016/j.ygeno.2003.09.025

Bashirzade, A. A. O., Cheresiz, S. V, Belova, A. S., Drobkov, A. V, Korotaeva, A. D., Azizi-Arani, S., Azimirad, A., Odle, E., Gild, E.-Y. V, Ardashov, O. V, Volcho, K. P., Bozhko, D. V, Myrov, V. O., Kolchanova, S. M., Polovian, A. I., Galumov, G. K., Salakhutdinov, N. F., Amstislavskaya, T. G., & Kalueff, A. V. (2022). MPTP-Treated Zebrafish Recapitulate "Late-Stage" Parkinson's-like Cognitive Decline. In *Toxics* (Vol. 10, Issue 2). https://doi.org/10.3390/toxics10020069

Bashirzade, A. A. O., Cheresiz, S. V, Belova, A. S., Drobkov, A. V, Korotaeva, A. D., Azizi-arani, S., Azimirad, A., Odle, E., Gild, E. V, Ardashov, O. V, Volcho, K. P., Bozhko, D. V, Myrov, V. O., Kolchanova, S. M., Polovian, A. I., Galumov, G. K., Salakhutdinov, N. F., & Amstislavskaya, T. G. (2022). Parkinson's-like Cognitive Decline. *Toxics*, 1–10.

Basnet, R. M., Zizioli, D., Taweedet, S., Finazzi, D., & Memo, M. (2019). Zebrafish Larvae as a Behavioral Model in Neuropharmacology. *Biomedicines*, *7*(1), 23. https://doi.org/10.3390/biomedicines7010023

Bauernfeind, F. G., Horvath, G., Stutz, A., Alnemri, E. S., MacDonald, K., Speert, D., Fernandes-Alnemri, T., Wu, J., Monks, B. G., Fitzgerald, K. A., Hornung, V., & Latz, E. (2009). Cutting edge: NF-kappaB activating pattern recognition and cytokine receptors license NLRP3 inflammasome activation by regulating NLRP3 expression. *Journal of Immunology (Baltimore, Md. : 1950)*, *183*(2), 787–791. https://doi.org/10.4049/jimmunol.0901363

Beach, T. G., Adler, C. H., Lue, L., Sue, L. I., Bachalakuri, J., Henry-Watson, J., Sasse, J., Boyer, S., Shirohi, S., Brooks, R., Eschbacher, J., White 3rd, C. L., Akiyama, H., Caviness, J., Shill, H. A., Connor, D. J., Sabbagh, M. N., Walker, D. G., & Consortium, A. P. D. (2009). Unified staging system for Lewy body disorders: correlation with nigrostriatal degeneration, cognitive impairment and motor dysfunction. *Acta Neuropathologica*, *117*(6), 613–634. https://doi.org/10.1007/s00401-009-0538-8

Beach, T. G., White, C. L., Hamilton, R. L., Duda, J. E., Iwatsubo, T., Dickson, D. W., Leverenz, J. B., Roncaroli, F., Buttini, M., Hladik, C. L., Sue, L. I., Noorigian, J. V, & Adler, C. H. (2008). Evaluation of alpha-synuclein immunohistochemical methods used by invited experts. *Acta Neuropathologica*, *116*(3), 277–288. https://doi.org/10.1007/s00401-008-0409-8

Boaru, S. G., Borkham-Kamphorst, E., Van de Leur, E., Lehnen, E., Liedtke, C., & Weiskirchen, R. (2015). NLRP3 inflammasome expression is driven by NF-κB in cultured hepatocytes. *Biochemical and Biophysical Research Communications*, *458*(3), 700–706. https://doi.org/10.1016/j.bbrc.2015.02.029

Boassa, D., Ambrosi, C., Qiu, F., Dahl, G., Gaietta, G., & Sosinsky, G. (2007). Pannexin1 channels contain a glycosylation site that targets the hexamer to the plasma membrane. *Journal of Biological Chemistry*, *282*(43), 31733–31743. https://doi.org/10.1074/jbc.M702422200

Bond, S. R., Wang, N., Leybaert, L., & Naus, C. C. (2012). Pannexin 1 Ohnologs in the Teleost Lineage. *The Journal of Membrane Biology*, *245*(8), 483–493. https://doi.org/10.1007/s00232-012-9497-4

Boyce, A. K. J., & Swayne, L. A. (2017). P2X7 receptor cross-talk regulates ATP-induced pannexin 1 internalization. *The Biochemical Journal*, *474*(13), 2133–2144. https://doi.org/10.1042/BCJ20170257

Breen, D. P., Halliday, G. M., & Lang, A. E. (2019). Gut–brain axis and the spread of α-synuclein pathology: Vagal highway or dead end? *Movement Disorders*, *34*(3), 307–316. https://doi.org/10.1002/mds.27556

Bretaud, S., Lee, S., & Guo, S. (2004). Sensitivity of zebrafish to environmental toxins implicated in Parkinson's disease. *Neurotoxicology and Teratology*, *26*(6), 857–864. https://doi.org/https://doi.org/10.1016/j.ntt.2004.06.014

Bronte-Stewart, H., Barberini, C., Koop, M. M., Hill, B. C., Henderson, J. M., & Wingeier, B. (2009). The STN beta-band profile in Parkinson's disease is stationary and shows prolonged attenuation after deep brain stimulation. *Experimental Neurology*, *215*(1), 20–28. https://doi.org/10.1016/j.expneurol.2008.09.008

Brown, S. J., Boussaad, I., Jarazo, J., Fitzgerald, J. C., Antony, P., Keatinge, M., Blechman, J., Schwamborn, J. C., Krüger, R., Placzek, M., & Bandmann, O. (2021). PINK1 deficiency impairs adult neurogenesis of dopaminergic neurons. *Scientific Reports*, *11*(1), 1–14. https://doi.org/10.1038/s41598-021-84278-7

Bruzzone, R., Hormuzdi, S. G., Barbe, M. T., Herb, A., & Monyer, H. (2003). Pannexins, a family of gap junction proteins expressed in brain. *Proceedings of the National Academy of Sciences*, *100*(23), 13644. https://doi.org/10.1073/pnas.2233464100

Camicioli, R., Moore, M. M., Kinney, A., Corbridge, E., Glassberg, K., & Kaye, J. A. (2003). Parkinson's disease is associated with hippocampal atrophy. *Movement Disorders : Official Journal of the Movement Disorder Society*, *18*(7), 784–790. https://doi.org/10.1002/mds.10444

Cao, L., & Hu, Y.-M. (2016). Beta Rebound in Visuomotor Adaptation: Still the Status Quo? *The Journal of Neuroscience : The Official Journal of the Society for Neuroscience*, *36*(24), 6365–6367. https://doi.org/10.1523/JNEUROSCI.1007-16.2016

Carey, G., Görmezoğlu, M., de Jong, J. J. A., Hofman, P. A. M., Backes, W. H., Dujardin, K., & Leentjens, A. F. G. (2021). Neuroimaging of Anxiety in Parkinson's Disease: A Systematic Review. *Movement Disorders*, *36*(2), 327–339. https://doi.org/https://doi.org/10.1002/mds.28404

Chekeni, F. B., Elliott, M. R., Sandilos, J. K., Walk, S. F., Kinchen, J. M., Lazarowski, E. R., Armstrong, A. J., Penuela, S., Laird, D. W., Salvesen, G. S., Isakson, B. E., Bayliss, D. A., & Ravichandran, K. S. (2010). Pannexin 1 channels mediate "find-me" signal release and membrane permeability during apoptosis. *Nature*, *467*(7317), 863–867. https://doi.org/10.1038/nature09413

Chen, K. W., Demarco, B., & Broz, P. (2020). Pannexin-1 promotes NLRP3 activation during apoptosis but is dispensable for canonical or noncanonical inflammasome activation. *European Journal of Immunology*, *50*(2), 170–177. https://doi.org/10.1002/eji.201948254

Chen, Wardill, T. J., Sun, Y., Pulver, S. R., Renninger, S. L., Baohan, A., Schreiter, E. R., Kerr, R. A., Orger, M. B., Jayaraman, V., Looger, L. L., Svoboda, K., & Kim, D. S. (2013). Ultrasensitive fluorescent proteins for imaging neuronal activity. *Nature*, *499*(7458), 295–300. https://doi.org/10.1038/nature12354

Chiu, Y.-H., Jin, X., Medina, C. B., Leonhardt, S. A., Kiessling, V., Bennett, B. C., Shu, S., Tamm, L. K., Yeager, M., Ravichandran, K. S., & Bayliss, D. A. (2017). A quantized mechanism for activation of pannexin channels. *Nature Communications*, *8*, 14324. https://doi.org/10.1038/ncomms14324

Christensen, C., Þorsteinsson, H., Maier, V. H., & Karlsson, K. Æ. (2020). Multi-parameter Behavioral Phenotyping of the MPP+ Model of Parkinson's Disease in Zebrafish . In *Frontiers in Behavioral Neuroscience* (Vol. 14). https://www.frontiersin.org/article/10.3389/fnbeh.2020.623924

Coll, R. C., Robertson, A. A. B., Chae, J. J., Higgins, S. C., Muñoz-Planillo, R., Inserra, M. C., Vetter, I., Dungan, L. S., Monks, B. G., Stutz, A., Croker, D. E., Butler, M. S., Haneklaus, M., Sutton, C. E., Núñez, G., Latz, E., Kastner, D. L., Mills, K. H. G., Masters, S. L., … O'Neill, L. A. J. (2015). A small-molecule inhibitor of the NLRP3 inflammasome for the treatment of inflammatory diseases. *Nature Medicine*, *21*(3), 248–255. https://doi.org/10.1038/nm.3806

Connaughton, V. P., Nelson, R., & Bender, A. M. (2008). Electrophysiological evidence of GABAA and GABAC receptors on zebrafish retinal bipolar cells. *Visual Neuroscience*, *25*(2), 139–153. https://doi.org/10.1017/S0952523808080322

Crespo, Yanguas, S., Willebrords, J., Johnstone, S. R., Maes, M., Decrock, E., De Bock, M., Leybaert, L., Cogliati, B., & Vinken, M. (2017). Pannexin1 as mediator of inflammation and cell death. *Biochimica et Biophysica Acta (BBA) - Molecular Cell Research*, *1864*(1), 51–61. https://doi.org/https://doi.org/10.1016/j.bbamcr.2016.10.006

Crespo, S. Y., Willebrords, J., Johnstone, S. R., Maes, M., Decrock, E., De Bock, M., Leybaert, L., Cogliati, B., & Vinken, M. (2017). Pannexin1 as mediator of inflammation and cell death. *Biochimica et Biophysica Acta. Molecular Cell Research*, *1864*(1), 51–61. https://doi.org/10.1016/j.bbamcr.2016.10.006

Crocetti, L., Guerrini, G., Puglioli, S., Giovannoni, M. P., Di Cesare Mannelli, L., Lucarini, E., Ghelardini, C., Wang, J., & Dahl, G. (2021). Design and synthesis of the first indole-based blockers of Panx-1 channel. *European Journal of Medicinal Chemistry*, *223*, 113650. https://doi.org/https://doi.org/10.1016/j.ejmech.2021.113650

Cruz, F. F., Leite, C. E., Kist, L. W., de Oliveira, G. M., Bogo, M. R., Bonan, C. D., Campos, M. M., & Morrone, F. B. (2017). Effects of caffeine on behavioral and inflammatory changes elicited by copper in zebrafish larvae: Role of adenosine receptors. *Comparative Biochemistry and Physiology Part C: Toxicology & Pharmacology*, *194*, 28–36. https://doi.org/https://doi.org/10.1016/j.cbpc.2017.01.007

Dahl, G. (2015). ATP release through pannexon channels. *Philosophical Transactions of the Royal Society B: Biological Sciences*, *370*(1672), 20140191. https://doi.org/10.1098/rstb.2014.0191

Dahl, G., & Keane, R. W. (2012). Pannexin: from discovery to bedside in 11±4 years? *Brain Research*, *1487*, 150–159. https://doi.org/10.1016/j.brainres.2012.04.058

Dahl, G., & Locovei, S. (2006). Pannexin: to gap or not to gap, is that a question? *IUBMB Life*, *58*(7), 409–419. https://doi.org/10.1080/15216540600794526

Di, T., Chen, P., Yuan, Z., Wang, Y., Sha, S., & Chen, L. (2019). Dorsal hypothalamic

dopaminergic neurons play an inhibitory role in the hypothalamic-pituitary-adrenal axis via activation of D2R in mice. *Acta Physiologica (Oxford, England)*, *225*(2), e13187. https://doi.org/10.1111/apha.13187

Diederich, N. J., Uchihara, T., Grillner, S., & Goetz, C. G. (2020). The Evolution-Driven Signature of Parkinson's Disease. *Trends in Neurosciences*, *43*(7), 475–492. https://doi.org/10.1016/j.tins.2020.05.001

Dissanayaka, N. N. N. W., White, E., O'Sullivan, J. D., Marsh, R., Pachana, N. A., & Byrne, G. J. (2014). The clinical spectrum of anxiety in Parkinson's disease. *Movement Disorders*, *29*(8), 967–975. https://doi.org/https://doi.org/10.1002/mds.25937

Du, Y., Guo, Q., Shan, M., Wu, Y., Huang, S., Zhao, H., Hong, H., Yang, M., Yang, X., Ren, L., Peng, J., Sun, J., Zhou, H., Li, S., & Su, B. (2016). Spatial and Temporal Distribution of Dopaminergic Neurons during Development in Zebrafish. *Frontiers in Neuroanatomy*, *10*, 115. https://doi.org/10.3389/fnana.2016.00115

Emran, F., Rihel, J., & Dowling, J. E. (2008). A behavioral assay to measure responsiveness of Zebrafish to changes in light intensities. *Journal of Visualized Experiments*, *20*, 1–6. https://doi.org/10.3791/923

Feddersen, B., Rémi, J., Einhellig, M., Stoyke, C., Krauss, P., & Noachtar, S. (2014). Parkinson's disease: Less epileptic seizures more status epilepticus. *Epilepsy Research*, *108*(2), 349–354. https://doi.org/https://doi.org/10.1016/j.eplepsyres.2013.11.013

Feldmann, L. K., Lofredi, R., Neumann, W. J., Al-Fatly, B., Roediger, J., Bahners, B. H., Nikolov, P., Denison, T., Saryyeva, A., Krauss, J. K., Faust, K., Florin, E., Schnitzler, A., Schneider, G. H., & Kühn, A. A. (2022). Toward therapeutic electrophysiology: beta-band suppression as a biomarker in chronic local field potential recordings. *Npj Parkinson's Disease*, *8*(1). https://doi.org/10.1038/s41531-022-00301-2

Feng, C.-W., Wen, Z.-H., Huang, S.-Y., Hung, H.-C., Chen, C.-H., Yang, S.-N., Chen, N.-F., Wang, H.-M., Hsiao, C.-D., & Chen, W.-F. (2014). Effects of 6-hydroxydopamine exposure on motor activity and biochemical expression in zebrafish (Danio rerio) larvae. *Zebrafish*, *11*(3), 227–239. https://doi.org/10.1089/zeb.2013.0950

Fett, M. E., Pilsl, A., Paquet, D., van Bebber, F., Haass, C., Tatzelt, J., Schmid, B., & Winklhofer, K. F. (2010). Parkin is protective against proteotoxic stress in a transgenic zebrafish model. *PloS One*, *5*(7), e11783–e11783. https://doi.org/10.1371/journal.pone.0011783

Fleming, S. M., Davis, A., & Simons, E. (2022). Targeting alpha-synuclein via the immune system in Parkinson's disease: Current vaccine therapies. *Neuropharmacology*, *202*, 108870. https://doi.org/https://doi.org/10.1016/j.neuropharm.2021.108870

Flores-Muñoz, C., Gómez, B., Mery, E., Mujica, P., Gajardo, I., Córdova, C., Lopez-Espíndola, D., Durán-Aniotz, C., Hetz, C., Muñoz, P., Gonzalez-Jamett, A. M., & Ardiles, Á. O. (2020). Acute Pannexin 1 Blockade Mitigates Early Synaptic Plasticity Defects in a Mouse Model of Alzheimer's Disease . In *Frontiers in Cellular Neuroscience* (Vol. 14). https://www.frontiersin.org/article/10.3389/fncel.2020.00046

Frederiksen, S. D., Wicki-Stordeur, L. E., Sanchez-Arias, J. C., & Swayne, L. A. (2019). Exploring the Pannexin 1 interactome: In silico cross-analyses with postsynaptic proteins and neuropsychiatric disorder susceptibility genes. *BioRxiv*, *1*(2018), 801563.

Gajardo, I., Salazar, C. S., Lopez-Espíndola, D., Estay, C., Flores-Muñoz, C., Elgueta, C., Gonzalez-Jamett, A. M., Martínez, A. D., Muñoz, P., & Ardiles, Á. O. (2018). Lack of Pannexin 1 Alters Synaptic GluN2 Subunit Composition and Spatial Reversal Learning in

Mice . In *Frontiers in Molecular Neuroscience* (Vol. 11). https://www.frontiersin.org/article/10.3389/fnmol.2018.00114

Gelb, D. J., Oliver, E., & Gilman, S. (1999). Diagnostic criteria for Parkinson disease. *Archives of Neurology*, *56*(1), 33–39. https://doi.org/10.1001/archneur.56.1.33

George, J. S., Strunk, J., Mak-McCully, R., Houser, M., Poizner, H., & Aron, A. R. (2013). Dopaminergic therapy in Parkinson's disease decreases cortical beta band coherence in the resting state and increases cortical beta band power during executive control. *NeuroImage. Clinical*, *3*, 261–270. https://doi.org/10.1016/j.nicl.2013.07.013

Grazia, S. M., Anthony, C. R., Ross, J., Masato, H., & Michel, G. (1998). α-Synuclein in filamentous inclusions of Lewy bodies from Parkinson's disease and dementia with Lewy bodies. *Proceedings of the National Academy of Sciences*, *95*(11), 6469–6473. https://doi.org/10.1073/pnas.95.11.6469

Guerra, A., Asci, F., Onofrio, V., Sveva, V., Bologna, M., Fabbrini, G., Berardelli, A., & Suppa, A. (2020). Enhancing Gamma Oscillations Restores Primary Motor Cortex Plasticity in Parkinson's Disease. *The Journal of Neuroscience*, *40*(24), 4788 LP – 4796. https://doi.org/10.1523/JNEUROSCI.0357-20.2020

Guerra, A., Colella, D., Giangrosso, M., Cannavacciuolo, A., Paparella, G., Fabbrini, G., Suppa, A., Berardelli, A., & Bologna, M. (2022). Driving motor cortex oscillations modulates bradykinesia in Parkinson's disease. *Brain : A Journal of Neurology*, *145*(1), 224–236. https://doi.org/10.1093/brain/awab257

Hamilton, T. J., Myggland, A., Duperreault, E., May, Z., Gallup, J., Powell, R. A., Schalomon, M., & Digweed, S. M. (2016). Episodic-like memory in zebrafish. *Animal Cognition*, *19*(6), 1071–1079. https://doi.org/10.1007/s10071-016-1014-1

Haque, M. E., Akther, M., Jakaria, M., Kim, I.-S., Azam, S., & Choi, D.-K. (2020). Targeting the microglial NLRP3 inflammasome and its role in Parkinson's disease. *Movement Disorders : Official Journal of the Movement Disorder Society*, *35*(1), 20–33. https://doi.org/10.1002/mds.27874

Heap, L. A., Vanwalleghem, G. C., Thompson, A. W., Favre-Bulle, I., Rubinsztein-Dunlop, H., & Scott, E. K. (2018). Hypothalamic Projections to the Optic Tectum in Larval Zebrafish. *Frontiers in Neuroanatomy*, *11*, 135. https://doi.org/10.3389/fnana.2017.00135

Herreras, O. (2016). Local Field Potentials: Myths and Misunderstandings . In *Frontiers in Neural Circuits* (Vol. 10). https://www.frontiersin.org/article/10.3389/fncir.2016.00101

Holbrook, J. A., Jarosz-Griffiths, H. H., Caseley, E., Lara-Reyna, S., Poulter, J. A., Williams-Gray, C. H., Peckham, D., & McDermott, M. F. (2021). Neurodegenerative Disease and the NLRP3 Inflammasome . In *Frontiers in Pharmacology* (Vol. 12). https://www.frontiersin.org/article/10.3389/fphar.2021.643254

Horsager, J., Andersen, K. B., Knudsen, K., Skjærbæk, C., Fedorova, T. D., Okkels, N., Schaeffer, E., Bonkat, S. K., Geday, J., Otto, M., Sommerauer, M., Danielsen, E. H., Bech, E., Kraft, J., Munk, O. L., Hansen, S. D., Pavese, N., Göder, R., Brooks, D. J., … Borghammer, P. (2020). Brain-first versus body-first Parkinson's disease: a multimodal imaging case-control study. *Brain*, *143*(10), 3077–3088. https://doi.org/10.1093/brain/awaa238

Horton, S. M., Luna Lopez, C., Blevins, E., Howarth, H., Weisberg, J., Shestopalov, V. I., Makarenkova, H. P., & Shah, S. B. (2017). Pannexin 1 Modulates Axonal Growth in Mouse Peripheral Nerves . In *Frontiers in Cellular Neuroscience* (Vol. 11). https://www.frontiersin.org/article/10.3389/fncel.2017.00365

Houser, M. C., & Tansey, M. G. (2017). The gut-brain axis: Is intestinal inflammation a silent driver of Parkinson's disease pathogenesis? *Npj Parkinson's Disease*, *3*(1). https://doi.org/10.1038/s41531-016-0002-0

Hughes, J. R. (2008). Gamma, fast, and ultrafast waves of the brain: Their relationships with epilepsy and behavior. *Epilepsy & Behavior*, *13*(1), 25–31. https://doi.org/https://doi.org/10.1016/j.yebeh.2008.01.011

Jackson, N., Cole, S. R., Voytek, B., & Swann, N. C. (2019). Characteristics of Waveform Shape in Parkinson's Disease Detected with Scalp Electroencephalography. *Eneuro*, *6*(3), ENEURO.0151-19.2019. https://doi.org/10.1523/ENEURO.0151-19.2019

Jiang, H., He, H., Chen, Y., Huang, W., Cheng, J., Ye, J., Wang, A., Tao, J., Wang, C., Liu, Q., Jin, T., Jiang, W., Deng, X., & Zhou, R. (2017). Identification of a selective and direct NLRP3 inhibitor to treat inflammatory disorders. *The Journal of Experimental Medicine*, *214*(11), 3219–3238. https://doi.org/10.1084/jem.20171419

Jiao, J., Zhao, G., Wang, Y., Ren, P., & Wu, M. (2020). MCC950, a Selective Inhibitor of NLRP3 Inflammasome, Reduces the Inflammatory Response and Improves Neurological Outcomes in Mice Model of Spinal Cord Injury. *Frontiers in Molecular Biosciences*, *7*, 37. https://doi.org/10.3389/fmolb.2020.00037

Jin, X., Leonhardt, S. A., Chiu, Y.-H., Purdy, M. D., McIntire, W. E., Bennett, B. C., Bayliss, D. A., & Yeager, M. (2021). A Constitutively Closed Pannexin1 Channel in Lipid Bilayer Nanodiscs Assembles as a Large-Pore Heptamer. *BioRxiv*, 2020.12.31.425019. https://doi.org/10.1101/2020.12.31.425019

Jin, Zhang, B., Zheng, X., Li, N., Xu, L., Xie, Y., Song, F., Bhat, E. A., Chen, Y., Gao, N., Guo, J., Zhang, X., & Ye, S. (2020). Cryo-EM structures of human pannexin 1 channel. *Cell Research*, *30*(5), 449–451. https://doi.org/10.1038/s41422-020-0310-0

Johnston, G. A. R. (2013). Advantages of an antagonist: bicuculline and other GABA antagonists. *British Journal of Pharmacology*, *169*(2), 328–336. https://doi.org/https://doi.org/10.1111/bph.12127

Kalyn, M., & Ekker, M. (2021). Cerebroventricular Microinjections of MPTP on Adult Zebrafish Induces Dopaminergic Neuronal Death, Mitochondrial Fragmentation, and Sensorimotor Impairments . In *Frontiers in Neuroscience* (Vol. 15). https://www.frontiersin.org/article/10.3389/fnins.2021.718244

Kamstra, K., Rizwan, M. Z., Grattan, D. R., Horsfield, J. A., & Tups, A. (2022). Leptin regulates glucose homeostasis via the canonical Wnt pathway in the zebrafish. *The FASEB Journal*, *36*(3), e22207. https://doi.org/https://doi.org/10.1096/fj.202101764R

Kanehisa, M., & Sato, Y. (2020). KEGG Mapper for inferring cellular functions from protein sequences. *Protein Science : A Publication of the Protein Society*, *29*(1), 28–35. https://doi.org/10.1002/pro.3711

Kanehisa, M., Sato, Y., & Kawashima, M. (2022). KEGG mapping tools for uncovering hidden features in biological data. *Protein Science*, *31*(1), 47–53. https://doi.org/10.1002/pro.4172

Kattla, S., & Lowery, M. M. (2010). Fatigue related changes in electromyographic coherence between synergistic hand muscles. *Experimental Brain Research*, *202*(1), 89–99. https://doi.org/10.1007/s00221-009-2110-0

Keller, P. J., Ahrens, M. B., & Freeman, J. (2015). Light-sheet imaging for systems neuroscience. *Nature Methods*, *12*(1), 27–29. https://doi.org/10.1038/nmeth.3214

Kelley, N., Jeltema, D., Duan, Y., & He, Y. (2019). The NLRP3 Inflammasome: An Overview of Mechanisms of Activation and Regulation. *International Journal of Molecular Sciences*,

20(13), 3328. https://doi.org/10.3390/ijms20133328

Klann, E. M., Dissanayake, U., Gurrala, A., Farrer, M., Shukla, A. W., Ramirez-Zamora, A., Mai, V., & Vedam-Mai, V. (2022). The Gut–Brain Axis and Its Relation to Parkinson's Disease: A Review . In *Frontiers in Aging Neuroscience* (Vol. 13). https://www.frontiersin.org/article/10.3389/fnagi.2021.782082

Koval, M., Cwiek, A., Carr, T., Good, M. E., Lohman, A. W., & Isakson, B. E. (2021). Pannexin 1 as a driver of inflammation and ischemia–reperfusion injury. *Purinergic Signalling*, *17*(4), 521–531. https://doi.org/10.1007/s11302-021-09804-8

Krack, P., Batir, A., Van Blercom, N., Chabardes, S., Fraix, V., Ardouin, C., Koudsie, A., Limousin, P. D., Benazzouz, A., LeBas, J. F., Benabid, A.-L., & Pollak, P. (2003). Five-year follow-up of bilateral stimulation of the subthalamic nucleus in advanced Parkinson's disease. *The New England Journal of Medicine*, *349*(20), 1925–1934. https://doi.org/10.1056/NEJMoa035275

Kurtenbach, S., Prochnow, N., Kurtenbach, S., Klooster, J., Zoidl, C., Dermietzel, R., Kamermans, M., & Zoidl, G. (2013). Pannexin1 Channel Proteins in the Zebrafish Retina Have Shared and Unique Properties. *PLOS ONE*, *8*(10), e77722-. https://doi.org/10.1371/journal.pone.0077722

Lai, C. P. K., Bechberger, J. F., Thompson, R. J., MacVicar, B. A., Bruzzone, R., & Naus, C. C. (2007). Tumor-suppressive effects of pannexin 1 in C6 glioma cells. *Cancer Research*, *67*(4), 1545–1554. https://doi.org/10.1158/0008-5472.CAN-06-1396

Lal, P., & Kawakami, K. (2022). Integrated Behavioral, Genetic and Brain Circuit Visualization Methods to Unravel Functional Anatomy of Zebrafish Amygdala . In *Frontiers in Neuroanatomy* (Vol. 16). https://www.frontiersin.org/article/10.3389/fnana.2022.837527

Lam, C. S., Korzh, V., & Strahle, U. (2005). Zebrafish embryos are susceptible to the dopaminergic neurotoxin MPTP. *The European Journal of Neuroscience*, *21*(6), 1758–1762. https://doi.org/10.1111/j.1460-9568.2005.03988.x

Langston, J. W., Irwin, I., Langston, E. B., & Forno, L. S. (1984). Pargyline Prevents MPTP-Induced Parkinsonism in Primates. *Science*, *225*(4669), 1480–1482. https://doi.org/10.1126/science.6332378

Lee, J., & Ziering, A. (1947). Piperidine derivatives; 2-phenyl- and 2-phenylalkyl-piperidines. *The Journal of Organic Chemistry*, *12*(6), 885–893. https://doi.org/10.1021/jo01170a021

Li, D., Ren, W., Jiang, Z., & Zhu, L. (2018). Regulation of the NLRP3 inflammasome and macrophage pyroptosis by the p38 MAPK signaling pathway in a mouse model of acute lung injury. *Molecular Medicine Reports*, *18*(5), 4399–4409. https://doi.org/10.3892/mmr.2018.9427

Li, S., Bjelobaba, I., & Stojilkovic, S. S. (2018). Interactions of Pannexin1 channels with purinergic and NMDA receptor channels. *Biochimica et Biophysica Acta (BBA) - Biomembranes*, *1860*(1), 166–173. https://doi.org/https://doi.org/10.1016/j.bbamem.2017.03.025

Liao, X. X., Dai, Y. Z., Zhao, Y. Z., & Nie, K. (2022). Gasdermin E: A Prospective Target for Therapy of Diseases. *Frontiers in Pharmacology*, *13*(April), 1–16. https://doi.org/10.3389/fphar.2022.855828

Lim, C.-S., Kim, M. J., Choi, J. E., Islam, M. A., Lee, Y.-K., Xiong, Y., Shim, K.-W., Yang, J., Lee, R. U., Lee, J., Park, P., Kwak, J.-H., Seo, H., Kim, C. H., Lee, J.-H., Lee, Y.-S., Hwang, S.-K., Lee, K., Lee, J.-A., & Kaang, B.-K. (2021). Dysfunction of NMDA receptors in neuronal models of an autism spectrum disorder patient with a DSCAM mutation and in

Dscam-knockout mice. *Molecular Psychiatry*, *26*(12), 7538–7549. https://doi.org/10.1038/s41380-021-01216-9

Limousin, P., Krack, P., Pollak, P., Benazzouz, A., Ardouin, C., Hoffmann, D., & Benabid, A. L. (1998). Electrical stimulation of the subthalamic nucleus in advanced Parkinson's disease. *The New England Journal of Medicine*, *339*(16), 1105–1111. https://doi.org/10.1056/NEJM199810153391603

Ling, Z.-M., Wang, Q., Ma, Y., Xue, P., Gu, Y., Cao, M.-H., & Wei, Z.-Y. (2021). Astrocyte Pannexin 1 Suppresses LPS-Induced Inflammatory Responses to Protect Neuronal SH-SY5Y Cells. *Frontiers in Cellular Neuroscience*, *15*, 710820. https://doi.org/10.3389/fncel.2021.710820

Little, S., & Brown, P. (2014). The functional role of beta oscillations in Parkinson's disease. *Parkinsonism & Related Disorders*, *20*, S44–S48. https://doi.org/https://doi.org/10.1016/S1353-8020(13)70013-0

Locovei, S., Wang, J., & Dahl, G. (2006). Activation of pannexin 1 channels by ATP through P2Y receptors and by cytoplasmic calcium. *FEBS Letters*, *580*(1), 239–244. https://doi.org/10.1016/j.febslet.2005.12.004

Love, M. I., Huber, W., & Anders, S. (2014). Moderated estimation of fold change and dispersion for RNA-seq data with DESeq2. *Genome Biology*, *15*(12), 550. https://doi.org/10.1186/s13059-014-0550-8

Luo, G., He, Y., Yang, F., Zhai, Z., Han, J., Xu, W., Zhang, J., Zhuang, L., Zhang, Y., Li, Y., Song, R., Luo, X., Liang, J., & Sun, E. (2022). Blocking GSDME-mediated pyroptosis in renal tubular epithelial cells alleviates disease activity in lupus mice. *Cell Death Discovery*, *8*(1), 113. https://doi.org/10.1038/s41420-022-00848-2

Luo, S., Yang, Y., Chen, J., Zhong, Z., Huang, H., Zhang, J., & Cui, L. (2016). Tanshinol stimulates bone formation and attenuates dexamethasone-induced inhibition of osteogenesis in larval zebrafish. *Journal of Orthopaedic Translation*, *4*, 35–45. https://doi.org/10.1016/j.jot.2015.07.002

MacDonald, H. J., Brittain, J.-S., Spitzer, B., Hanslmayr, S., & Jenkinson, N. (2019). Memory deficits in Parkinson's disease are associated with reduced beta power modulation. *Brain Communications*, *1*(1), fcz040–fcz040. https://doi.org/10.1093/braincomms/fcz040

MacPhail, R. C., Brooks, J., Hunter, D. L., Padnos, B., Irons, T. D., & Padilla, S. (2009). Locomotion in larval zebrafish: Influence of time of day, lighting and ethanol. *Neurotoxicology*, *30*(1), 52–58. https://doi.org/10.1016/j.neuro.2008.09.011

Makarenkova, H. P., Shah, S. B., & Shestopalov, V. I. (2018). The two faces of pannexins: new roles in inflammation and repair. *Journal of Inflammation Research*, *11*, 273–288. https://doi.org/10.2147/JIR.S128401

Mallet, N., Pogosyan, A., Sharott, A., Csicsvari, J., Bolam, J. P., Brown, P., & Magill, P. J. (2008). Disrupted dopamine transmission and the emergence of exaggerated beta oscillations in subthalamic nucleus and cerebral cortex. *The Journal of Neuroscience : The Official Journal of the Society for Neuroscience*, *28*(18), 4795–4806. https://doi.org/10.1523/JNEUROSCI.0123-08.2008

Maximino, C., Puty, B., Matos Oliveira, K. R., & Herculano, A. M. (2013). Behavioral and neurochemical changes in the zebrafish leopard strain. *Genes, Brain, and Behavior*, *12*(5), 576–582. https://doi.org/10.1111/gbb.12047

McGrath, P., & Li, C. Q. (2008). Zebrafish: a predictive model for assessing drug-induced toxicity. *Drug Discovery Today*, *13*(9–10), 394–401.

https://doi.org/10.1016/j.drudis.2008.03.002
McKinley, E. T., Baranowski, T. C., Blavo, D. O., Cato, C., Doan, T. N., & Rubinstein, A. L. (2005). Neuroprotection of MPTP-induced toxicity in zebrafish dopaminergic neurons. *Brain Research. Molecular Brain Research*, *141*(2), 128–137. https://doi.org/10.1016/j.molbrainres.2005.08.014
Medina, C. B., Mehrotra, P., Arandjelovic, S., Perry, J. S. A., Guo, Y., Morioka, S., Barron, B., Walk, S. F., Ghesquière, B., Krupnick, A. S., Lorenz, U., & Ravichandran, K. S. (2020). Metabolites released from apoptotic cells act as tissue messengers. *Nature*, *580*(7801), 130–135. https://doi.org/10.1038/s41586-020-2121-3
Meredith, G. E., & Rademacher, D. J. (2011). MPTP mouse models of Parkinson's disease: an update. *Journal of Parkinson's Disease*, *1*(1), 19–33. https://doi.org/10.3233/JPD-2011-11023
Mi, H., Muruganujan, A., Ebert, D., Huang, X., & Thomas, D. (2019). *PANTHER version 14 : more genomes , a new PANTHER GO-slim and improvements in enrichment analysis tools*. *47*(November 2018), 419–426. https://doi.org/10.1093/nar/gky1038
Michalski, K., Henze, E., Nguyen, P., Lynch, P., & Kawate, T. (2018). The weak voltage dependence of pannexin 1 channels can be tuned by N-terminal modifications. *The Journal of General Physiology*, *150*(12), 1758–1768. https://doi.org/10.1085/jgp.201711804
Michalski, K., Syrjanen, J. L., Henze, E., Kumpf, J., Furukawa, H., & Kawate, T. (2020). The Cryo-EM structure of pannexin 1 reveals unique motifs for ion selection and inhibition. *ELife*, *9*, e54670. https://doi.org/10.7554/eLife.54670
Mim, C., Perkins, G., & Dahl, G. (2021). Structure versus function: Are new conformations of pannexin 1 yet to be resolved? *Journal of General Physiology*, *153*(5), e202012754. https://doi.org/10.1085/jgp.202012754
Mou, L., Ke, M., Song, M., Shan, Y., Xiao, Q., Liu, Q., Li, J., Sun, K., Pu, L., Guo, L., Geng, J., Wu, J., & Deng, D. (2020). Structural basis for gating mechanism of Pannexin 1 channel. *Cell Research*, *30*(5), 452–454. https://doi.org/10.1038/s41422-020-0313-x
Mousseau, M., Burma, N. E., Lee, K. Y., Leduc-Pessah, H., Kwok, C. H. T., Reid, A. R., O'Brien, M., Sagalajev, B., Stratton, J. A., Patrick, N., Stemkowski, P. L., Biernaskie, J., Zamponi, G. W., Salo, P., McDougall, J. J., Prescott, S. A., Matyas, J. R., & Trang, T. (2018). Microglial pannexin-1 channel activation is a spinal determinant of joint pain. *Science Advances*, *4*(8), eaas9846–eaas9846. https://doi.org/10.1126/sciadv.aas9846
Muñoz-Manchado, A. B., Villadiego, J., Romo-Madero, S., Suárez-Luna, N., Bermejo-Navas, A., Rodríguez-Gómez, J. A., Garrido-Gil, P., Labandeira-García, J. L., Echevarría, M., López-Barneo, J., & Toledo-Aral, J. J. (2016). Chronic and progressive Parkinson's disease MPTP model in adult and aged mice. *Journal of Neurochemistry*, *136*(2), 373–387. https://doi.org/https://doi.org/10.1111/jnc.13409
Muralidharan, A., Zhang, J., Ghosh, D., Johnson, M. D., Baker, K. B., & Vitek, J. L. (2017). Modulation of Neuronal Activity in the Motor Thalamus during GPi-DBS in the MPTP Nonhuman Primate Model of Parkinson's Disease. *Brain Stimulation*, *10*(1), 126–138. https://doi.org/10.1016/j.brs.2016.10.005
Mustapha, M., & Mat Taib, C. N. (2021). MPTP-induced mouse model of Parkinson's disease: A promising direction of therapeutic strategies. *Bosnian Journal of Basic Medical Sciences*, *21*(4 SE-Reviews), 422–433. https://doi.org/10.17305/bjbms.2020.5181
Muthuraman, M., Bange, M., Koirala, N., Ciolac, D., Pintea, B., Glaser, M., Tinkhauser, G., Brown, P., Deuschl, G., & Groppa, S. (2020). Cross-frequency coupling between gamma

oscillations and deep brain stimulation frequency in Parkinson's disease. *Brain*, *143*(11), 3393–3407. https://doi.org/10.1093/brain/awaa297

Nakai, J., Ohkura, M., & Imoto, K. (2001). A high signal-to-noise Ca2+ probe composed of a single green fluorescent protein. *Nature Biotechnology*, *19*(2), 137–141. https://doi.org/10.1038/84397

Nasri, H., & Rafieian-Kopaei, M. (2014). Metformin: Current knowledge. *Journal of Research in Medical Sciences : The Official Journal of Isfahan University of Medical Sciences*, *19*(7), 658–664. https://pubmed.ncbi.nlm.nih.gov/25364368

Navis, K. E., Fan, C. Y., Trang, T., Thompson, R. J., & Derksen, D. J. (2020). Pannexin 1 Channels as a Therapeutic Target: Structure, Inhibition, and Outlook. *ACS Chemical Neuroscience*, *11*(15), 2163–2172. https://doi.org/10.1021/acschemneuro.0c00333

Nellore, J., & Nandita, P. (2015). Paraquat exposure induces behavioral deficits in larval zebrafish during the window of dopamine neurogenesis. *Toxicology Reports*, *2*, 950–956. https://doi.org/https://doi.org/10.1016/j.toxrep.2015.06.007

Nyitrai, G., Kékesi, K. A., Dobolyi, A., Pungor, K., & Juhász, G. (1997). Single low dose of MPTP decreases extracellular levels of noradrenaline and monoamine metabolites in the ventrobasal thalamus of the rats. *Neurobiology (Budapest, Hungary)*, *5*(2), 249–261.

Ofori, S., & Schorderet, M. (1987). Effects of 1-methyl-4-phenyl-1,2,3,6-tetrahydropyridine (MPTP) on dopamine synthesis and release in the rabbit retina in vitro. *Neuropharmacology*, *26*(11), 1607–1610. https://doi.org/10.1016/0028-3908(87)90009-8

Ortiz, F. C., & Puebla, C. (2020). Pannexin 1-based channels activity as a novel regulator of multiple sclerosis progression. *Neural Regeneration Research*, *15*(1), 65–66. https://doi.org/10.4103/1673-5374.264450

Panchin, Y., Kelmanson, I., Matz, M., Lukyanov, K., Usman, N., & Lukyanov, S. (2000). A ubiquitous family of putative gap junction molecules. *Current Biology*, *10*(13), R473–R474. https://doi.org/10.1016/S0960-9822(00)00576-5

Pelegrin, P., Barroso-Gutierrez, C., & Surprenant, A. (2008). P2X7 Receptor Differentially Couples to Distinct Release Pathways for IL-1β in Mouse Macrophage. *The Journal of Immunology*, *180*(11), 7147. https://doi.org/10.4049/jimmunol.180.11.7147

Penuela, S., Bhalla, R., Gong, X.-Q., Cowan, K. N., Celetti, S. J., Cowan, B. J., Bai, D., Shao, Q., & Laird, D. W. (2007). Pannexin 1 and pannexin 3 are glycoproteins that exhibit many distinct characteristics from the connexin family of gap junction proteins. *Journal of Cell Science*, *120*(Pt 21), 3772–3783. https://doi.org/10.1242/jcs.009514

Penuela, S., Bhalla, R., Nag, K., & Laird, D. W. (2009). Glycosylation regulates pannexin intermixing and cellular localization. *Molecular Biology of the Cell*, *20*(20), 4313–4323. https://doi.org/10.1091/mbc.e09-01-0067

Penuela, S., Celetti, S. J., Bhalla, R., Shao, Q., & Laird, D. W. (2008). Diverse subcellular distribution profiles of pannexin1 and pannexin3. *Cell Communication and Adhesion*, *15*(1–2), 133–142. https://doi.org/10.1080/15419060802014115

Penuela, S., Harland, L., Simek, J., & Laird, D. W. (2014). Pannexin channels and their links to human disease. *The Biochemical Journal*, *461*(3), 371–381. https://doi.org/10.1042/BJ20140447

Pfaffl, M. W., Horgan, G. W., & Dempfle, L. (2002). *Relative expression software tool (REST ©) for group-wise comparison and statistical analysis of relative expression results in real-time PCR*. *30*(9).

Poewe, W., & Mahlknecht, P. (2009). The clinical progression of Parkinson's disease.

Parkinsonism & Related Disorders, *15*, S28–S32. https://doi.org/https://doi.org/10.1016/S1353-8020(09)70831-4

Porras, G., Li, Q., & Bezard, E. (2012). Modeling Parkinson's disease in primates: The MPTP model. *Cold Spring Harbor Perspectives in Medicine*, *2*(3), a009308–a009308. https://doi.org/10.1101/cshperspect.a009308

Pretegiani, E., Vanegas-Arroyave, N., FitzGibbon, E. J., Hallett, M., & Optican, L. M. (2019). Evidence From Parkinson's Disease That the Superior Colliculus Couples Action and Perception. *Movement Disorders : Official Journal of the Movement Disorder Society*, *34*(11), 1680–1689. https://doi.org/10.1002/mds.27861

Prochnow, N., Abdulazim, A., Kurtenbach, S., Wildförster, V., Dvoriantchikova, G., Hanske, J., Petrasch-Parwez, E., Shestopalov, V. I., Dermietzel, R., Manahan-Vaughan, D., & Zoidl, G. (2012). Pannexin1 Stabilizes Synaptic Plasticity and Is Needed for Learning. *PLOS ONE*, *7*(12), e51767. https://doi.org/10.1371/journal.pone.0051767

Prochnow, N., Hoffmann, S., Dermietze, R., & Zoidl, G. (2009). *Replacement of a single cysteine in the fourth transmembrane region of zebrafish pannexin1 alters hemichannel gating behavior*. 255–264. https://doi.org/10.1007/s00221-009-1957-4

Przedborski, S., Jackson-Lewis, V., Djaldetti, R., Liberatore, G., Vila, M., Vukosavic, S., & Almer, G. (2000). The parkinsonian toxin MPTP: action and mechanism. *Restorative Neurology and Neuroscience*, *16*(2), 135–142.

Qu, Y., Misaghi, S., Newton, K., Gilmour, L. L., Louie, S., Cupp, J. E., Dubyak, G. R., Hackos, D., & Dixit, V. M. (2011). Pannexin-1 Is Required for ATP Release during Apoptosis but Not for Inflammasome Activation. *The Journal of Immunology*, *186*(11), 6553 LP – 6561. https://doi.org/10.4049/jimmunol.1100478

Ravichandran, K. S. (2010). Find-me and eat-me signals in apoptotic cell clearance: progress and conundrums. *The Journal of Experimental Medicine*, *207*(9), 1807–1817. https://doi.org/10.1084/jem.20101157

Ray, A., Zoidl, G., Wahle, P., & Dermietzel, R. (2006). Pannexin expression in the cerebellum. *Cerebellum (London, England)*, *5*(3), 189–192. https://doi.org/10.1080/14734220500530082

Ray, A., Zoidl, G., Weickert, S., Wahle, P., & Dermietzel, R. (2005). Site-specific and developmental expression of pannexin1 in the mouse nervous system. *The European Journal of Neuroscience*, *21*(12), 3277–3290. https://doi.org/10.1111/j.1460-9568.2005.04139.x

Razali, K., Othman, N., Mohd Nasir, M. H., Doolaanea, A. A., Kumar, J., Ibrahim, W. N., Mohamed Ibrahim, N., & Mohamed, W. M. Y. (2021). The Promise of the Zebrafish Model for Parkinson's Disease: Today's Science and Tomorrow's Treatment. *Frontiers in Genetics*, *12*, 655550. https://doi.org/10.3389/fgene.2021.655550

Richardson, J. R., Caudle, W. M., Guillot, T. S., Watson, J. L., Nakamaru-Ogiso, E., Seo, B. B., Sherer, T. B., Greenamyre, J. T., Yagi, T., Matsuno-Yagi, A., & Miller, G. W. (2007). Obligatory role for complex I inhibition in the dopaminergic neurotoxicity of 1-methyl-4-phenyl-1,2,3,6-tetrahydropyridine (MPTP). *Toxicological Sciences : An Official Journal of the Society of Toxicology*, *95*(1), 196–204. https://doi.org/10.1093/toxsci/kfl133

Rink, E., & Guo, S. (2004). The too few mutant selectively affects subgroups of monoaminergic neurons in the zebrafish forebrain. *Neuroscience*, *127*(1), 147–154. https://doi.org/10.1016/j.neuroscience.2004.05.004

Roberts, A., Bill, B., & Glanzman, D. (2013). Learning and memory in zebrafish larvae . In

Frontiers in Neural Circuits (Vol. 7). https://www.frontiersin.org/article/10.3389/fncir.2013.00126

Royer, L. A., Lemon, W. C., Chhetri, R. K., Wan, Y., Coleman, M., Myers, E. W., & Keller, P. J. (2016). Adaptive light-sheet microscopy for long-term, high-resolution imaging in living organisms. *Nature Biotechnology*, *34*(12), 1267–1278. https://doi.org/10.1038/nbt.3708

Rubinstein, A. L. (2003). Zebrafish : From disease modeling to drug discovery Amy L Rubinstein. *Current Opinion in Drug Discovery & Development*, 218–223.

Safarian, Houshangi-Tabrizi, S., Zoidl, C., & Zoidl, G. R. (2021). Panx1b Modulates the Luminance Response and Direction of Locomotion in the Zebrafish. *International Journal of Molecular Sciences*, *22*(21). https://doi.org/10.3390/ijms222111750

Safarian, N. (2021). *Roles of Panx1 channels in larval zebrafish: From genes to visual-motor behavior*.

Safarian, Whyte-Fagundes, P., Zoidl, C., Zoidl, G., & Grigull, J. (2020). *Visuomotor deficiency in panx1a knockout zebrafish is linked to dopaminergic signaling*.

Sahu, G., Sukumaran, S., & Bera, A. K. (2014). Pannexins form gap junctions with electrophysiological and pharmacological properties distinct from connexins. *Scientific Reports*, *4*(1), 4955. https://doi.org/10.1038/srep04955

Sanchez-Arias, J. C., Liu, M., Choi, C. S. W., Ebert, S. N., Brown, C. E., & Swayne, L. A. (2019). Pannexin 1 Regulates Network Ensembles and Dendritic Spine Development in Cortical Neurons. *ENeuro*, *6*(3), ENEURO.0503-18.2019. https://doi.org/10.1523/ENEURO.0503-18.2019

Sandall, C. F., Ziehr, B. K., & Macdonald, J. A. (2020). *ATP-Binding and Hydrolysis in Inflammasome Activation*.

Satapathy, S. K., Dehuri, S., Jagadev, A. K., & Mishra, S. (2019). *Chapter 1 - Introduction* (S. K. Satapathy, S. Dehuri, A. K. Jagadev, & S. B. T.-E. E. G. B. S. C. for E. S. D. D. Mishra (eds.); pp. 1–25). Academic Press. https://doi.org/https://doi.org/10.1016/B978-0-12-817426-5.00001-6

Schwerdt, H. N., Amemori, K., Gibson, D. J., Stanwicks, L. L., Yoshida, T., Bichot, N. P., Amemori, S., Desimone, R., Langer, R., Cima, M. J., & Graybiel, A. M. (2022). Dopamine and beta-band oscillations differentially link to striatal value and motor control. *Science Advances*, *6*(39), eabb9226. https://doi.org/10.1126/sciadv.abb9226

Sheng, D., Qu, D., Kwok, K. H. H., Ng, S. S., Lim, A. Y. M., Aw, S. S., Lee, C. W. H., Sung, W. K., Tan, E. K., Lufkin, T., Jesuthasan, S., Sinnakaruppan, M., & Liu, J. (2010). Deletion of the WD40 domain of LRRK2 in Zebrafish causes Parkinsonism-like loss of neurons and locomotive defect. *PLoS Genetics*, *6*(4), e1000914. https://doi.org/10.1371/journal.pgen.1000914

Shi, Y., Lv, Q., Zheng, M., Sun, H., & Shi, F. (2021). NLRP3 inflammasome inhibitor INF39 attenuated NLRP3 assembly in macrophages. *International Immunopharmacology*, *92*, 107358. https://doi.org/10.1016/j.intimp.2020.107358

Shuo, Bjelobaba, I., & Stojilkovic, S. S. (2018). Interactions of Pannexin1 channels with purinergic and NMDA receptor channels. *Biochimica et Biophysica Acta. Biomembranes*, *1860*(1), 166–173. https://doi.org/10.1016/j.bbamem.2017.03.025

Siegel, M. S., & Isacoff, E. Y. (1997). A Genetically Encoded Optical Probe of Membrane Voltage. *Neuron*, *19*(4), 735–741. https://doi.org/https://doi.org/10.1016/S0896-6273(00)80955-1

Silverman, de Rivero Vaccari, J. P., Locovei, S., Qiu, F., Carlsson, S. K., Scemes, E., Keane, R.

W., & Dahl, G. (2009). The pannexin 1 channel activates the inflammasome in neurons and astrocytes. *The Journal of Biological Chemistry*, *284*(27), 18143–18151. https://doi.org/10.1074/jbc.M109.004804

Silverman, Locovei, S., & Dahl, G. (2008a). Probenecid, a gout remedy, inhibits pannexin 1 channels. *American Journal of Physiology. Cell Physiology*, *295*(3), C761–C767. https://doi.org/10.1152/ajpcell.00227.2008

Silverman, W., Locovei, S., & Dahl, G. (2008b). *Probenecid , a gout remedy , inhibits pannexin 1 channels*. *33101*, 761–767. https://doi.org/10.1152/ajpcell.00227.2008.

Sison, M., & Gerlai, R. (2011). Behavioral performance altering effects of MK-801 in zebrafish (Danio rerio). *Behavioural Brain Research*, *220*(2), 331–337. https://doi.org/10.1016/j.bbr.2011.02.019

Son, A. Y., Biagioni, M. C., Kaminski, D., Gurevich, A., Stone, B., & Di Rocco, A. (2016). Parkinson's Disease and Cryptogenic Epilepsy. *Case Reports in Neurological Medicine*, *2016*, 3745631. https://doi.org/10.1155/2016/3745631

Song, X., Jensen, M. Ø., Jogini, V., Stein, R. A., Lee, C.-H., Mchaourab, H. S., Shaw, D. E., & Gouaux, E. (2018). Mechanism of NMDA receptor channel block by MK-801 and memantine. *Nature*, *556*(7702), 515–519. https://doi.org/10.1038/s41586-018-0039-9

Suadicani, S. O., Iglesias, R., Wang, J., Dahl, G., Spray, D. C., & Scemes, E. (2012). ATP signaling is deficient in cultured Pannexin1-null mouse astrocytes. *Glia*, *60*(7), 1106–1116. https://doi.org/10.1002/glia.22338

Suzuki, D. G., Pérez-Fernández, J., Wibble, T., Kardamakis, A. A., & Grillner, S. (2019). The role of the optic tectum for visually evoked orienting and evasive movements. *Proceedings of the National Academy of Sciences of the United States of America*, *116*(30), 15272–15281. https://doi.org/10.1073/pnas.1907962116

Swann, N. C., de Hemptinne, C., Miocinovic, S., Qasim, S., Wang, S. S., Ziman, N., Ostrem, J. L., San Luciano, M., Galifianakis, N. B., & Starr, P. A. (2016). Gamma Oscillations in the Hyperkinetic State Detected with Chronic Human Brain Recordings in Parkinson's Disease. *The Journal of Neuroscience : The Official Journal of the Society for Neuroscience*, *36*(24), 6445–6458. https://doi.org/10.1523/JNEUROSCI.1128-16.2016

Szklarczyk, D., Gable, A. L., Lyon, D., Junge, A., Wyder, S., Huerta-Cepas, J., Simonovic, M., Doncheva, N. T., Morris, J. H., Bork, P., Jensen, L. J., & Mering, C. von. (2019). STRING v11: protein-protein association networks with increased coverage, supporting functional discovery in genome-wide experimental datasets. *Nucleic Acids Research*, *47*(D1), D607–D613. https://doi.org/10.1093/nar/gky1131

Szklarczyk, D., Gable, A. L., Nastou, K. C., Lyon, D., Kirsch, R., Pyysalo, S., Doncheva, N. T., Legeay, M., Fang, T., Bork, P., Jensen, L. J., & von Mering, C. (2021). The STRING database in 2021: customizable protein-protein networks, and functional characterization of user-uploaded gene/measurement sets. *Nucleic Acids Research*, *49*(D1), D605–D612. https://doi.org/10.1093/nar/gkaa1074

Tanner, J. J., McFarland, N. R., & Price, C. C. (2017). Striatal and Hippocampal Atrophy in Idiopathic Parkinson's Disease Patients without Dementia: A Morphometric Analysis . In *Frontiers in Neurology* (Vol. 8). https://www.frontiersin.org/article/10.3389/fneur.2017.00139

Teleńczuk, B., Dehghani, N., Le Van Quyen, M., Cash, S. S., Halgren, E., Hatsopoulos, N. G., & Destexhe, A. (2017). Local field potentials primarily reflect inhibitory neuron activity in human and monkey cortex. *Scientific Reports*, *7*, 40211. https://doi.org/10.1038/srep40211

Thompson, J. A., Lanctin, D., Ince, N. F., & Abosch, A. (2014). Clinical implications of local field potentials for understanding and treating movement disorders. *Stereotactic and Functional Neurosurgery*, *92*(4), 251–263. https://doi.org/10.1159/000364913

Timmermann, L., & Florin, E. (2012). Parkinson's disease and pathological oscillatory activity: is the beta band the bad guy? - New lessons learned from low-frequency deep brain stimulation. *Experimental Neurology*, *233*(1), 123–125. https://doi.org/10.1016/j.expneurol.2011.10.022

Tinkhauser, G., Pogosyan, A., Tan, H., Herz, D. M., Kühn, A. A., & Brown, P. (2017). Beta burst dynamics in Parkinson's disease OFF and ON dopaminergic medication. *Brain : A Journal of Neurology*, *140*(11), 2968–2981. https://doi.org/10.1093/brain/awx252

Ünal, İ., Üstündağ, Ü. V, Ateş, P. S., Eğilmezer, G., Alturfan, A. A., Yiğitbaşı, T., & Emekli-Alturfan, E. (2019). Rotenone impairs oxidant/antioxidant balance both in brain and intestines in zebrafish. *The International Journal of Neuroscience*, *129*(4), 363–368. https://doi.org/10.1080/00207454.2018.1538141

van Deursen, J. A., Vuurman, E. F. P. M., Verhey, F. R. J., van Kranen-Mastenbroek, V. H. J. M., & Riedel, W. J. (2008). Increased EEG gamma band activity in Alzheimer's disease and mild cognitive impairment. *Journal of Neural Transmission (Vienna, Austria : 1996)*, *115*(9), 1301–1311. https://doi.org/10.1007/s00702-008-0083-y

van Ham, T. J., Mapes, J., Kokel, D., & Peterson, R. T. (2010). Live imaging of apoptotic cells in zebrafish. *FASEB Journal : Official Publication of the Federation of American Societies for Experimental Biology*, *24*(11), 4336–4342. https://doi.org/10.1096/fj.10-161018

Vandepoele, K., De Vos, W., Taylor, J. S., Meyer, A., & Van de Peer, Y. (2004). Major events in the genome evolution of vertebrates: Paranome age and size differ considerably between ray-finned fishes and land vertebrates. *Proceedings of the National Academy of Sciences*, *101*(6), 1638–1643. https://doi.org/10.1073/pnas.0307968100

Vargas, R., Thorsteinsson, H., & Karlsson, K. A. E. (2012). Spontaneous neural activity of the anterodorsal lobe and entopeduncular nucleus in adult zebrafish: a putative homologue of hippocampal sharp waves. *Behavioural Brain Research*, *229*(1), 10–20. https://doi.org/10.1016/j.bbr.2011.12.025

Vaz, R. L., Outeiro, T. F., & Ferreira, J. J. (2018). Zebrafish as an Animal Model for Drug Discovery in Parkinson's Disease and Other Movement Disorders: A Systematic Review . In *Frontiers in Neurology* (Vol. 9). https://www.frontiersin.org/article/10.3389/fneur.2018.00347

Veldman, M. B., & Lin, S. (2008). Zebrafish as a Developmental Model Organism for. *Pediatric Research*, *64*(5), 470–476.

Vijayanathan, Y., Lim, F. T., Lim, S. M., Long, C. M., Tan, M. P., Majeed, A. B. A., & Ramasamy, K. (2017). 6-OHDA-Lesioned Adult Zebrafish as a Useful Parkinson's Disease Model for Dopaminergic Neuroregeneration. *Neurotoxicity Research*, *32*(3), 496–508. https://doi.org/10.1007/s12640-017-9778-x

von Trotha, J. W., Vernier, P., & Bally-Cuif, L. (2014). Emotions and motivated behavior converge on an amygdala-like structure in the zebrafish. *The European Journal of Neuroscience*, *40*(9), 3302–3315. https://doi.org/10.1111/ejn.12692

Wang, J., Ambrosi, C., Qiu, F., Jackson, D. G., Sosinsky, G., & Dahl, G. (2014). The membrane protein Pannexin1 forms two open-channel conformations depending on the mode of activation. *Science Signaling*, *7*(335), ra69. https://doi.org/10.1126/scisignal.2005431

Wang, Liu, W., Yang, J., Wang, F., Sima, Y., Zhong, Z.-M., Wang, H., Hu, L.-F., & Liu, C.-F.

(2017). Parkinson's disease-like motor and non-motor symptoms in rotenone-treated zebrafish. *Neurotoxicology*, *58*, 103–109. https://doi.org/10.1016/j.neuro.2016.11.006

Wang, Peng, J., Xie, X., Zhang, Z., Li, M., & Yang, M. (2021). Gasdermin E-mediated programmed cell death: An unpaved path to tumor suppression. *Journal of Cancer*, *12*(17), 5241–5248. https://doi.org/10.7150/jca.48989

Wang, Souders, C. L. 2nd, Zhao, Y. H., & Martyniuk, C. J. (2018). Paraquat affects mitochondrial bioenergetics, dopamine system expression, and locomotor activity in zebrafish (Danio rerio). *Chemosphere*, *191*, 106–117. https://doi.org/10.1016/j.chemosphere.2017.10.032

Wang, Streeter, M., Liu, Y.-P., & Zhao, H.-B. (2009). Identification and characterization of pannexin expression in the mammalian cochlea. *The Journal of Comparative Neurology*, *512*(3), 336–346. https://doi.org/10.1002/cne.21898

Weil, R. S., Schrag, A. E., Warren, J. D., Crutch, S. J., Lees, A. J., & Morris, H. R. (2016). Visual dysfunction in Parkinson's disease. *Brain*, *139*(11), 2827–2843. https://doi.org/10.1093/brain/aww175

Weinberger, M., Mahant, N., Hutchison, W. D., Lozano, A. M., Moro, E., Hodaie, M., Lang, A. E., & Dostrovsky, J. O. (2006). Beta Oscillatory Activity in the Subthalamic Nucleus and Its Relation to Dopaminergic Response in Parkinson's Disease. *Journal of Neurophysiology*, *96*(6), 3248–3256. https://doi.org/10.1152/jn.00697.2006

Whyte-Fagundes, P., Kurtenbach, S., Zoidl, C., Shestopalov, V. I., Carlen, P. L., & Zoidl, G. (2018). A potential compensatory role of Panx3 in the VNO of a Panx1 knock out mouse model. *Frontiers in Molecular Neuroscience*, *11*(April), 1–16. https://doi.org/10.3389/fnmol.2018.00135

Whyte-Fagundes, P., Taskina, D., Safarian, N., Zoidl, C., Carlen, P. L., Donaldson, L. W., & Zoidl, G. R. (2022). Panx1 channels promote both anti- and pro-seizure-like activities in the zebrafish via p2rx7 receptors and ATP signaling. *Communications Biology*, *5*(1), 472. https://doi.org/10.1038/s42003-022-03356-2

Whyte-Fagundes, P., & Zoidl, G. (2018). Mechanisms of pannexin1 channel gating and regulation. *Biochimica et Biophysica Acta - Biomembranes*, *1860*(1), 65–71. https://doi.org/10.1016/j.bbamem.2017.07.009

Wilkaniec, A., Gąssowska, M., Czapski, G. A., Cieślik, M., Sulkowski, G., & Adamczyk, A. (2017). P2X7 receptor-pannexin 1 interaction mediates extracellular alpha-synuclein-induced ATP release in neuroblastoma SH-SY5Y cells. *Purinergic Signalling*, *13*(3), 347–361. https://doi.org/10.1007/s11302-017-9567-2

Yan, Y.-Q., Fang, Y., Zheng, R., Pu, J.-L., & Zhang, B.-R. (2020). NLRP3 Inflammasomes in Parkinson's disease and their Regulation by Parkin. *Neuroscience*, *446*, 323–334. https://doi.org/https://doi.org/10.1016/j.neuroscience.2020.08.004

Yang, Y., Delalio, L. J., Best, A. K., Macal, E., Milstein, J., Donnelly, I., Miller, A. M., McBride, M., Shu, X., Koval, M., Isakson, B. E., & Johnstone, S. R. (2020). Endothelial Pannexin 1 Channels Control Inflammation by Regulating Intracellular Calcium. *The Journal of Immunology*, ji1901089. https://doi.org/10.4049/jimmunol.1901089

Zhou, B., & Abbott, D. W. (2021). Gasdermin E permits interleukin-1 beta release in distinct sublytic and pyroptotic phases. *Cell Reports*, *35*(2). https://doi.org/10.1016/j.celrep.2021.108998

Zoidl, G., Petrasch-Parwez, E., Ray, A., Meier, C., Bunse, S., Habbes, H.-W., Dahl, G., & Dermietzel, R. (2007). Localization of the pannexin1 protein at postsynaptic sites in the

cerebral cortex and hippocampus. *Neuroscience*, *146*(1), 9–16. https://doi.org/10.1016/J.NEUROSCIENCE.2007.01.061

8. Supplementary Information

8.1 RNA-seq Inflammasome

Supplementary Table S1. The log2FC values of inflammasome genes from the DESeq2 analysis. The RNA-seq data was sorted for protein coding mRNAs with a padj (<0.01).

Gene	TL vs Panx1a-KO	TL vs TL MPTP	Panx1a-KO vs Panx1a-KO MPTP	TL MPTP vs Panx1a-KO MPTP
hsp90aa1.2	0	0.827287	1.510336	0
ikbkg	0	3.467043	2.374303	0
map3k7	0	6.132984	0	0
mapk14a	0	0.677304	0.78068	0
mapk3	0	0.519115	0	0
nlrx1	0	0.570114	0.652361	0
ptgs2b	0	1.421092	0	0
tab2	0	7.112244	7.414056	0
txnipa	0	1.0465	1.76458	0
birc2	0	-0.6918	-0.69987	0
caspb	0	-5.25794	-9.80945	-4.68048
ctsba	-0.92574	-10.4984	0.739767	0
fadd	0	-0.74596	0	0
hsp90ab1	-4.75574	-4.42194	6.505541	2.968968
ifih1	0	-2.24154	-1.92889	0
il1b	0	-3.08633	-2.8692	0
irf1b	0	-1.73109	-1.72907	0
irf2	0	-2.15515	0.940664	0
mapk8a	0	-0.96174	0	0
mavs	0	-3.19989	-3.8686	3.70979
nfkb1	0	-0.47537	0	-0.5168
nfkbib	0	-0.62809	-0.59611	0
rela	0	-0.27843	0	0
tbk1	0	-0.56389	0	0
traf2a	0	-5.40836	0	0
ccl27a	0	0	5.209253	0
chuk	0	0	0.40401	0
cxcl19	0	0	2.389303	0
ifngr1	0	0	0.560527	0
irak1	0	0	0.719953	0
irf5	0	0	1.061991	0
mapk12a	0	0	0.912133	1.160048
mapk3	0	0	0.703294	0
nlrb5	-4.9207	0	5.937486	0
p2rx7	-1.1265	0	1.121332	0
panx1a	-2.7253	0	2.345613	0

tnfsf11	0	0	1.129229	0
xiap	0	0	1.020049	0.866899
mapk11	0	0	-0.68651	0
nfkbiab	0	0	0.87982	0
pstpip1a	0	0	-1.72704	0

8.2 RT-qPCR Statistics

Supplementary Table S2. Comparison between control TL and MPTP-treated TL larvae (50µM MPTP). Expression levels and statistical tests were performed using the REST 2009 software. P(H1) is the probability of the alternate hypothesis that the difference between sample and control groups is due only to chance. 95% C.I. is the confidence interval. Results shows whether the gene tested was significantly up- or down-regulated. Significance was determined as P-value (<0.05).

Gene	Expression	Std. Error	95% C.I.	P(H1)	Results
caspa 3	0.832	0.277 - 2.466	0.197 - 3.490	0.549	
capsa 7	0.795	0.302 - 2.229	0.187 - 3.910	0.446	
caspa 9	1.038	0.421 - 2.897	0.251 - 3.945	0.868	
caspa 1	1.256	0.462 - 3.382	0.332 - 5.057	0.434	
ATP5pf	0.465	0.035 - 2.839	0.018 - 4.823	0.221	
COX4i1	1.329	0.682 - 2.710	0.473 - 4.724	0.235	
Ndufa10	0.886	0.447 - 2.137	0.379 - 3.387	0.596	
Uqcrq	1.982	1.399 - 2.748	1.042 - 3.945	0	UP
CFTR	3.158	1.383 - 7.531	0.865 - 10.339	0	UP
EEF2K	1.277	0.553 - 2.811	0.358 - 3.655	0.304	
PCK1	2.567	0.654 - 10.874	0.233 - 21.857	0.059	
PFKFB3	2.101	1.062 - 4.254	0.768 - 6.320	0.004	UP
IL-1B	1.644	0.428 - 13.011	0.235 - 19.306	0.334	
panIL-16	1.003	0.585 - 1.614	0.384 - 2.102	0.984	
NLRP3	1.051	0.483 - 2.445	0.287 - 6.453	0.873	
Pycard	1.221	0.612 - 2.572	0.363 - 4.377	0.407	

Gasdermin E	0.598	0.289 - 1.127	0.153 - 1.729	0.043	DOWN

Supplementary Table S3. Comparison between control Panx1a-KO and MPTP-treated Panx1a-KO larvae (50μM MPTP). Expression levels and statistical tests were performed using the REST 2009 software. P(H1) is the probability of the alternate hypothesis that the difference between sample and control groups is due only to chance. 95% C.I. is the confidence interval. Results shows whether the gene tested was significantly up- or down-regulated. Significance was determined as P-value (<0.05).

Gene	Expression	Std. Error	95% C.I.	P(H1)	Results
caspa 3	0.673	0.280 - 1.694	0.111 - 3.665	0.245	
capsa 7	0.595	0.238 - 1.385	0.148 - 2.745	0.096	
caspa 9	1.11	0.478 - 3.170	0.230 - 4.332	0.72	
caspa 1	1.382	0.561 - 3.689	0.282 - 6.385	0.29	
ATP5pf	1.486	1.004 - 2.201	0.763 - 3.434	0.01	UP
COX4i1	1.291	0.680 - 2.233	0.418 - 3.182	0.193	
Ndufa10	1.225	0.670 - 2.339	0.412 - 4.170	0.34	
Uqcrq	1.411	0.860 - 2.212	0.532 - 3.010	0.046	UP
CFTR	5.794	3.856 - 8.815	3.294 - 11.551	0	UP
EEF2K	1.38	0.912 - 2.046	0.683 - 2.657	0.026	UP
PCK1	2.705	1.258 - 5.524	1.050 - 8.168	0.001	UP
PFKFB3	1.789	1.071 - 3.233	0.758 - 4.287	0.006	UP
IL-1B	0.847	0.473 - 1.322	0.236 - 2.085	0.414	
panIL-16	1.489	0.972 - 2.301	0.642 - 3.420	0.024	UP
NLRP3	0.574	0.309 - 0.960	0.204 - 1.729	0.019	DOWN
Pycard	0.661	0.360 - 1.130	0.243 - 1.853	0.051	
Gasdermin E	0.818	0.457 - 1.485	0.287 - 2.173	0.328	

8.3 ATP Assay Statistical Information

Supplementary Table S4. Extracellular ATP concentration values after four hours of MPTP treatment. TL and Panx1a-KO *Danio rerio* larvae at 6dpf ATP concentrations were compared before and after MPTP treatment. Statistical significance was calculated using GraphPad Prism. A Welch's t-test was applied. Significance was determined as P-value (<0.05).

Treatment	P value	P value summary	Welch-corrected t, df	ATP Concentration Control (nm/µg)	ATP Concentration MPTP (nm/µg)
Control TL vs MPTP (10µM) TL	0.0229	*	t=6.459, df=2.008	2.709	0.9587
Control Panx1a-KO vs MPTP (10µM) Panx1a-KO	0.8566	ns	t=0.1980, df=2.783	1.018	0.946

8.4 LFP Statistical Information

8.4.1 LFP: Beta Peak Frequency

Supplementary Table S5. The comparison of beta band peak frequency before and after probenecid treatment. The TL and Panx1a-KO larvae were placed under the electrophysiology setup and baseline recordings were performed from the DM, DL and OT regions. After baseline recordings in the light and dark, the larvae were treated with probenecid for 30 minutes. After incubation with the drug the larvae's brain activity was recorded in the light and the dark. NeuroExplorer was used to calculate the power spectral density. The beta band peak frequency was compared before and after treatment using a Paired t-test. Significance was determined as P-value (<0.05).

Genotype and Treatment	P-value	Significant?	T ratio and Degrees of freedom (df)	Mean of Control	Mean of Treatment
TL DM Dark	0.7305	No	t=0.3781, df=3	0.03372	0.03857
TL DM Light	0.3667	No	t=1.061, df=3	0.03814	0.06128
TL DL Dark	0.2642	No	t=1.370, df=3	0.08904	0.01893
TL DL Light	0.4399	No	t=0.8882, df=3	0.09177	0.0429
TL OT Dark	0.2646	No	t=1.213, df=7	0.05221	0.03897
TL OT Light	0.6926	No	t=0.4120, df=7	0.05703	0.05081
Panx1a-KO DM Dark	0.896	No	t=0.1420, df=3	0.04217	0.04579
Panx1a-KO DM Light	0.6357	No	t=0.5253, df=3	0.03677	0.0445
Panx1a-KO DL Dark	0.617	No	t=0.5863, df=2	0.03417	0.04377

Panx1a-KO DL Light	0.3207	No	t=1.309, df=2	0.02959	0.03635
Panx1a-KO OT Dark	0.5219	No	t=0.7011, df=4	0.03544	0.03048
Panx1a-KO OT Light	0.6034	No	t=0.5632, df=4	0.03044	0.03596

Supplementary Table S6. The comparison of beta band peak frequency before and after bicuculline treatment. The TL and Panx1a-KO larvae were placed under the electrophysiology setup and baseline recordings were performed from the DM, DL and OT regions. After baseline recordings in the light and dark, the larvae were treated with bicuculline for 30 minutes. After incubation with the drug the larvae's brain activity was recorded in the light and the dark. NeuroExplorer was used to calculate the power spectral density. The beta band peak frequency was compared before and after treatment using a Paired t-test. Significance was determined as P-value (<0.05).

Genotype and Treatment	P-value	Significant?	T ratio and Degrees of freedom (df)	Mean of Control	Mean of Treatment
TL DM Dark	0.6349	No	t=0.5132, df=4	0.03739	0.0319
TL DM Light	0.6478	No	t=0.4931, df=4	0.04608	0.03809
TL DL Dark	0.5735	No	t=0.6299, df=3	0.06545	0.05826
TL DL Light	0.609	No	t=0.5693, df=3	0.07608	0.08946
TL OT Dark	0.535	No	t=0.6482, df=8	0.04467	0.05204
TL OT Light	0.2913	No	t=1.130, df=8	0.05248	0.08013
Panx1a-KO DM Dark	0.1345	No	t=2.037, df=3	0.0497	0.03006
Panx1a-KO DM Light	0.2893	No	t=1.284, df=3	0.05178	0.02944
Panx1a-KO DL Dark	0.0101	*	t=9.888, df=2	0.07894	0.04407
Panx1a-KO DL Light	0.0134	*	t=8.551, df=2	0.08532	0.04549
Panx1a-KO OT Dark	0.0485	*	t=2.385, df=7	0.0626	0.03993
Panx1a-KO OT Light	0.0082	**	t=3.651, df=7	0.0614	0.03228

Supplementary Table S7. The comparison of beta band peak frequency before and after MK-801 treatment. The TL and Panx1a-KO larvae were placed under the electrophysiology setup and baseline recordings were performed from the DM, DL and OT regions. After baseline recordings in the light and dark, the larvae were treated with MK-801 for 30 minutes. After incubation with the drug the larvae's brain activity was recorded in the light and the dark. NeuroExplorer was used to calculate the power spectral density. The beta band peak frequency was compared before and after treatment using a Paired t-test. Significance was determined as P-value (<0.05).

Genotype and Treatment	P-value	Significant?	T ratio and Degrees of freedom (df)	Mean of Control	Mean of Treatment

TL DM Dark	0.7741	No	t=0.3140, df=3	0.03387	0.02952
TL DM Light	0.0477	*	t=3.245, df=3	0.04082	0.02432
TL DL Dark	0.1163	No	t=2.670, df=2	0.04362	0.0292
TL DL Light	0.0668	No	t=3.673, df=2	0.05128	0.02754
TL OT Dark	0.2804	No	t=1.186, df=6	0.04222	0.03118
TL OT Light	0.7347	No	t=0.3550, df=6	0.03511	0.03362
Panx1a-KO DM Dark	0.403	No	t=0.9345, df=4	0.03806	0.03078
Panx1a-KO DM Light	0.113	No	t=2.024, df=4	0.04774	0.02926
Panx1a-KO DL Dark	0.9624	No	t=0.05318, df=2	0.02792	0.0275
Panx1a-KO DL Light	0.1436	No	t=2.346, df=2	0.03487	0.0219
Panx1a-KO OT Dark	0.0239	*	t=3.202, df=5	0.04288	0.0308
Panx1a-KO OT Light	0.0221	*	t=3.273, df=5	0.04534	0.02957

Supplementary Table S8. The comparison of beta band peak frequency before and after MPTP treatment. The TL and Panx1a-KO were incubated with MPTP for four hours in the dark. After incubation the larvae's brain activity was recorded in the light and the dark. NeuroExplorer was used to calculate the power spectral density. The beta band peak frequency was compared before and after treatment using a Welch's t-test. Significance was determined as P-value (<0.05).

Genotype and Treatment	P-value	Significant?	T ratio and Degrees of freedom (df)	Mean of Control	Mean of Treatment
TL DM Dark	0.7798	No	t=0.2924, df=6.000	0.03372	0.03039
TL DM Light	0.0942	No	t=1.987, df=5.985	0.04905	0.03441
TL DL Dark	0.441	No	t=0.8837, df=3.046	0.08904	0.0433
TL DL Light	0.3022	No	t=1.234, df=3.113	0.09177	0.0355
TL OT Dark	0.1322	No	t=1.614, df=12.14	0.05221	0.04041
TL OT Light	0.6158	No	t=0.5133, df=13.95	0.05703	0.04941
Panx1a-KO DM Dark	0.7173	No	t=0.3828, df=5.084	0.04217	0.03648
Panx1a-KO DM Light	0.821	No	t=0.2364, df=5.998	0.03677	0.03918
Panx1a-KO DL Dark	0.107	No	t=2.115, df=3.722	0.03417	0.08315
Panx1a-KO DL Light	0.1411	No	t=1.934, df=3.264	0.02959	0.05644

Panx1a-KO OT Dark	0.0392	*	t=2.514, df=7.227	0.03677	0.08414
Panx1a-KO OT Light	0.0414	*	t=2.304, df=11.16	0.03224	0.05953

8.4.2 LFP: Gamma Peak Frequency

Supplementary Table S9. The comparison of gamma band peak frequency before and after probenecid treatment. The TL and Panx1a-KO larvae were placed under the electrophysiology setup and baseline recordings were performed from the DM, DL and OT regions. After baseline recordings in the light and dark, the larvae were treated with probenecid for 30 minutes. After incubation with the drug the larvae's brain activity was recorded in the light and the dark. NeuroExplorer was used to calculate the power spectral density. The gamma band peak frequency was compared before and after treatment using a Paired t-test. Significance was determined as P-value (<0.05).

Genotype and Treatment	P-value	Significant?	T ratio and Degrees of freedom (df)	Mean of Control	Mean of Treatment
TL DM Dark	0.3636	No	t=1.069, df=3	2.195	3.736
TL DM Light	0.0504	No	t=3.173, df=3	2.85	4.241
TL DL Dark	0.1691	No	t=1.803, df=3	1.39	1.687
TL DL Light	0.9065	No	t=0.1276, df=3	1.792	1.505
TL OT Dark	0.3029	No	t=1.112, df=7	1.911	3.054
TL OT Light	0.3586	No	t=0.9825, df=7	2.199	3.482
Panx1a-KO DM Dark	0.3562	No	t=1.088, df=3	0.91	0.3548
Panx1a-KO DM Light	0.2746	No	t=1.334, df=3	0.9811	0.2394
Panx1a-KO DL Dark	0.4197	No	t=1.008, df=2	0.414	1.175
Panx1a-KO DL Light	0.4654	No	t=0.8946, df=2	1.268	1.412
Panx1a-KO OT Dark	0.0635	No	t=2.547, df=4	3.128	0.9536
Panx1a-KO OT Light	0.8235	No	t=0.2382, df=4	2.384	2.272

Supplementary Table S10. The comparison of gamma band peak frequency before and after bicuculline treatment. The TL and Panx1a-KO larvae were placed under the electrophysiology setup and baseline recordings were performed from the DM, DL and OT regions. After baseline recordings in the light and

dark, the larvae were treated with bicuculline for 30 minutes. After incubation with the drug the larvae's brain activity was recorded in the light and the dark. NeuroExplorer was used to calculate the power spectral density. The gamma band peak frequency was compared before and after treatment using a Paired t-test. Significance was determined as P-value (<0.05).

Genotype and Treatment	P-value	Significant?	T ratio and Degrees of freedom (df)	Mean of Control	Mean of Treatment
TL DM Dark	0.0966	No	t=2.163, df=4	1.124	2.311
TL DM Light	0.5893	No	t=0.5861, df=4	2.008	1.464
TL DL Dark	0.1806	No	t=1.738, df=3	1.917	1.032
TL DL Light	0.385	No	t=1.015, df=3	1.68	1.228
TL OT Dark	0.2176	No	t=1.338, df=8	1.551	1.248
TL OT Light	0.6399	No	t=0.4861, df=8	1.418	1.227
Panx1a-KO DM Dark	0.1216	No	t=2.142, df=3	0.8535	4.024
Panx1a-KO DM Light	0.0726	No	t=2.719, df=3	1.414	5.006
Panx1a-KO DL Dark	0.2516	No	t=1.596, df=2	0.2943	0.0384
Panx1a-KO DL Light	0.2608	No	t=1.552, df=2	0.05855	0.02289
Panx1a-KO OT Dark	0.7787	No	t=0.2920, df=7	1.586	1.833
Panx1a-KO OT Light	0.0452	*	t=2.433, df=7	0.7489	2.097

Supplementary Table S11. The comparison of gamma band peak frequency before and after MK-801 treatment. The TL and Panx1a-KO larvae were placed under the electrophysiology setup and baseline recordings were performed from the DM, DL and OT regions. After baseline recordings in the light and dark, the larvae were treated with MK-801 for 30 minutes. After incubation with the drug the larvae's brain activity was recorded in the light and the dark. NeuroExplorer was used to calculate the power spectral density. The gamma band peak frequency was compared before and after treatment using a Paired t-test. Significance was determined as P-value (<0.05).

Genotype and Treatment	P-value	Significant?	T ratio and Degrees of freedom (df)	Mean of Control	Mean of Treatment
TL DM Dark	0.1271	No	t=2.096, df=3	0.2745	2.966
TL DM Light	0.1988	No	t=1.644, df=3	0.5532	3.159

TL DL Dark	0.1977	No	t=1.901, df=2	1.238	1.07
TL DL Light	0.1374	No	t=2.412, df=2	1.086	1.369
TL OT Dark	0.8267	No	t=0.2387, df=3	2.468	2.083
TL OT Light	0.6528	No	t=0.4978, df=3	2.845	2.417
Panx1a-KO DM Dark	0.6662	No	t=0.4649, df=4	2.094	1.859
Panx1a-KO DM Light	0.2043	No	t=1.515, df=4	1.36	2.665
Panx1a-KO DL Dark	0.3313	No	t=1.272, df=2	1.656	0.4371
Panx1a-KO DL Light	0.4327	No	t=0.9742, df=2	1.594	0.4647
Panx1a-KO OT Dark	0.2506	No	t=1.299, df=5	1.641	2.509
Panx1a-KO OT Light	0.0827	No	t=2.164, df=5	1.191	2.885

Supplementary Table S12. The comparison of gamma band peak frequency before and after MPTP treatment. The TL and Panx1a-KO were incubated with MPTP for four hours in the dark. After incubation the larvae's brain activity was recorded in the light and the dark. NeuroExplorer was used to calculate the power spectral density. The gamma band peak frequency was compared before and after treatment using a Welch's t-test. Significance was determined as P-value (<0.05).

Genotype and Treatment	P-value	Significant?	T ratio and Degrees of freedom (df)	Mean of Control	Mean of Treatment
TL DM Dark	0.5951	No	t=0.5658, df=5.194	2.195	1.198
TL DM Light	0.6332	No	t=0.5026, df=5.975	2.85	1.77
TL DL Dark	0.4043	No	t=0.9625, df=3.123	1.39	0.3136
TL DL Light	0.3974	No	t=0.9731, df=3.242	1.792	0.3872
TL OT Dark	0.0475	*	t=2.173, df=14.00	1.911	4.725
TL OT Light	0.0815	No	t=1.969, df=8.733	2.523	5.336
Panx1a-KO DM Dark	0.3912	No	t=0.9961, df=3.064	0.91	0.2009
Panx1a-KO DM Light	0.4096	No	t=0.9486, df=3.158	0.9811	0.2764
Panx1a-KO DL Dark	0.5736	No	t=0.6252, df=3.201	0.414	0.8552
Panx1a-KO DL Light	0.8088	No	t=0.2628, df=3.179	1.268	0.9

Panx1a-KO OT Dark	0.2831	No	t=1.157, df=7.431	3.128	1.539
Panx1a-KO OT Light	0.787	No	t=0.2796, df=7.880	2.384	1.95

8.4.3 LFP: Beta Average Frequency

Supplementary Table S13. The comparison of average beta band power before and after probenecid treatment. The TL and Panx1a-KO larvae were placed under the electrophysiology setup and baseline recordings were performed from the DM, DL and OT regions. After baseline recordings in the light and dark, the larvae were treated with probenecid for 30 minutes. After incubation with the drug the larvae's brain activity was recorded in the light and the dark. NeuroExplorer was used to calculate the power spectral density. The beta band (12-30Hz) average frequency power was compared before and after treatment using a Paired t-test. Significance was determined as P-value (<0.05).

Larva and Treatment	P-value	Significant?	T ratio and Degrees of freedom (df)	Mean of Control	Mean of Treatment
TL DM Dark	<0.0001	****	t=9.180, df=101	0.01118	0.01447
TL DM Light	<0.0001	****	t=8.877, df=101	0.01003	0.01274
TL DL Dark	<0.0001	****	t=12.02, df=101	0.01525	0.00726
TL DL Light	0.0002	***	t=3.924, df=101	0.01748	0.01483
TL OT Dark	<0.0001	****	t=22.08, df=101	0.01722	0.00992
TL OT Light	<0.0001	****	t=15.54, df=101	0.01791	0.01296
Panx1a-KO DM Dark	<0.0001	****	t=5.200, df=101	0.01922	0.02077
Panx1a-KO DM Light	<0.0001	****	t=17.74, df=101	0.01217	0.01795
Panx1a-KO DL Dark	<0.0001	****	t=18.58, df=107	0.009643	0.01513
Panx1a-KO DL Light	<0.0001	****	t=17.18, df=107	0.009016	0.01359
Panx1a-KO OT Dark	<0.0001	****	t=8.362, df=107	0.01055	0.01227
Panx1a-KO OT Light	<0.0001	****	t=14.57, df=107	0.009621	0.01258

Supplementary Table S14. The comparison of average beta band power before and after bicuculline treatment. The TL and Panx1a-KO larvae were placed under the electrophysiology setup and baseline recordings were performed from the DM, DL and OT regions. After baseline recordings in the light and

dark, the larvae were treated with bicuculline for 30 minutes. After incubation with the drug the larvae's brain activity was recorded in the light and the dark. NeuroExplorer was used to calculate the power spectral density. The beta band (12-30Hz) average frequency power was compared before and after treatment using a Paired t-test. Significance was determined as P-value (<0.05).

Larva and Treatment	P-value	Significant?	T ratio and Degrees of freedom (df)	Mean of Control	Mean of Treatment
TL DM Dark	<0.0001	****	t=13.12, df=107	0.01246	0.01061
TL DM Light	0.0077	**	t=2.718, df=107	0.0113	0.01215
TL DL Dark	<0.0001	****	t=21.14, df=106	0.02596	0.01942
TL DL Light	<0.0001	****	t=5.621, df=106	0.02897	0.02667
TL OT Dark	<0.0001	****	t=9.746, df=107	0.01715	0.01567
TL OT Light	0.001	***	t=3.385, df=107	0.01886	0.02
Panx1a-KO DM Dark	<0.0001	****	t=21.37, df=107	0.02206	0.008986
Panx1a-KO DM Light	<0.0001	****	t=14.89, df=107	0.0208	0.008901
Panx1a-KO DL Dark	<0.0001	****	t=27.39, df=107	0.03219	0.01494
Panx1a-KO DL Light	<0.0001	****	t=16.11, df=107	0.02598	0.01416
Panx1a-KO OT Dark	<0.0001	****	t=28.55, df=107	0.02199	0.01357
Panx1a-KO OT Light	<0.0001	****	t=17.89, df=107	0.02264	0.0111

Supplementary Table S15. The comparison of average beta band power before and after MK-801 treatment. The TL and Panx1a-KO larvae were placed under the electrophysiology setup and baseline recordings were performed from the DM, DL and OT regions. After baseline recordings in the light and dark, the larvae were treated with MK-801 for 30 minutes. After incubation with the drug the larvae's brain activity was recorded in the light and the dark. NeuroExplorer was used to calculate the power spectral density. The beta band (12-30Hz) average frequency power was compared before and after treatment using a Paired t-test. Significance was determined as P-value (<0.05).

Larva and Treatment	P-value	Significant?	T ratio and Degrees of freedom (df)	Mean of Control	Mean of Treatment
TL DM Dark	<0.0001	****	t=17.39, df=101	0.01505	0.01194
TL DM Light	<0.0001	****	t=21.42, df=101	0.01575	0.01088
TL DL Dark	<0.0001	****	t=27.82, df=107	0.02094	0.01302
TL DL Light	<0.0001	****	t=28.61, df=107	0.02324	0.01234
TL OT Dark	<0.0001	****	t=12.86, df=107	0.01046	0.01234
TL OT Light	<0.0001	****	t=9.490, df=107	0.009228	0.01081

Panx1a-KO DM Dark	0.0002	***	t=3.868, df=107	0.01341	0.01423
Panx1a-KO DM Light	<0.0001	****	t=10.41, df=107	0.01521	0.009592
Panx1a-KO DL Dark	0.5218	No	t=0.6427, df=107	0.01009	0.009979
Panx1a-KO DL Light	<0.0001	****	t=11.18, df=107	0.01236	0.008641
Panx1a-KO OT Dark	<0.0001	****	t=18.79, df=107	0.01351	0.008155
Panx1a-KO OT Light	<0.0001	****	t=14.17, df=107	0.01539	0.008503

Supplementary Table S16. The comparison of average beta band power before and after MPTP treatment. The TL and Panx1a-KO were incubated with MPTP for four hours in the dark. After incubation the larvae's brain activity was recorded in the light and the dark. NeuroExplorer was used to calculate the power spectral density. The beta band (12-30Hz) average frequency power was compared before and after treatment using a Welch's t-test. Significance was determined as P-value (<0.05).

Larva and Treatment	P-value	Significant?	T ratio and Degrees of freedom (df)	Mean of Control	Mean of Treatment
TL DM Dark	<0.0001	****	t=4.940, df=198.7	0.01118	0.0145
TL DM Light	<0.0001	****	t=6.978, df=201.8	0.01003	0.01452
TL DL Dark	<0.0001	****	t=4.894, df=197.7	0.01525	0.02044
TL DL Light	0.1159	No	t=1.580, df=181.4	0.01748	0.01581
TL OT Dark	<0.0001	****	t=5.777, df=192.1	0.01722	0.01277
TL OT Light	<0.0001	****	t=7.832, df=196.3	0.01791	0.01145
Panx1a-KO DM Dark	0.0665	No	t=1.846, df=185.9	0.01922	0.01748
Panx1a-KO DM Light	<0.0001	****	t=5.802, df=193.8	0.01217	0.01713
Panx1a-KO DL Dark	<0.0001	****	t=15.71, df=144.6	0.009643	0.03367
Panx1a-KO DL Light	<0.0001	****	t=10.45, df=147.2	0.009016	0.02165
Panx1a-KO OT Dark	<0.0001	****	t=19.47, df=140.0	0.01055	0.03665
Panx1a-KO OT Light	<0.0001	****	t=13.73, df=148.5	0.009621	0.02475

8.4.4 LFP: Gamma Average Frequency

Supplementary Table S17. The comparison of average gamma band power before and after probenecid treatment. The TL and Panx1a-KO larvae were placed under the electrophysiology setup and baseline recordings were performed from the DM, DL and OT regions. After baseline recordings in the light and dark, the larvae were treated with probenecid for 30 minutes. After incubation with the drug the larvae's

brain activity was recorded in the light and the dark. NeuroExplorer was used to calculate the power spectral density.The gamma band (35-45Hz) average frequency power was compared before and after treatment using a Paired t-test. Significance was determined as P-value (<0.05).

Larva and Treatment	P-value	Significant?	T ratio and Degrees of freedom (df)	Mean of Control	Mean of Treatment
TL DM Dark	<0.0001	****	t=4.575, df=59	0.4858	0.7175
TL DM Light	0.0077	**	t=2.760, df=59	0.6737	0.7856
TL DL Dark	0.795	No	t=0.2610, df=59	0.3135	0.3171
TL DL Light	<0.0001	****	t=4.856, df=59	0.337	0.2727
TL OT Dark	<0.0001	****	t=4.988, df=59	0.3611	0.5737
TL OT Light	<0.0001	****	t=5.135, df=59	0.4183	0.6306
Panx1a-KO DM Dark	<0.0001	****	t=5.274, df=59	0.1733	0.07283
Panx1a-KO DM Light	<0.0001	****	t=5.751, df=59	0.1776	0.05369
Panx1a-KO DL Dark	<0.0001	****	t=5.558, df=59	0.08333	0.2172
Panx1a-KO DL Light	0.6815	No	t=0.4124, df=59	0.2544	0.2446
Panx1a-KO OT Dark	<0.0001	****	t=5.570, df=59	0.5494	0.1759
Panx1a-KO OT Light	0.0024	**	t=3.167, df=59	0.4185	0.3642

Supplementary Table S18. The comparison of average gamma band power before and after bicuculline treatment. The TL and Panx1a-KO larvae were placed under the electrophysiology setup and baseline recordings were performed from the DM, DL and OT regions. After baseline recordings in the light and dark, the larvae were treated with bicuculline for 30 minutes. After incubation with the drug the larvae's brain activity was recorded in the light and the dark. NeuroExplorer was used to calculate the power spectral density. The gamma band (35-45Hz) average frequency power was compared before and after treatment using a Paired t-test. Significance was determined as P-value (<0.05).

Larva and Treatment	P-value	Significant?	T ratio and Degrees of freedom (df)	Mean of Control	Mean of Treatment
TL DM Dark	0.0002	***	t=3.908, df=59	0.2504	0.3848
TL DM Light	<0.0001	****	t=4.392, df=59	0.377	0.2528
TL DL Dark	<0.0001	****	t=6.010, df=59	0.4084	0.1895
TL DL Light	0.0047	**	t=2.941, df=59	0.2987	0.2144
TL OT Dark	0.0065	**	t=2.824, df=59	0.2838	0.255

TL OT Light	0.0241	*	t=2.314, df=59	0.2695	0.2377
Panx1a-KO DM Dark	<0.0001	****	t=6.364, df=59	0.1831	0.7544
Panx1a-KO DM Light	<0.0001	****	t=6.204, df=59	0.2972	0.7734
Panx1a-KO DL Dark	<0.0001	****	t=7.930, df=59	0.07475	0.0111
Panx1a-KO DL Light	<0.0001	****	t=9.064, df=59	0.01877	0.008288
Panx1a-KO OT Dark	0.7851	No	t=0.2739, df=59	0.3268	0.3218
Panx1a-KO OT Light	<0.0001	****	t=5.338, df=59	0.17	0.3837

Supplementary Table S19. The comparison of average gamma band power before and after MK-801 treatment. The TL and Panx1a-KO larvae were placed under the electrophysiology setup and baseline recordings were performed from the DM, DL and OT regions. After baseline recordings in the light and dark, the larvae were treated with MK-801 for 30 minutes. After incubation with the drug the larvae's brain activity was recorded in the light and the dark. NeuroExplorer was used to calculate the power spectral density. The gamma band (35-45Hz) average frequency power was compared before and after treatment using a Paired t-test. Significance was determined as P-value (<0.05).

Larva and Treatment	P-value	Significant?	T ratio and Degrees of freedom (df)	Mean of Control	Mean of Treatment
TL DM Dark	<0.0001	****	t=6.184, df=59	0.05693	0.3942
TL DM Light	<0.0001	****	t=5.670, df=59	0.09263	0.4275
TL DL Dark	<0.0001	****	t=4.406, df=59	0.2954	0.1731
TL DL Light	0.0014	**	t=3.354, df=59	0.2003	0.2696
TL OT Dark	0.0174	*	t=2.448, df=59	0.4676	0.3861
TL OT Light	0.0027	**	t=3.133, df=59	0.5476	0.4542
Panx1a-KO DM Dark	0.0248	*	t=2.303, df=59	0.433	0.3828
Panx1a-KO DM Light	<0.0001	****	t=5.687, df=59	0.3117	0.5212
Panx1a-KO DL Dark	<0.0001	****	t=5.672, df=59	0.3107	0.1003
Panx1a-KO DL Light	<0.0001	****	t=4.602, df=59	0.2227	0.07631
Panx1a-KO OT Dark	<0.0001	****	t=5.043, df=59	0.313	0.4448
Panx1a-KO OT Light	<0.0001	****	t=5.900, df=59	0.235	0.504

Supplementary Table S20. The comparison of average gamma band power before and after MPTP treatment. The TL and Panx1a-KO were incubated with MPTP for four hours in the dark. After incubation the larvae's brain activity was recorded in the light and the dark. NeuroExplorer was used to calculate the power spectral density. The gamma band (35-45Hz) average frequency power was compared before and after treatment using a Welch's t-test. Significance was determined as P-value (<0.05).

Larva and Treatment	P-value	Significant?	T ratio and Degrees of freedom (df)	Mean of Control	Mean of Treatment
TL DM Dark	0.0019	**	t=3.212, df=84.79	0.4858	0.224
TL DM Light	0.0025	**	t=3.109, df=86.86	0.6737	0.3417
TL DL Dark	<0.0001	****	t=5.032, df=61.70	0.3135	0.06554
TL DL Light	<0.0001	****	t=4.654, df=62.87	0.337	0.07477
TL OT Dark	0.0014	**	t=3.304, df=83.38	0.3611	0.8205
TL OT Light	0.0079	**	t=2.721, df=86.13	0.4183	0.8247
Panx1a-KO DM Dark	<0.0001	****	t=4.420, df=63.61	0.1733	0.05078
Panx1a-KO DM Light	0.0003	***	t=3.830, df=68.52	0.1776	0.06688
Panx1a-KO DL Dark	0.0012	**	t=3.358, df=79.94	0.08333	0.1783
Panx1a-KO DL Light	0.0071	**	t=2.759, df=87.82	0.2544	0.1309
Panx1a-KO OT Dark	0.0127	*	t=2.547, df=84.75	0.5494	0.2851
Panx1a-KO OT Light	0.3724	No	t=0.8955, df=113.2	0.4185	0.339

8.4.5 LFP: Coherence Statistics

Supplementary Table S21. The comparison of coherence between the DM and OT and the DL and OT regions before and after probenecid treatment. TL and Panx1a-KO larvae were recorded at baseline and after 30-minute probenecid treatment. The coherence between ascending visual pathway regions was calculated using NeuroExplorer and split into five frequency bands: delta, theta, alpha, beta and gamma. A 2-way ANOVA analysis with Tukey's multiple comparison was performed on each frequency band using GraphPad Prism. DM stands for the coherence between the DM and OT regions. DL stands for the coherence between the DL and OT regions.

Delta

Tukey's multiple comparisons test	Mean Diff.	95.00% CI of diff.	Below threshold?	Summary	Adjusted P Value
TL DM Baseline Dark vs Control Light	0.03615	-0.1675 to 0.2398	No	ns	0.9673
TL DM Baseline Dark vs PROB (20µM) Dark	-0.1187	-0.3224 to 0.08493	No	ns	0.431
TL DM Baseline Light vs PROB (20µM) Light	-0.03597	-0.2396 to 0.1677	No	ns	0.9678
TL DM PROB (20µM) Dark vs PROB (20µM) Light	0.1189	-0.08475 to 0.3226	No	ns	0.4296

TL DL Baseline Dark vs Control Light	0.006263	-0.2331 to 0.2456	No	ns	0.9999
TL DL Baseline Dark vs PROB (20µM) Dark	-0.09529	-0.3346 to 0.1440	No	ns	0.7292
TL DL Baseline Light vs PROB (20µM) Light	-0.1272	-0.3665 to 0.1122	No	ns	0.5132
TL DL PROB (20µM) Dark vs PROB (20µM) Light	-0.02561	-0.2649 to 0.2137	No	ns	0.9925
Panx1a-KO DM Baseline Dark vs Control Light	-0.2233	-0.4031 to -0.04342	Yes	**	0.0083
Panx1a-KO DM Baseline Dark vs PROB (20µM) Dark	-0.4784	-0.6583 to -0.2986	Yes	****	<0.0001
Panx1a-KO DM Baseline Light vs PROB (20µM) Light	-0.1595	-0.3394 to 0.02034	No	ns	0.1016
Panx1a-KO DM PROB (20µM) Dark vs PROB (20µM) Light	0.09564	-0.08421 to 0.2755	No	ns	0.5125
Panx1a-KO DL Baseline Dark vs Control Light	0.005796	-0.2481 to 0.2597	No	ns	>0.9999
Panx1a-KO DL Baseline Dark vs PROB (20µM) Dark	0.04036	-0.2136 to 0.2943	No	ns	0.9761
Panx1a-KO DL Baseline Light vs PROB (20µM) Light	0.00355	-0.2504 to 0.2575	No	ns	>0.9999
Panx1a-KO DL PROB (20µM) Dark vs PROB (20µM) Light	-0.03101	-0.2849 to 0.2229	No	ns	0.9889

Theta

Tukey's multiple comparisons test	**Mean Diff.**	**95.00% CI of diff.**	**Below threshold?**	**Summary**	**Adjusted P Value**
TL DM Baseline Dark vs Control Light	0.008017	-0.1192 to 0.1353	No	ns	0.9985
TL DM Baseline Dark vs PROB (20µM) Dark	-0.04197	-0.1692 to 0.08526	No	ns	0.8292
TL DM Baseline Light vs PROB (20µM) Light	-0.06535	-0.1926 to 0.06189	No	ns	0.5464

TL DM PROB (20µM) Dark vs PROB (20µM) Light	-0.01536	-0.1426 to 0.1119	No	ns	0.9895
TL DL Baseline Dark vs Control Light	-0.02265	-0.1809 to 0.1356	No	ns	0.9827
TL DL Baseline Dark vs PROB (20µM) Dark	-0.1036	-0.2618 to 0.05474	No	ns	0.3305
TL DL Baseline Light vs PROB (20µM) Light	-0.141	-0.2993 to 0.01730	No	ns	0.1
TL DL PROB (20µM) Dark vs PROB (20µM) Light	-0.06008	-0.2184 to 0.09821	No	ns	0.7605
Panx1a-KO DM Baseline Dark vs Control Light	-0.1403	-0.2538 to -0.02683	Yes	**	0.0084
Panx1a-KO DM Baseline Dark vs PROB (20µM) Dark	-0.3876	-0.5011 to -0.2742	Yes	****	<0.0001
Panx1a-KO DM Baseline Light vs PROB (20µM) Light	-0.1354	-0.2488 to -0.02192	Yes	*	0.012
Panx1a-KO DM PROB (20µM) Dark vs PROB (20µM) Light	0.1119	-0.001522 to 0.2254	No	ns	0.0547
Panx1a-KO DL Baseline Dark vs Control Light	0.03276	-0.1331 to 0.1987	No	ns	0.9566
Panx1a-KO DL Baseline Dark vs PROB (20µM) Dark	0.01011	-0.1558 to 0.1760	No	ns	0.9986
Panx1a-KO DL Baseline Light vs PROB (20µM) Light	-0.01752	-0.1834 to 0.1484	No	ns	0.9929
Panx1a-KO DL PROB (20µM) Dark vs PROB (20µM) Light	0.005134	-0.1608 to 0.1710	No	ns	0.9998

Alpha

Tukey's multiple comparisons test	**Mean Diff.**	**95.00% CI of diff.**	**Below threshold?**	**Summary**	**Adjusted P Value**
TL DM Baseline Dark vs Control Light	0.05676	-0.03570 to 0.1492	No	ns	0.3888
TL DM Baseline Dark vs PROB (20µM) Dark	0.0507	-0.04176 to 0.1432	No	ns	0.4905

TL DM Baseline Light vs PROB (20µM) Light	0.03763	-0.05483 to 0.1301	No	ns	0.7197
TL DM PROB (20µM) Dark vs PROB (20µM) Light	0.04369	-0.04877 to 0.1361	No	ns	0.6148
TL DL Baseline Dark vs Control Light	-0.01683	-0.1353 to 0.1017	No	ns	0.9832
TL DL Baseline Dark vs PROB (20µM) Dark	-0.07206	-0.1906 to 0.04644	No	ns	0.3979
TL DL Baseline Light vs PROB (20µM) Light	-0.145	-0.2635 to -0.02648	Yes	**	0.0093
TL DL PROB (20µM) Dark vs PROB (20µM) Light	-0.08975	-0.2083 to 0.02876	No	ns	0.2076
Panx1a-KO DM Baseline Dark vs Control Light	-0.0853	-0.1671 to -0.003486	Yes	*	0.0373
Panx1a-KO DM Baseline Dark vs PROB (20µM) Dark	-0.3005	-0.3823 to -0.2187	Yes	****	<0.0001
Panx1a-KO DM Baseline Light vs PROB (20µM) Light	-0.121	-0.2028 to -0.03917	Yes	***	0.0009
Panx1a-KO DM PROB (20µM) Dark vs PROB (20µM) Light	0.09421	0.01239 to 0.1760	Yes	*	0.0166
Panx1a-KO DL Baseline Dark vs Control Light	0.03273	-0.09960 to 0.1651	No	ns	0.9195
Panx1a-KO DL Baseline Dark vs PROB (20µM) Dark	0.00024	-0.1321 to 0.1326	No	ns	>0.9999
Panx1a-KO DL Baseline Light vs PROB (20µM) Light	-0.04885	-0.1812 to 0.08348	No	ns	0.7763
Panx1a-KO DL PROB (20µM) Dark vs PROB (20µM) Light	-0.01636	-0.1487 to 0.1160	No	ns	0.9888

Beta

Tukey's multiple comparisons test	**Mean Diff.**	**95.00% CI of diff.**	**Below threshold?**	**Summary**	**Adjusted P Value**
TL DM Baseline Dark vs Control Light	0.02365	-0.01914 to 0.06643	No	ns	0.486

TL DM Baseline Dark vs PROB (20μM) Dark	-0.00894	-0.05173 to 0.03384	No	ns	0.9498
TL DM Baseline Light vs PROB (20μM) Light	0.0217	-0.02108 to 0.06449	No	ns	0.56
TL DM PROB (20μM) Dark vs PROB (20μM) Light	0.05429	0.01150 to 0.09707	Yes	**	0.0062
TL DL Baseline Dark vs Control Light	-0.02604	-0.09374 to 0.04167	No	ns	0.7555
TL DL Baseline Dark vs PROB (20μM) Dark	-0.04614	-0.1138 to 0.02156	No	ns	0.2967
TL DL Baseline Light vs PROB (20μM) Light	-0.07629	-0.1440 to -0.008583	Yes	*	0.0199
TL DL PROB (20μM) Dark vs PROB (20μM) Light	-0.05618	-0.1239 to 0.01152	No	ns	0.1427
Panx1a-KO DM Baseline Dark vs Control Light	-0.01798	-0.04184 to 0.005887	No	ns	0.2128
Panx1a-KO DM Baseline Dark vs PROB (20μM) Dark	-0.1266	-0.1505 to -0.1027	Yes	****	<0.0001
Panx1a-KO DM Baseline Light vs PROB (20μM) Light	-0.08763	-0.1115 to -0.06376	Yes	****	<0.0001
Panx1a-KO DM PROB (20μM) Dark vs PROB (20μM) Light	0.02101	-0.002856 to 0.04488	No	ns	0.1069
Panx1a-KO DL Baseline Dark vs Control Light	0.01431	-0.03829 to 0.06691	No	ns	0.8972
Panx1a-KO DL Baseline Dark vs PROB (20μM) Dark	-0.06796	-0.1205 to -0.01541	Yes	**	0.005
Panx1a-KO DL Baseline Light vs PROB (20μM) Light	-0.1216	-0.1741 to -0.06903	Yes	****	<0.0001
Panx1a-KO DL PROB (20μM) Dark vs PROB (20μM) Light	-0.03931	-0.09170 to 0.01309	No	ns	0.2161
Gamma					
Tukey's multiple comparisons test	**Mean Diff.**	**95.00% CI of diff.**	**Below threshold?**	**Summary**	**Adjusted P Value**

TL DM Baseline Dark vs Control Light	-0.1329	-0.1876 to -0.07825	Yes	****	<0.0001
TL DM Baseline Dark vs PROB (20µM) Dark	-0.1275	-0.1822 to -0.07285	Yes	****	<0.0001
TL DM Baseline Light vs PROB (20µM) Light	-0.0164	-0.07106 to 0.03827	No	ns	0.8669
TL DM PROB (20µM) Dark vs PROB (20µM) Light	-0.0218	-0.07647 to 0.03286	No	ns	0.7336
TL DL Baseline Dark vs Control Light	-0.1106	-0.1798 to -0.04141	Yes	***	0.0003
TL DL Baseline Dark vs PROB (20µM) Dark	-0.2081	-0.2773 to -0.1389	Yes	****	<0.0001
TL DL Baseline Light vs PROB (20µM) Light	-0.02404	-0.09326 to 0.04517	No	ns	0.8078
TL DL PROB (20µM) Dark vs PROB (20µM) Light	0.07341	0.004194 to 0.1426	Yes	*	0.0327
Panx1a-KO DM Baseline Dark vs Control Light	-0.03386	-0.09332 to 0.02560	No	ns	0.4585
Panx1a-KO DM Baseline Dark vs PROB (20µM) Dark	-0.00058	-0.06003 to 0.05888	No	ns	>0.9999
Panx1a-KO DM Baseline Light vs PROB (20µM) Light	0.0386	-0.02086 to 0.09806	No	ns	0.3395
Panx1a-KO DM PROB (20µM) Dark vs PROB (20µM) Light	0.005317	-0.05414 to 0.06477	No	ns	0.9957
Panx1a-KO DL Baseline Dark vs Control Light	-0.1312	-0.1847 to -0.07782	Yes	****	<0.0001
Panx1a-KO DL Baseline Dark vs PROB (20µM) Dark	-0.06047	-0.1139 to -0.007042	Yes	*	0.0192
Panx1a-KO DL Baseline Light vs PROB (20µM) Light	-0.05755	-0.1110 to -0.004113	Yes	*	0.029
Panx1a-KO DL PROB (20µM) Dark vs PROB (20µM) Light	-0.1283	-0.1818 to -0.07489	Yes	****	<0.0001

Supplementary Table S22. The comparison of coherence between the DM and OT and the DL and OT regions before and after bicuculline treatment. TL and Panx1a-KO larvae were recorded at baseline and after 30-minute bicuculline treatment. The coherence between ascending visual pathway regions was calculated using NeuroExplorer and split into five frequency bands: delta, theta, alpha, beta and gamma. A 2-way ANOVA analysis with Tukey's multiple comparison was performed on each frequency band using GraphPad Prism. DM stands for the coherence between the DM and OT regions. DL stands for the coherence between the DL and OT regions.

Delta

Tukey's multiple comparisons test	Mean Diff.	95.00% CI of diff.	Below threshold?	Summary	Adjusted P Value
TL DM Baseline Dark vs Control Light	-0.1281	-0.2820 to 0.02579	No	ns	0.1391
TL DM Baseline Dark vs Bicuculline (100µM) Dark	0.08498	-0.06893 to 0.2389	No	ns	0.4816
TL DM Baseline Light vs Bicuculline (100µM) Light	-0.06906	-0.2230 to 0.08486	No	ns	0.651
TL DM Bicuculline (100µM) Dark vs Bicuculline (100µM) Light	-0.2822	-0.4361 to -0.1282	Yes	****	<0.0001
TL DL Baseline Dark vs Control Light	0.04251	0.005157 to 0.07986	Yes	*	0.0188
TL DL Baseline Dark vs Bicuculline (100µM) Dark	-0.07856	-0.1159 to -0.04120	Yes	****	<0.0001
TL DL Baseline Light vs Bicuculline (100µM) Light	-0.1129	-0.1503 to -0.07558	Yes	****	<0.0001
TL DL Bicuculline (100µM) Dark vs Bicuculline (100µM) Light	0.008132	-0.02922 to 0.04548	No	ns	0.942
Panx1a-KO DM Baseline Dark vs Control Light	-0.06923	-0.1702 to 0.03176	No	ns	0.2863
Panx1a-KO DM Baseline Dark vs Bicuculline (100µM) Dark	0.1504	0.04936 to 0.2514	Yes	***	0.0009
Panx1a-KO DM Baseline Light vs Bicuculline (100µM) Light	0.129	0.02802 to 0.2300	Yes	**	0.0062
Panx1a-KO DM Bicuculline (100µM) Dark vs Bicuculline (100µM) Light	-0.09057	-0.1916 to 0.01042	No	ns	0.0958

Panx1a-KO DL Baseline Dark vs Control Light	-0.09151	-0.1285 to -0.05452	Yes	****	<0.0001
Panx1a-KO DL Baseline Dark vs Bicuculline (100µM) Dark	-0.1136	-0.1506 to -0.07659	Yes	****	<0.0001
Panx1a-KO DL Baseline Light vs Bicuculline (100µM) Light	-0.02092	-0.05791 to 0.01606	No	ns	0.4541
Panx1a-KO DL Bicuculline (100µM) Dark vs Bicuculline (100µM) Light	0.001141	-0.03585 to 0.03813	No	ns	0.9998

Theta

Tukey's multiple comparisons test	**Mean Diff.**	**95.00% CI of diff.**	**Below threshold?**	**Summary**	**Adjusted P Value**
TL DM Baseline Dark vs Control Light	-0.02086	-0.1355 to 0.09380	No	ns	0.9657
TL DM Baseline Dark vs Bicuculline (100µM) Dark	-0.216	-0.3307 to -0.1014	Yes	****	<0.0001
TL DM Baseline Light vs Bicuculline (100µM) Light	-0.2778	-0.3924 to -0.1631	Yes	****	<0.0001
TL DM Bicuculline (100µM) Dark vs Bicuculline (100µM) Light	-0.08259	-0.1973 to 0.03207	No	ns	0.2478
TL DL Baseline Dark vs Control Light	0.03026	-0.006898 to 0.06741	No	ns	0.1542
TL DL Baseline Dark vs Bicuculline (100µM) Dark	-0.09779	-0.1349 to -0.06063	Yes	****	<0.0001
TL DL Baseline Light vs Bicuculline (100µM) Light	-0.1303	-0.1675 to -0.09318	Yes	****	<0.0001
TL DL Bicuculline (100µM) Dark vs Bicuculline (100µM) Light	-0.0023	-0.03945 to 0.03486	No	ns	0.9985
Panx1a-KO DM Baseline Dark vs Control Light	-0.1408	-0.2141 to -0.06748	Yes	****	<0.0001
Panx1a-KO DM Baseline Dark vs Bicuculline (100µM) Dark	0.1047	0.03139 to 0.1780	Yes	**	0.0015
Panx1a-KO DM Baseline Light vs Bicuculline (100µM) Light	0.2365	0.1632 to 0.3098	Yes	****	<0.0001

Panx1a-KO DM Bicuculline (100µM) Dark vs Bicuculline (100µM) Light	-0.00897	-0.08226 to 0.06432	No	ns	0.989
Panx1a-KO DL Baseline Dark vs Control Light	-0.06154	-0.08533 to -0.03774	Yes	****	<0.0001
Panx1a-KO DL Baseline Dark vs Bicuculline (100µM) Dark	-0.09649	-0.1203 to -0.07270	Yes	****	<0.0001
Panx1a-KO DL Baseline Light vs Bicuculline (100µM) Light	-0.03947	-0.06327 to -0.01568	Yes	***	0.0002
Panx1a-KO DL Bicuculline (100µM) Dark vs Bicuculline (100µM) Light	-0.00452	-0.02831 to 0.01928	No	ns	0.9608

Alpha

Tukey's multiple comparisons test	**Mean Diff.**	**95.00% CI of diff.**	**Below threshold?**	**Summary**	**Adjusted P Value**
TL DM Baseline Dark vs Control Light	-0.02763	-0.1411 to 0.08589	No	ns	0.9232
TL DM Baseline Dark vs Bicuculline (100µM) Dark	-0.1276	-0.2411 to -0.01403	Yes	*	0.0205
TL DM Baseline Light vs Bicuculline (100µM) Light	-0.2043	-0.3178 to -0.09079	Yes	****	<0.0001
TL DM Bicuculline (100µM) Dark vs Bicuculline (100µM) Light	-0.1044	-0.2179 to 0.009137	No	ns	0.0842
TL DL Baseline Dark vs Control Light	-0.0022	-0.02972 to 0.02532	No	ns	0.9969
TL DL Baseline Dark vs Bicuculline (100µM) Dark	-0.1227	-0.1502 to -0.09513	Yes	****	<0.0001
TL DL Baseline Light vs Bicuculline (100µM) Light	-0.1312	-0.1587 to -0.1036	Yes	****	<0.0001
TL DL Bicuculline (100µM) Dark vs Bicuculline (100µM) Light	-0.0107	-0.03823 to 0.01682	No	ns	0.7473
Panx1a-KO DM Baseline Dark vs Control Light	-0.1334	-0.1935 to -0.07320	Yes	****	<0.0001
Panx1a-KO DM Baseline Dark vs Bicuculline (100µM) Dark	0.1766	0.1165 to 0.2368	Yes	****	<0.0001

Panx1a-KO DM Baseline Light vs Bicuculline (100µM) Light	0.3852	0.3250 to 0.4453	Yes	****	<0.0001
Panx1a-KO DM Bicuculline (100µM) Dark vs Bicuculline (100µM) Light	0.07518	0.01502 to 0.1353	Yes	**	0.0074
Panx1a-KO DL Baseline Dark vs Control Light	-0.05821	-0.07916 to -0.03726	Yes	****	<0.0001
Panx1a-KO DL Baseline Dark vs Bicuculline (100µM) Dark	-0.06064	-0.08159 to -0.03969	Yes	****	<0.0001
Panx1a-KO DL Baseline Light vs Bicuculline (100µM) Light	0.004925	-0.01602 to 0.02587	No	ns	0.9294
Panx1a-KO DL Bicuculline (100µM) Dark vs Bicuculline (100µM) Light	0.007355	-0.01359 to 0.02830	No	ns	0.8005

Beta

Tukey's multiple comparisons test	**Mean Diff.**	**95.00% CI of diff.**	**Below threshold?**	**Summary**	**Adjusted P Value**
TL DM Baseline Dark vs Control Light	-0.00827	-0.06236 to 0.04582	No	ns	0.9794
TL DM Baseline Dark vs Bicuculline (100µM) Dark	-0.03702	-0.09111 to 0.01707	No	ns	0.2932
TL DM Baseline Light vs Bicuculline (100µM) Light	-0.1101	-0.1642 to -0.05600	Yes	****	<0.0001
TL DM Bicuculline (100µM) Dark vs Bicuculline (100µM) Light	-0.08134	-0.1354 to -0.02725	Yes	***	0.0007
TL DL Baseline Dark vs Control Light	-0.0448	-0.06773 to -0.02187	Yes	****	<0.0001
TL DL Baseline Dark vs Bicuculline (100µM) Dark	-0.122	-0.1449 to -0.09905	Yes	****	<0.0001
TL DL Baseline Light vs Bicuculline (100µM) Light	-0.09876	-0.1217 to -0.07583	Yes	****	<0.0001
TL DL Bicuculline (100µM) Dark vs Bicuculline (100µM) Light	-0.02159	-0.04452 to 0.001341	No	ns	0.0735
Panx1a-KO DM Baseline Dark vs Control Light	-0.1474	-0.1834 to -0.1114	Yes	****	<0.0001

Panx1a-KO DM Baseline Dark vs Bicuculline (100µM) Dark	0.1788	0.1428 to 0.2147	Yes	****	<0.0001
Panx1a-KO DM Baseline Light vs Bicuculline (100µM) Light	0.3379	0.3019 to 0.3739	Yes	****	<0.0001
Panx1a-KO DM Bicuculline (100µM) Dark vs Bicuculline (100µM) Light	0.01169	-0.02430 to 0.04768	No	ns	0.8374
Panx1a-KO DL Baseline Dark vs Control Light	-0.06286	-0.07793 to -0.04780	Yes	****	<0.0001
Panx1a-KO DL Baseline Dark vs Bicuculline (100µM) Dark	0.009202	-0.005862 to 0.02427	No	ns	0.395
Panx1a-KO DL Baseline Light vs Bicuculline (100µM) Light	0.04773	0.03267 to 0.06279	Yes	****	<0.0001
Panx1a-KO DL Bicuculline (100µM) Dark vs Bicuculline (100µM) Light	-0.02434	-0.03940 to -0.009273	Yes	***	0.0002

Gamma

Tukey's multiple comparisons test	**Mean Diff.**	**95.00% CI of diff.**	**Below threshold?**	**Summary**	**Adjusted P Value**
TL DM Baseline Dark vs Control Light	-0.01534	-0.07051 to 0.03983	No	ns	0.8909
TL DM Baseline Dark vs Bicuculline (100µM) Dark	-0.06324	-0.1184 to -0.008070	Yes	*	0.0171
TL DM Baseline Light vs Bicuculline (100µM) Light	-0.08227	-0.1374 to -0.02711	Yes	***	0.0008
TL DM Bicuculline (100µM) Dark vs Bicuculline (100µM) Light	-0.03438	-0.08955 to 0.02079	No	ns	0.3769
TL DL Baseline Dark vs Control Light	0.003562	-0.05667 to 0.06379	No	ns	0.9987
TL DL Baseline Dark vs Bicuculline (100µM) Dark	0.02989	-0.03034 to 0.09012	No	ns	0.5773
TL DL Baseline Light vs Bicuculline (100µM) Light	0.03794	-0.02229 to 0.09818	No	ns	0.3667
TL DL Bicuculline (100µM) Dark vs Bicuculline (100µM) Light	0.01161	-0.04862 to 0.07185	No	ns	0.9599

Panx1a-KO DM Baseline Dark vs Control Light	-0.01789	-0.07906 to 0.04328	No	ns	0.8753
Panx1a-KO DM Baseline Dark vs Bicuculline (100µM) Dark	-0.3052	-0.3664 to -0.2441	Yes	****	<0.0001
Panx1a-KO DM Baseline Light vs Bicuculline (100µM) Light	-0.2511	-0.3123 to -0.1899	Yes	****	<0.0001
Panx1a-KO DM Bicuculline (100µM) Dark vs Bicuculline (100µM) Light	0.03623	-0.02494 to 0.09740	No	ns	0.4228
Panx1a-KO DL Baseline Dark vs Control Light	0.09802	0.03667 to 0.1594	Yes	***	0.0003
Panx1a-KO DL Baseline Dark vs Bicuculline (100µM) Dark	-0.04733	-0.1087 to 0.01401	No	ns	0.1935
Panx1a-KO DL Baseline Light vs Bicuculline (100µM) Light	-0.1026	-0.1639 to -0.04125	Yes	***	0.0001
Panx1a-KO DL Bicuculline (100µM) Dark vs Bicuculline (100µM) Light	0.04275	-0.01859 to 0.1041	No	ns	0.2761

Supplementary Table S23. The comparison of coherence between the DM and OT and the DL and OT regions before and after MK-801 treatment. TL and Panx1a-KO larvae were recorded at baseline and after 30-minute MK-801 treatment. The coherence between ascending visual pathway regions was calculated using NeuroExplorer and split into five frequency bands: delta, theta, alpha, beta and gamma. A 2-way ANOVA analysis with Tukey's multiple comparison was performed on each frequency band using GraphPad Prism. DM stands for the coherence between the DM and OT regions. DL stands for the coherence between the DL and OT regions.

Delta

Tukey's multiple comparisons test	Mean Diff.	95.00% CI of diff.	Below threshold?	Summary	Adjusted P Value
TL DM Baseline Dark vs Control Light	-0.1465	-0.2950 to 0.001888	No	ns	0.0544
TL DM Baseline Dark vs MK-801 (20µM) Dark	-0.2123	-0.3608 to -0.06390	Yes	**	0.0016
TL DM Baseline Light vs MK-801 (20µM) Light	-0.0423	-0.1907 to 0.1061	No	ns	0.8804
TL DM MK-801 (20µM) Dark vs MK-801 (20µM) Light	0.02348	-0.1249 to 0.1719	No	ns	0.9765
TL DL Baseline Dark vs Control Light	0.02747	-0.2653 to 0.3202	No	ns	0.9948

TL DL Baseline Dark vs MK-801 (20µM) Dark	-0.1361	-0.4289 to 0.1566	No	ns	0.6184
TL DL Baseline Light vs MK-801 (20µM) Light	-0.1622	-0.4550 to 0.1306	No	ns	0.4726
TL DL MK-801 (20µM) Dark vs MK-801 (20µM) Light	0.001414	-0.2914 to 0.2942	No	ns	>0.9999
Panx1a-KO DM Baseline Dark vs Control Light	-0.1101	-0.2633 to 0.04300	No	ns	0.2471
Panx1a-KO DM Baseline Dark vs MK-801 (20µM) Dark	0.03287	-0.1203 to 0.1860	No	ns	0.9447
Panx1a-KO DM Baseline Light vs MK-801 (20µM) Light	0.107	-0.04613 to 0.2601	No	ns	0.2713
Panx1a-KO DM MK-801 (20µM) Dark vs MK-801 (20µM) Light	-0.03601	-0.1891 to 0.1171	No	ns	0.929
Panx1a-KO DL Baseline Dark vs Control Light	-0.1087	-0.2914 to 0.07399	No	ns	0.4088
Panx1a-KO DL Baseline Dark vs MK-801 (20µM) Dark	0.2538	0.07115 to 0.4365	Yes	**	0.0025
Panx1a-KO DL Baseline Light vs MK-801 (20µM) Light	0.3291	0.1465 to 0.5118	Yes	****	<0.0001
Panx1a-KO DL MK-801 (20µM) Dark vs MK-801 (20µM) Light	-0.03337	-0.2161 to 0.1493	No	ns	0.9638

Theta

Tukey's multiple comparisons test	**Mean Diff.**	**95.00% CI of diff.**	**Below threshold?**	**Summary**	**Adjusted P Value**
TL DM Baseline Dark vs Control Light	-0.06516	-0.1650 to 0.03466	No	ns	0.3326
TL DM Baseline Dark vs MK-801 (20µM) Dark	-0.1402	-0.2401 to -0.04041	Yes	**	0.0019
TL DM Baseline Light vs MK-801 (20µM) Light	-0.05773	-0.1576 to 0.04209	No	ns	0.4421
TL DM MK-801 (20µM) Dark vs MK-801 (20µM) Light	0.01734	-0.08248 to 0.1172	No	ns	0.9698
TL DL Baseline Dark vs Control Light	0.00667	-0.1868 to 0.2001	No	ns	0.9997
TL DL Baseline Dark vs MK-801 (20µM) Dark	-0.1652	-0.3587 to 0.02825	No	ns	0.1233
TL DL Baseline Light vs MK-801 (20µM) Light	-0.1946	-0.3881 to -0.001156	Yes	*	0.048
TL DL MK-801 (20µM) Dark vs MK-801 (20µM) Light	-0.02273	-0.2162 to 0.1707	No	ns	0.9902

Panx1a-KO DM Baseline Dark vs Control Light	-0.1472	-0.2574 to -0.03699	Yes	**	0.0035
Panx1a-KO DM Baseline Dark vs MK-801 (20µM) Dark	0.008324	-0.1019 to 0.1185	No	ns	0.9974
Panx1a-KO DM Baseline Light vs MK-801 (20µM) Light	0.1504	0.04025 to 0.2607	Yes	**	0.0027
Panx1a-KO DM MK-801 (20µM) Dark vs MK-801 (20µM) Light	-0.00507	-0.1153 to 0.1051	No	ns	0.9994
Panx1a-KO DL Baseline Dark vs Control Light	-0.1429	-0.2842 to -0.001620	Yes	*	0.0463
Panx1a-KO DL Baseline Dark vs MK-801 (20µM) Dark	0.222	0.08065 to 0.3633	Yes	***	0.0004
Panx1a-KO DL Baseline Light vs MK-801 (20µM) Light	0.3069	0.1656 to 0.4482	Yes	****	<0.0001
Panx1a-KO DL MK-801 (20µM) Dark vs MK-801 (20µM) Light	-0.05802	-0.1993 to 0.08328	No	ns	0.7117

Alpha

Tukey's multiple comparisons test	**Mean Diff.**	**95.00% CI of diff.**	**Below threshold?**	**Summary**	**Adjusted P Value**
TL DM Baseline Dark vs Control Light	-0.04064	-0.1424 to 0.06115	No	ns	0.7317
TL DM Baseline Dark vs MK-801 (20µM) Dark	-0.05143	-0.1532 to 0.05036	No	ns	0.5609
TL DM Baseline Light vs MK-801 (20µM) Light	0.01667	-0.08512 to 0.1185	No	ns	0.9746
TL DM MK-801 (20µM) Dark vs MK-801 (20µM) Light	0.02746	-0.07433 to 0.1293	No	ns	0.8984
TL DL Baseline Dark vs Control Light	-0.00807	-0.1428 to 0.1266	No	ns	0.9987
TL DL Baseline Dark vs MK-801 (20µM) Dark	-0.2588	-0.3935 to -0.1241	Yes	****	<0.0001
TL DL Baseline Light vs MK-801 (20µM) Light	-0.2759	-0.4106 to -0.1412	Yes	****	<0.0001
TL DL MK-801 (20µM) Dark vs MK-801 (20µM) Light	-0.02521	-0.1599 to 0.1095	No	ns	0.9626
Panx1a-KO DM Baseline Dark vs Control Light	-0.1813	-0.2735 to -0.08916	Yes	****	<0.0001
Panx1a-KO DM Baseline Dark vs MK-801 (20µM) Dark	-0.01494	-0.1071 to 0.07721	No	ns	0.9754

Panx1a-KO DM Baseline Light vs MK-801 (20µM) Light	0.1859	0.09371 to 0.2780	Yes	****	<0.0001
Panx1a-KO DM MK-801 (20µM) Dark vs MK-801 (20µM) Light	0.01948	-0.07267 to 0.1116	No	ns	0.9479
Panx1a-KO DL Baseline Dark vs Control Light	-0.1436	-0.2757 to -0.01146	Yes	*	0.0272
Panx1a-KO DL Baseline Dark vs MK-801 (20µM) Dark	0.1937	0.06160 to 0.3259	Yes	**	0.0011
Panx1a-KO DL Baseline Light vs MK-801 (20µM) Light	0.3182	0.1860 to 0.4503	Yes	****	<0.0001
Panx1a-KO DL MK-801 (20µM) Dark vs MK-801 (20µM) Light	-0.01917	-0.1513 to 0.1130	No	ns	0.9819

Beta

Tukey's multiple comparisons test	**Mean Diff.**	**95.00% CI of diff.**	**Below threshold?**	**Summary**	**Adjusted P Value**
TL DM Baseline Dark vs Control Light	-0.04494	-0.09352 to 0.003628	No	ns	0.0814
TL DM Baseline Dark vs MK-801 (20µM) Dark	-0.06225	-0.1108 to -0.01368	Yes	**	0.0055
TL DM Baseline Light vs MK-801 (20µM) Light	-0.00493	-0.05350 to 0.04365	No	ns	0.9938
TL DM MK-801 (20µM) Dark vs MK-801 (20µM) Light	0.01238	-0.03619 to 0.06096	No	ns	0.9135
TL DL Baseline Dark vs Control Light	-0.00187	-0.07008 to 0.06635	No	ns	0.9999
TL DL Baseline Dark vs MK-801 (20µM) Dark	-0.1768	-0.2451 to -0.1086	Yes	****	<0.0001
TL DL Baseline Light vs MK-801 (20µM) Light	-0.2012	-0.2694 to -0.1330	Yes	****	<0.0001
TL DL MK-801 (20µM) Dark vs MK-801 (20µM) Light	-0.02618	-0.09439 to 0.04203	No	ns	0.7563
Panx1a-KO DM Baseline Dark vs Control Light	-0.1571	-0.2003 to -0.1139	Yes	****	<0.0001
Panx1a-KO DM Baseline Dark vs MK-801 (20µM) Dark	-0.04855	-0.09172 to -0.005376	Yes	*	0.0202
Panx1a-KO DM Baseline Light vs MK-801 (20µM) Light	0.2033	0.1601 to 0.2464	Yes	****	<0.0001

Panx1a-KO DM MK-801 (20µM) Dark vs MK-801 (20µM) Light	0.0947	0.05153 to 0.1379	Yes	****	<0.0001
Panx1a-KO DL Baseline Dark vs Control Light	-0.1295	-0.1959 to -0.06298	Yes	****	<0.0001
Panx1a-KO DL Baseline Dark vs MK-801 (20µM) Dark	0.1598	0.09329 to 0.2262	Yes	****	<0.0001
Panx1a-KO DL Baseline Light vs MK-801 (20µM) Light	0.2273	0.1608 to 0.2938	Yes	****	<0.0001
Panx1a-KO DL MK-801 (20µM) Dark vs MK-801 (20µM) Light	-0.06192	-0.1284 to 0.004560	No	ns	0.0783

Gamma

Tukey's multiple comparisons test	**Mean Diff.**	**95.00% CI of diff.**	**Below threshold?**	**Summary**	**Adjusted P Value**
TL DM Baseline Dark vs Control Light	-0.1298	-0.1800 to -0.07952	Yes	****	<0.0001
TL DM Baseline Dark vs MK-801 (20µM) Dark	-0.1256	-0.1759 to -0.07537	Yes	****	<0.0001
TL DM Baseline Light vs MK-801 (20µM) Light	-0.1292	-0.1794 to -0.07895	Yes	****	<0.0001
TL DM MK-801 (20µM) Dark vs MK-801 (20µM) Light	-0.1333	-0.1836 to -0.08310	Yes	****	<0.0001
TL DL Baseline Dark vs Control Light	0.008288	-0.06527 to 0.08185	No	ns	0.9915
TL DL Baseline Dark vs MK-801 (20µM) Dark	-0.05022	-0.1238 to 0.02334	No	ns	0.2941
TL DL Baseline Light vs MK-801 (20µM) Light	-0.1919	-0.2655 to -0.1183	Yes	****	<0.0001
TL DL MK-801 (20µM) Dark vs MK-801 (20µM) Light	-0.1334	-0.2069 to -0.05982	Yes	****	<0.0001
Panx1a-KO DM Baseline Dark vs Control Light	0.0257	-0.02870 to 0.08011	No	ns	0.6169
Panx1a-KO DM Baseline Dark vs MK-801 (20µM) Dark	-0.1279	-0.1824 to -0.07354	Yes	****	<0.0001
Panx1a-KO DM Baseline Light vs MK-801 (20µM) Light	-0.1518	-0.2062 to -0.09740	Yes	****	<0.0001

Panx1a-KO DM MK-801 (20µM) Dark vs MK-801 (20µM) Light	0.00185	-0.05255 to 0.05626	No	ns	0.9998
Panx1a-KO DL Baseline Dark vs Control Light	-0.00786	-0.07276 to 0.05705	No	ns	0.9895
Panx1a-KO DL Baseline Dark vs MK-801 (20µM) Dark	-0.04388	-0.1088 to 0.02103	No	ns	0.3027
Panx1a-KO DL Baseline Light vs MK-801 (20µM) Light	-0.01301	-0.07791 to 0.05189	No	ns	0.955
Panx1a-KO DL MK-801 (20µM) Dark vs MK-801 (20µM) Light	0.02301	-0.04189 to 0.08791	No	ns	0.7974

Supplementary Table S24. The comparison of coherence between the DM and OT and the DL and OT regions before and after MPTP treatment. TL and Panx1a-KO larvae were recorded after four hours of MPTP treatment in the dark. The coherence between ascending visual pathway regions was calculated using NeuroExplorer and split into five frequency bands: delta, theta, alpha, beta and gamma. A 2-way ANOVA analysis with Tukey's multiple comparison was performed on each frequency band using GraphPad Prism. DM stands for the coherence between the DM and OT regions. DL stands for the coherence between the DL and OT regions.

Delta

Tukey's multiple comparisons test	Mean Diff.	95.00% CI of diff.	Below threshold?	Summary	Adjusted P Value
TL DM Baseline Dark vs Control Light	0.03615	-0.1364 to 0.2087	No	ns	0.9478
TL DM Baseline Dark vs MPTP (50µM) Dark	0.3923	0.2197 to 0.5648	Yes	****	<0.0001
TL DM Baseline Light vs MPTP (50µM) Light	0.3626	0.1901 to 0.5351	Yes	****	<0.0001
TL DM MPTP (50µM) Dark vs MPTP (50µM) Light	0.006482	-0.1660 to 0.1790	No	ns	0.9997
TL DL Baseline Dark vs Control Light	0.006263	-0.2170 to 0.2295	No	ns	0.9999
TL DL Baseline Dark vs MPTP (50µM) Dark	-0.04488	-0.2681 to 0.1783	No	ns	0.9535
TL DL Baseline Light vs MPTP (50µM) Light	-0.09705	-0.3203 to 0.1262	No	ns	0.6716
TL DL MPTP (50µM) Dark vs MPTP (50µM) Light	-0.04591	-0.2691 to 0.1773	No	ns	0.9505
Panx1a-KO DM Baseline Dark vs Control Light	-0.2233	-0.3381 to -0.1085	Yes	****	<0.0001
Panx1a-KO DM Baseline Dark vs MPTP (50µM) Dark	-0.7294	-0.8442 to -0.6145	Yes	****	<0.0001

Panx1a-KO DM Baseline Light vs MPTP (50µM) Light	-0.5419	-0.6568 to -0.4271	Yes	****	<0.0001
Panx1a-KO DM MPTP (50µM) Dark vs MPTP (50µM) Light	-0.03586	-0.1507 to 0.07896	No	ns	0.8488
Panx1a-KO DL Baseline Dark vs Control Light	0.005796	-0.1976 to 0.2092	No	ns	0.9999
Panx1a-KO DL Baseline Dark vs MPTP (50µM) Dark	-0.2752	-0.4949 to -0.05552	Yes	**	0.0077
Panx1a-KO DL Baseline Light vs MPTP (50µM) Light	-0.3015	-0.5212 to -0.08181	Yes	**	0.0028
Panx1a-KO DL MPTP (50µM) Dark vs MPTP (50µM) Light	-0.02049	-0.2553 to 0.2144	No	ns	0.9958

Theta

Tukey's multiple comparisons test	**Mean Diff.**	**95.00% CI of diff.**	**Below threshold?**	**Summary**	**Adjusted P Value**
TL DM Baseline Dark vs Control Light	0.008017	-0.1080 to 0.1240	No	ns	0.998
TL DM Baseline Dark vs MPTP (50µM) Dark	0.321	0.2050 to 0.4369	Yes	****	<0.0001
TL DM Baseline Light vs MPTP (50µM) Light	0.3376	0.2216 to 0.4536	Yes	****	<0.0001
TL DM MPTP (50µM) Dark vs MPTP (50µM) Light	0.02466	-0.09133 to 0.1406	No	ns	0.9467
TL DL Baseline Dark vs Control Light	-0.02265	-0.1715 to 0.1262	No	ns	0.9794
TL DL Baseline Dark vs MPTP (50µM) Dark	-0.04876	-0.1976 to 0.1001	No	ns	0.8321
TL DL Baseline Light vs MPTP (50µM) Light	-0.07336	-0.2222 to 0.07550	No	ns	0.5806
TL DL MPTP (50µM) Dark vs MPTP (50µM) Light	-0.04724	-0.1961 to 0.1016	No	ns	0.8449
Panx1a-KO DM Baseline Dark vs Control Light	-0.1403	-0.2111 to -0.06951	Yes	****	<0.0001
Panx1a-KO DM Baseline Dark vs MPTP (50µM) Dark	-0.6359	-0.7067 to -0.5651	Yes	****	<0.0001
Panx1a-KO DM Baseline Light vs MPTP (50µM) Light	-0.5058	-0.5766 to -0.4350	Yes	****	<0.0001
Panx1a-KO DM MPTP (50µM) Dark vs MPTP (50µM) Light	-0.01022	-0.08101 to 0.06057	No	ns	0.9823
Panx1a-KO DL Baseline Dark vs Control Light	0.03276	-0.1018 to 0.1673	No	ns	0.9224

Panx1a-KO DL Baseline Dark vs MPTP (50µM) Dark	-0.2547	-0.4001 to -0.1094	Yes	****	<0.0001
Panx1a-KO DL Baseline Light vs MPTP (50µM) Light	-0.2918	-0.4372 to -0.1465	Yes	****	<0.0001
Panx1a-KO DL MPTP (50µM) Dark vs MPTP (50µM) Light	-0.00436	-0.1597 to 0.1510	No	ns	0.9999

Alpha

Tukey's multiple comparisons test	**Mean Diff.**	**95.00% CI of diff.**	**Below threshold?**	**Summary**	**Adjusted P Value**
TL DM Baseline Dark vs Control Light	0.05676	-0.02241 to 0.1359	No	ns	0.2516
TL DM Baseline Dark vs MPTP (50µM) Dark	0.3711	0.2919 to 0.4502	Yes	****	<0.0001
TL DM Baseline Light vs MPTP (50µM) Light	0.3192	0.2401 to 0.3984	Yes	****	<0.0001
TL DM MPTP (50µM) Dark vs MPTP (50µM) Light	0.004923	-0.07424 to 0.08409	No	ns	0.9985
TL DL Baseline Dark vs Control Light	-0.01683	-0.1191 to 0.08548	No	ns	0.9744
TL DL Baseline Dark vs MPTP (50µM) Dark	-0.05732	-0.1670 to 0.05240	No	ns	0.5336
TL DL Baseline Light vs MPTP (50µM) Light	-0.08779	-0.1975 to 0.02192	No	ns	0.1669
TL DL MPTP (50µM) Dark vs MPTP (50µM) Light	-0.04731	-0.1594 to 0.06477	No	ns	0.697
Panx1a-KO DM Baseline Dark vs Control Light	-0.0853	-0.1418 to -0.02881	Yes	***	0.0007
Panx1a-KO DM Baseline Dark vs MPTP (50µM) Dark	-0.5142	-0.5707 to -0.4577	Yes	****	<0.0001
Panx1a-KO DM Baseline Light vs MPTP (50µM) Light	-0.4537	-0.5101 to -0.3972	Yes	****	<0.0001
Panx1a-KO DM MPTP (50µM) Dark vs MPTP (50µM) Light	-0.02474	-0.08123 to 0.03174	No	ns	0.6708
Panx1a-KO DL Baseline Dark vs Control Light	0.03273	-0.07153 to 0.1370	No	ns	0.8492
Panx1a-KO DL Baseline Dark vs MPTP (50µM) Dark	-0.2806	-0.3932 to -0.1680	Yes	****	<0.0001

Panx1a-KO DL Baseline Light vs MPTP (50µM) Light	-0.3522	-0.4648 to -0.2396	Yes	****	<0.0001
Panx1a-KO DL MPTP (50µM) Dark vs MPTP (50µM) Light	-0.03889	-0.1593 to 0.08150	No	ns	0.838

Beta

Tukey's multiple comparisons test	**Mean Diff.**	**95.00% CI of diff.**	**Below threshold?**	**Summary**	**Adjusted P Value**
TL DM Baseline Dark vs Control Light	0.02365	-0.02363 to 0.07092	No	ns	0.5717
TL DM Baseline Dark vs MPTP (50µM) Dark	0.2323	0.1850 to 0.2796	Yes	****	<0.0001
TL DM Baseline Light vs MPTP (50µM) Light	0.2086	0.1614 to 0.2559	Yes	****	<0.0001
TL DM MPTP (50µM) Dark vs MPTP (50µM) Light	-2.3E-05	-0.04730 to 0.04725	No	ns	>0.9999
TL DL Baseline Dark vs Control Light	-0.02604	-0.08327 to 0.03119	No	ns	0.6458
TL DL Baseline Dark vs MPTP (50µM) Dark	-0.08573	-0.1426 to -0.02889	Yes	***	0.0006
TL DL Baseline Light vs MPTP (50µM) Light	-0.07229	-0.1291 to -0.01546	Yes	**	0.006
TL DL MPTP (50µM) Dark vs MPTP (50µM) Light	-0.0126	-0.06822 to 0.04302	No	ns	0.9373
Panx1a-KO DM Baseline Dark vs Control Light	-0.01798	-0.04690 to 0.01094	No	ns	0.3794
Panx1a-KO DM Baseline Dark vs MPTP (50µM) Dark	-0.438	-0.4669 to -0.4091	Yes	****	<0.0001
Panx1a-KO DM Baseline Light vs MPTP (50µM) Light	-0.4376	-0.4665 to -0.4087	Yes	****	<0.0001
Panx1a-KO DM MPTP (50µM) Dark vs MPTP (50µM) Light	-0.01757	-0.04649 to 0.01135	No	ns	0.4005
Panx1a-KO DL Baseline Dark vs Control Light	0.01432	-0.02788 to 0.05651	No	ns	0.8188
Panx1a-KO DL Baseline Dark vs MPTP (50µM) Dark	-0.4423	-0.4879 to -0.3968	Yes	****	<0.0001

Panx1a-KO DL Baseline Light vs MPTP (50µM) Light	-0.473	-0.5186 to -0.4274	Yes	****	<0.0001
Panx1a-KO DL MPTP (50µM) Dark vs MPTP (50µM) Light	-0.01634	-0.06506 to 0.03238	No	ns	0.824
Gamma					
Tukey's multiple comparisons test	**Mean Diff.**	**95.00% CI of diff.**	**Below threshold?**	**Summary**	**Adjusted P Value**
TL DM Baseline Dark vs Control Light	-0.1329	-0.1964 to -0.06946	Yes	****	<0.0001
TL DM Baseline Dark vs MPTP (50µM) Dark	0.04833	-0.01236 to 0.1090	No	ns	0.1709
TL DM Baseline Light vs MPTP (50µM) Light	0.1401	0.07945 to 0.2008	Yes	****	<0.0001
TL DM MPTP (50µM) Dark vs MPTP (50µM) Light	-0.04111	-0.09264 to 0.01042	No	ns	0.1696
TL DL Baseline Dark vs Control Light	-0.1106	-0.1810 to -0.04024	Yes	***	0.0003
TL DL Baseline Dark vs MPTP (50µM) Dark	-0.05736	-0.1277 to 0.01302	No	ns	0.1545
TL DL Baseline Light vs MPTP (50µM) Light	0.0069	-0.06348 to 0.07728	No	ns	0.9944
TL DL MPTP (50µM) Dark vs MPTP (50µM) Light	-0.04636	-0.1167 to 0.02402	No	ns	0.3263
Panx1a-KO DM Baseline Dark vs Control Light	-0.03386	-0.09676 to 0.02904	No	ns	0.5085
Panx1a-KO DM Baseline Dark vs MPTP (50µM) Dark	0.03924	-0.02366 to 0.1021	No	ns	0.3755
Panx1a-KO DM Baseline Light vs MPTP (50µM) Light	0.02501	-0.03789 to 0.08792	No	ns	0.7354
Panx1a-KO DM MPTP (50µM) Dark vs MPTP (50µM) Light	-0.04809	-0.1110 to 0.01481	No	ns	0.2009
Panx1a-KO DL Baseline Dark vs Control Light	-0.1312	-0.1945 to -0.06802	Yes	****	<0.0001
Panx1a-KO DL Baseline Dark vs MPTP (50µM) Dark	-0.1032	-0.1715 to -0.03489	Yes	***	0.0006

Panx1a-KO DL Baseline Light vs MPTP (50µM) Light	-0.08533	-0.1536 to -0.01704	Yes	**	0.0074
Panx1a-KO DL MPTP (50µM) Dark vs MPTP (50µM) Light	-0.1134	-0.1864 to -0.04038	Yes	***	0.0004

8.5 Behavioral Assay Statistics

Supplementary Table S25. The distance travelled by TL and Panx1a-KO larvae in a light ramp assay. Larvae were incubated with adenosine ± MPTP for four hours in the dark prior to recording. The data was recorded using the Zebrabox and processed using Fast Data Monitor. The total distance travelled of each larva between 2100 and 2300 seconds was extracted and analyzed using GraphPad Prism. Significance was calculated using a Welch's t-test.

Treatment	P value	Significant (P < 0.05)?	Welch-corrected t, df	Control (mm)	Adenosine (0.1µM) (mm)	MPTP (10µM) (mm)	Adenosine (0.1µM) + MPTP (10µM) (mm)
Control TL vs Adenosine (0.1µM) TL	<0.0001	****	t=5.246, df=951.0	25.57	21.77		
Control Panx1a-KO vs Adenosine (0.1µM) Panx1a-KO	<0.0001	****	t=6.391, df=945.6	21.12	16.92		
Control TL vs Adenosine (0.1µM)+ MPTP (10µM) TL	<0.0001	****	t=25.59, df=1074	25.57			10.76
Control Panx1a-KO vs Adenosine (0.1µM)+ MPTP (10µM) Panx1a-KO	<0.0001	****	t=29.63, df=894.9	21.12			5.963
TL MPTP vs Adenosine+MPTP	<0.0001	****	t=4.370, df=467.7			14.29	10.76
Panx1a-KO MPTP vs Adenosine+MPTP	<0.0001	****	t=3.858, df=421.5			8.839	5.963

Supplementary Table S26. The distance travelled by TL and Panx1a-KO larvae in a light ramp assay. Larvae were incubated with caffeine ± MPTP for four hours in the dark prior to recording. The data was recorded using the Zebrabox and processed using Fast Data Monitor. The total distance travelled of each

larva between 2100 and 2300 seconds was extracted and analyzed using GraphPad Prism. Significance was calculated using a Welch's t-test.

Treatment	P value	Significant (P < 0.05)?	Welch-corrected t, df	Control (mm)	Caffeine (100µM) (mm)	MPTP (10µM) (mm)	Caffeine (100µM) + MPTP (10µM) (mm)
Control TL vs Caffeine (100µM) TL	<0.0001	****	t=14.74, df=1054	25.57	15.91		
Control Panx1a-KO vs Caffeine (100µM) Panx1a-KO	0.007	**	t=2.703, df=935.2	21.12	19.32		
Control TL vs Caffeine (100µM)+ MPTP (10µM) TL	<0.0001	****	t=20.34, df=969.1	25.57			11.05
Control Panx1a-KO vs Caffeine (100µM)+ MPTP (10µM) Panx1a-KO	<0.0001	****	t=22.49, df=858.4	21.12			9.844
TL MPTP vs Caffeine+MPTP	0.0004	***	t=3.565, df=636.9			14.29	11.05
Panx1a-KO MPTP vs Caffeine+MPTP	0.1746	ns	t=1.360, df=407.7			8.839	9.844

Supplementary Table S27. The distance travelled by TL and Panx1a-KO larvae in a light ramp assay. Larvae were incubated with CY-09 ± MPTP for four hours in the dark prior to recording. The data was recorded using the Zebrabox and processed using Fast Data Monitor. The total distance travelled of each larva between 2100 and 2300 seconds was extracted and analyzed using GraphPad Prism. Significance was calculated using a Welch's t-test.

Treatment	P value	Significant (P < 0.05)?	Welch-corrected t, df	Control (mm)	CY-09 (1µM) (mm)	MPTP (10µM) (mm)	CY-09 (1µM) + MPTP (10µM) (mm)
Control TL vs CY-09 (1µM) TL	<0.0001	****	t=17.34, df=1160	25.57	14.12		
Control Panx1a-KO vs CY-09 (1µM) Panx1a-KO	<0.0001	****	t=10.50, df=1087	21.12	14.58		

Control TL vs CY-09 (1µM)+MPTP (10µM) TL	<0.0001	****	t=26.63, df=1072	25.57			10.2
Control Panx1a-KO vs CY-09 (1µM)+MPTP (10µM) Panx1a-KO	<0.0001	****	t=20.64, df=998.2	21.12			9.518
TL MPTP vs CY-09+MPTP	<0.0001	****	t=5.076, df=465.6			14.29	10.2
Panx1a-KO MPTP vs CY-09+MPTP	0.3852	ns	t=0.8692, df=492.0			8.839	9.518

Supplementary Table S28. The distance travelled by TL and Panx1a-KO larvae in a light ramp assay. Larvae were incubated with dexamethasone ± MPTP for four hours in the dark prior to recording. The data was recorded using the Zebrabox and processed using Fast Data Monitor. The total distance travelled of each larva between 2100 and 2300 seconds was extracted and analyzed using GraphPad Prism. Significance was calculated using a Welch's t-test.

Treatment	**P value**	**Significant (P < 0.05)?**	**Welch-corrected t, df**	**Control (mm)**	**Dexamethasone (10µM) (mm)**	**MPTP (10µM) (mm)**	**Dexamethasone (10µM) + MPTP (10µM) (mm)**
Control TL vs Dexamethasone (10µM) TL	0.2783	ns	t=1.085, df=751.8	25.57	24.61		
Control Panx1a-KO vs Dexamethasone (10µM) Panx1a-KO	<0.0001	****	t=5.883, df=790.9	21.12	16.54		
Control TL vs Dexamethasone (10µM) + MPTP (10µM) TL	<0.0001	****	t=20.94, df=962.3	25.57			12.35
Control Panx1a-KO vs Dexamethasone (10µM) + MPTP (10µM) Panx1a-KO	<0.0001	****	t=16.37, df=809.5	21.12			10.34

TL MPTP vs Dexamethasone+MPTP	0.0217	*	t=2.302, df=528.5		14.29	12.35
Panx1a-KO MPTP vs Dexamethasone+MPTP	0.0781	ns	t=1.765, df=595.6		8.839	10.34

Supplementary Table S29. The distance travelled by TL and Panx1a-KO larvae in a light ramp assay. Larvae were incubated with INF39 ± MPTP for four hours in the dark prior to recording. The data was recorded using the Zebrabox and processed using Fast Data Monitor. The total distance travelled of each larva between 2100 and 2300 seconds was extracted and analyzed using GraphPad Prism. Significance was calculated using a Welch's t-test.

Treatment	P value	Significant (P < 0.05)?	Welch-corrected t, df	Control (mm)	INF-39 (10µM) (mm)	MPTP (10µM) (mm)	INF-39 (10µM) + MPTP (10µM) (mm)
Control TL vs INF39 (10µM) TL	<0.0001	****	t=4.000, df=563.3	25.57	21.76		
Control Panx1a-KO vs INF39 (10µM) Panx1a-KO	<0.0001	****	t=23.81, df=902.2	21.12	7.028		
Control TL vs INF39 (10µM) + MPTP(10µM) TL	<0.0001	****	t=10.23, df=872.6	25.57			18.57
Control Panx1a-KO vs INF39 (10µM) + MPTP(10µM) Panx1a-KO	<0.0001	****	t=20.80, df=901.8	21.12			8.801
TL MPTP vs INF39+MPTP	<0.0001	****	t=4.827, df=584.1			14.29	18.57
Panx1a-KO MPTP vs INF39+MPTP	0.9619	ns	t=0.04781, df=524.7			8.839	8.801

Supplementary Table S30. The distance travelled by TL and Panx1a-KO larvae in a light ramp assay. Larvae were incubated with MCC950 ± MPTP for four hours in the dark prior to recording. The data was recorded using the Zebrabox and processed using Fast Data Monitor. The total distance travelled of each larva between 2100 and 2300 seconds was extracted and analyzed using GraphPad Prism. Significance was calculated using a Welch's t-test.

Treatment	P value	Significant (P < 0.05)?	Welch-corrected t, df	Control (mm)	MCC-950 (1µM) (mm)	MPTP (10µM) (mm)	MCC-950 (1µM) + MPTP (10µM) (mm)
Control TL vs MCC950 (1µM) TL	0.0002	***	t=3.697, df=873.0	25.57	28.89		
Control Panx1a-KO vs MCC950 (1µM) Panx1a-KO	0.4202	ns	t=0.8065, df=963.1	21.12	21.72		
Control TL vs MCC950 (1µM) + MPTP (10µM) TL	<0.0001	****	t=11.57, df=651.5	25.57			15.84
Control Panx1a-KO vs MCC950 (1µM) + MPTP (10µM) Panx1a-KO	<0.0001	****	t=21.95, df=818.0	21.12			6.796
TL MPTP vs MCC950+MPTP	0.128	ns	t=1.524, df=667.6			14.29	15.84
Panx1a-KO MPTP vs MCC950+MPTP	0.0163	*	t=2.409, df=590.4			8.839	6.796

Supplementary Table S31. The distance travelled by TL and Panx1a-KO larvae in a light ramp assay. Larvae were incubated with metformin ± MPTP for four hours in the dark prior to recording. The data was recorded using the Zebrabox and processed using Fast Data Monitor. The total distance travelled of each larva between 2100 and 2300 seconds was extracted and analyzed using GraphPad Prism. Significance was calculated using a Welch's t-test.

Treatment	P value	Significantly different (P < 0.05)?	Welch-corrected t, df	Control (mm)	Metformin (10µM) (mm)	MPTP (10µM) (mm)	Metformin (10µM)+ MPTP (10µM) (mm)

Control TL vs Metformin (10µM) TL	<0.0001	****	t=9.340, df=1019	25.57	19.21		
Control panx1a vs Metformin (10µM) panx1a	<0.0001	****	t=12.06, df=886.4	21.12	12.66		
Control TL vs Metformin (10µM)+ MPTP (10µM) TL	<0.0001	****	t=20.61, df=1076	25.57			12.48
Control panx1a vs Metformin (10µM)+ MPTP (10µM) panx1a	<0.0001	****	t=25.19, df=989.2	21.12			7.188
TL MPTP vs Metformin+MPTP	0.0327	*	t=2.142, df=543.4			14.29	12.48
Panx1a-KO MPTP vs Metformin+MPTP	0.0335	*	t=2.132, df=479.3			8.839	7.188